THREE DIMENSIONAL STRAIN DISTRIBUTION AND DEFORMATION TEMPERATURE INTERPRETED FROM QUARTZ MICROSTRUCTURES AND PETROFABRICS IN THE OKANAGAN VALLEY SHEAR ZONE, SOUTHERN CANADIAN CORDILLERA

by

Vincent Twomey

B.Sc., University College Cork, 2011

Thesis Submitted in Partial Fulfilment of the

Requirements for the Degree of

Master of Science

in the

Department of Earth Sciences

Faculty of Science

SIMON FRASER UNIVERSITY

Summer 2014

Approval

Name: **Vincent Twomey**

Degree: **Master of Science**

Title:

Three dimensional strain distribution and deformation temperature interpreted from quartz microstructures and petrofabrics in the Okanagan Valley shear zone, southern Canadian Cordillera

Examining Committee: **Chair: Dr. Andrew Calvert**
Professor

Dr. Dan Gibson
Senior Supervisor
Associate Professor

Dr. Dan Marshall
Supervisor
Professor

Dr. Derek Thorkelson
Supervisor
Professor

Dr. Laurent Godin
Supervisor
Adjunct

Dr. Lori Kennedy
External Examiner
UBC

Date Defended/Approved: July 18, 2014

Partial Copyright Licence

Abstract

The Eocene Okanagan Valley shear zone (OVsz) is a ~1-1.5 km thick, <30° west-dipping, extensional, crustal-scale detachment that facilitated exhumation of the southwestern Shuswap metamorphic complex in the southern Canadian Cordillera. Kinematic indicators suggest a predominantly top-to-the-WNW sense of shear with quartz a-axis patterns suggesting general plane strain conditions with possible constriction in the upper 150m of the shear zone. Deformation temperatures derived from recrystallization mechanisms and crystallographic orientations of quartz progressively, yet anomalously rapidly, increase from ~280 to >650 °C down the 1-1.5 km structural section. Higher temperature fabrics formed at structurally lower levels within the shear zone are interpreted to have been 'locked-in' after migrating out of the progressively narrowing active zone of deformation during exhumation of the footwall to upper crustal levels. These fabrics were passively exhumed along a trajectory resulting in their progressive juxtaposition against lower temperature fabrics being generated in the still active part of the OVsz higher in the crust.

Keywords: Quartz crystallographic preferred orientations (CPOs); quartz recrystallization mechanisms; deformation temperatures; strain; exhumation; Okanagan Valley shear zone (OVsz); Shuswap metamorphic complex

Acknowledgements

I want to thank Dan Gibson for giving me the chance to study in Canada and to experience life in a new continent. I would also like to thank him for his support for support, mentorship and academic insight. The exact same can be said for Laurent Godin. I am also thankful to Derek Thorkelson, Dan Marshall, and Lori Kennedy for taking the time to make suggestions and provide discussions which helped improve this thesis.

I am very thankful to Kevin Cameron for the bit of banter and giving me great labs to TA. Also a very special mention to all the lads at SFU particularly Luke, Ivanka, Flavien, Jaap, Sarah, Anja, Francesca and many others who have made my time at SFU enjoyable and great craic altogether. This thesis was initially the product of a few pints to many back in Ireland with Brendan Murphy and my good friend John Reavy who helped convince me to give Canada a shot.

I would like to thank Dr. Martin Wong from Colgate University for allowing me to use his EBSD detector. His knowledge of the software made my life demonstrably easier during my data collection. Also, cheers to Kyle Larson (UBC-O) for the FA scans. I am also very appreciative of the staff at the Earth Sciences department of SFU; particularly the assistance of Glenda, Tarja, Matt and Rodney.

I'd like to give a particularly big shout out to my field assistant Zac for doing a great job, as well as putting up with me for the guts of an entire Summer, as well as providing m with some good company when out camping. Special thanks to Andy Okulitch for sharing his expertise in my study area. Also thanks to Rick Lawton for hitting me up with some accommodation in the Okanagan. Thanks to all who helped in Kingston too.

My biggest thanks goes out to my Mammy and Daddy as well as my brothers and sister for their support and motivation while I pursue my studies. This would be by no means possible without them. I cannot write an acknowledgements section without a special referral to Hazel for her endless support, motivation and friendship.

Table of Contents

List of Tables

List of Figures

Chapter 1.

Introduction to the regional geology of the southeastern Canadian Cordillera, the Okanagan Valley shear zone, and a statement of problems and research objectives

1.1. Introduction

Low-angle extensional brittle-ductile shear zones, which can accommodate kilometre-scale horizontal crustal stretching, are interpreted to play a significant role in the exhumation of metamorphic core complexes in the North American Cordillera (Coney, 1980; Wernicke, 1981; Coney and Harms, 1984; Axen, 2004). A comprehensive examination of the thermo-kinematic evolution of these shear zones is required to understand processes that contribute to the exhumation of mid-crustal rocks. Constituent minerals within mylonitic rocks in ductile shear zones are commonly characterized by recrystallization textures and steady-state microfabrics, with a consistent grain size distribution, shape-preferred orientation, and crystallographic preferred orientation (Passchier and Trouw, 2005). The balance between individual strain-accommodating processes, petrofabric development and different recrystallization mechanisms is related to the succession of physical conditions that accompanied deformation, including temperature, strain rate, strain geometry, shear sense, grain size and fluid activity (Lister, 1978; Law, 1990; Law

et al., 2004; Toy et al., 2008; Stipp et al, 2002a, b; Barth et al., 2010; Sullivan and Beane, 2010; Law et al., 2010).

Current uncertainties regarding the structural character and thermo-kinematic evolution of the Okanagan Valley shear zone (OVsz) in southern British Columbia has led to discrepancies regarding the interpreted significance of the OVsz as a crustal-scale shear zone and its role in the exhumation of the Shuswap metamorphic complex. This thesis uses field data, microstructural and petrofabric analysis of quartz, and previously-published geochronological and thermochronological data to resolve the spatial and temporal development of strain and temperature of deformation associated with the OVsz.

1.2. Geology of the southern Canadian Cordillera

The tectonic framework of the Canadian Cordillera consists of a "collage" of allochthonous arc and oceanic terranes accreted to the western margin of the Laurentian craton from the early Mesozoic to the late Paleocene (Helwig, 1974; Davis et al., 1978; Coney et al., 1980; Monger et al., 1982; Colpron and Nelson, 2007). The Intermontane terranes were largely accreted to the North American western paleomargin during Late Permian to Early Jurassic time (Monger et al. 1982; Nelson et al. 2006; Beranek et al., 2010) followed by the progressive Late Jurassic to mid-Cretaceous accretion of the Insular terranes unto the sedimentary sequences that accumulated onto the ancestral western North American paleomargin (Monger et al, 1982; Monger and Price, 2002; Colpron et al., 2007 Inset Fig. 1.1). This, combined with westward underthrusting of the North American craton, resulted in crustal thickening in excess of 50–60-km, widespread high-temperature metamorphism and crustal anatexis in the southern Canadian Cordillera (Coney and Harms, 1984; Bardoux and Mareschal, 1994; Whitney et al., 2004; Gibson et al., 2008).

During the Paleocene, the obliquity of convergence between the North American plate and subducting Kula plate increased due to a change in plate kinematics. The increased obliquity produced a dextral transtensional regime that resulted in cessation of crustal contraction and orogenic thickening, and the initiation of Eocene extensional collapse in the southeastern Canadian Cordillera (Ewing, 1980; Engebretson et al., 1984; Price and Carmichael, 1986; Parrish et al., 1988; Harms and Price, 1992; Struik, 1993; Monger and Price, 2002). The extensional collapse was accompanied by decompression melting and rapid exhumation of mid-crustal rocks within the overthickened orogenic wedge in south-central British Columbia and adjacent Washington (Figs 1.1; 1.2; Ewing, 1980; Okulitch, 1984; Tempelman-Kluit and Parkinson, 1986; Johnson and Brown, 1996; Johnson, 2006). Eocene exhumation was primarily facilitated by a system of crustal-scale, north-south striking normal sense detachment faults and shear zones (Ewing, 1980; Okulitch, 1984; Johnson and Brown, 1996; Parrish et al., 1988). Two of the crustal detachments include the west-side-down Okanagan Valley shear zone (OVsz) and the east-side-down Columbia River fault defining the western and eastern boundaries of the southern Shuswap metamorphic complex, respectively (Figs 1.1; 1.2; Templeman-Kluit and Parkinson, 1986; Parrish et al., 1988; Johnson and Brown, 1996; Brown et al, 2012).

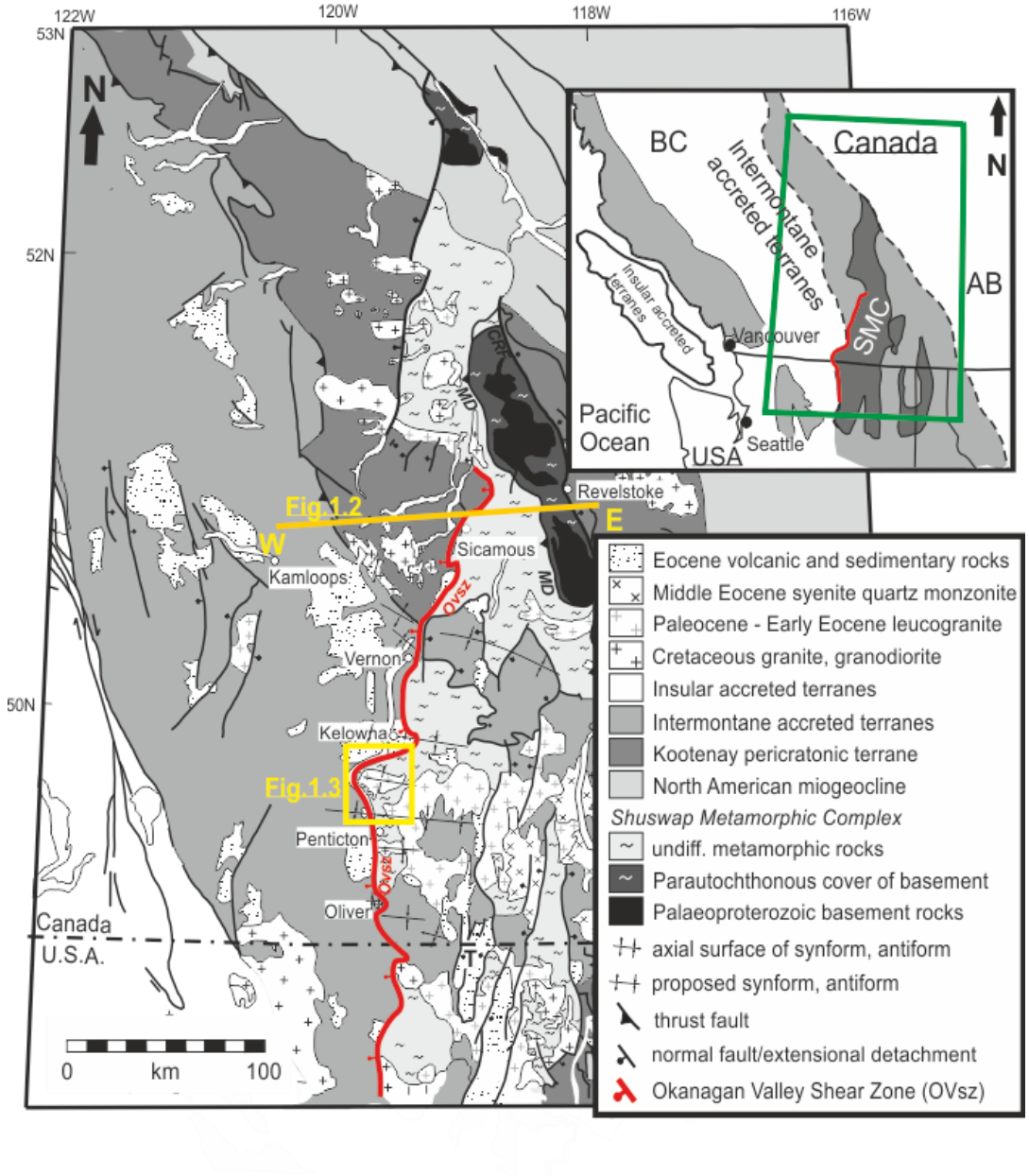

Figure 1.1. Generalized geological map of the southern Canadian Cordillera

Locations of cross-section in Fig 1.2 and study area (yellow box) in Fig. 1.3 are also highlighted (modified from Johnson et al., 2006, and Brown et al., 2012). OVsz, Okanagan Valley shear zone; MD, Monashee décollement; CRF, Columbia River fault.

1.3. The significance of the Okanagan Valley shear zone as an extensional detachment

The OVsz represents a fundamental structural boundary between the high grade Shuswap metamorphic complex in the footwall to the east and the predominantly sub-greenschist to greenschist-facies hanging wall rocks to the west (Figs.1.2; 1.3). The OVsz is characterised by a <30° west-dipping, 1-2 km thick, brittle to ductile shear zone consisting of mylonitic amphibolite facies orthogneiss and paragneiss with abundant syntectonic leucocratic intrusions (Fig. 1.3; Bardoux, 1993; Brown et al., 2012; this study).

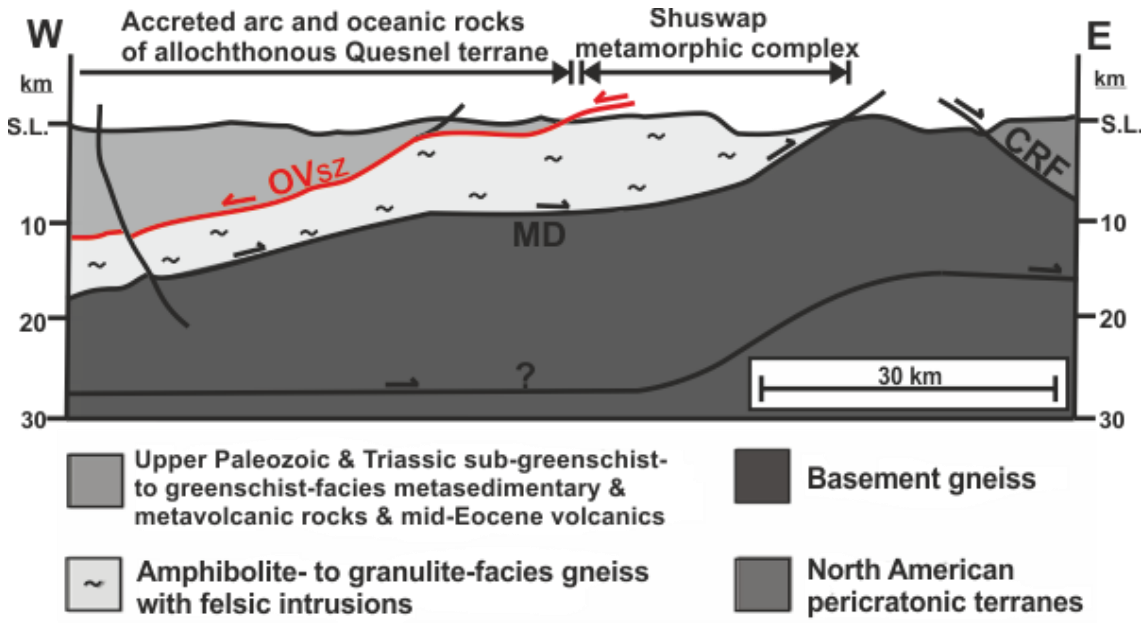

Figure 1.2. Simplified present-day west-east crustal cross-section of the southern Canadian Cordillera

Major crustal detachments include; the Okanagan Valley shear zone (OVsz), the Monashee décollement (MD), and the Columbia River fault (CRF) (See Fig. 1.1 for line of section) (Modified from Johnson and Brown, 1996).

Footwall rock types consist of amphibolite- to granulite-facies gneisses and abundant leucocratic intrusions (Figs.1.1; 1.2). These rocks contain a penetrative ductile fabric characterized by a shallowly dipping foliation, interpreted to be the result of the Early Jurassic to early Paleogene contraction and orogenic thickening (Figs.1.1; 1.2; Price and Mountjoy, 1970; Brown and Journeay, 1987; Parrish et al., 1988; Johnson and Brown, 1996; Gibson et al., 2005; 2008). Paleozoic to Early Triassic sub-greenschist to greenschist facies metasedimentary and metavolcanic rocks, along with local Eocene volcanic and sedimentary sequences and unconformably overlying stratified syn-extensional half graben basins are found in the hanging wall west of the OVsz (Fig.1.2; 1.3; Tempelman-Kluit and Parkinson, 1986: McClaughry and Gaylord, 2005; Brown et al., 2012). The steep metamorphic gradient and disparity in argon cooling ages exhibited across the trace of the OVsz, and the degree of anatectic Eocene melting, ductile deformation and mylonitization within the footwall gneiss readily demonstrate that the exhumation of mid-crustal footwall rocks was achieved through lithospheric extension (Bardoux and Mareschal, 1994; Johnson and Brown, 1996; Brown et al., 2012).

The base of the OVsz is marked by undeformed granitoid plutons and gneissic units (Bardoux, 1993; Brown et al., 2012; this study). Top-to-the-WNW solid-state deformation fabrics increase in intensity up the structural section grading from penetratively deformed amphibolite facies orthogneiss and paragneiss to greenschist-facies mylonite and cataclasite within the uppermost part of the shear zone (Fig. 1.3). Previous studies have characterized the detachment system as a brittle-ductile shear zone >1 km thick in many places overprinted by a brittle detachment at the top, thus referring to the system as the Okanagan crustal shear (Tempelman-Kluit and Parkinson, 1986) or Okanagan Valley fault (Parrish et al., 1988 and references therein). In this study, we continue with the terminology proposed by Brown (2010) and Brown et al. (2012) choosing to refer to the detachment system as the Okanagan Valley shear zone

(OVsz), since it is a km's thick distributed shear zone that includes both the brittle and ductile fabric components.

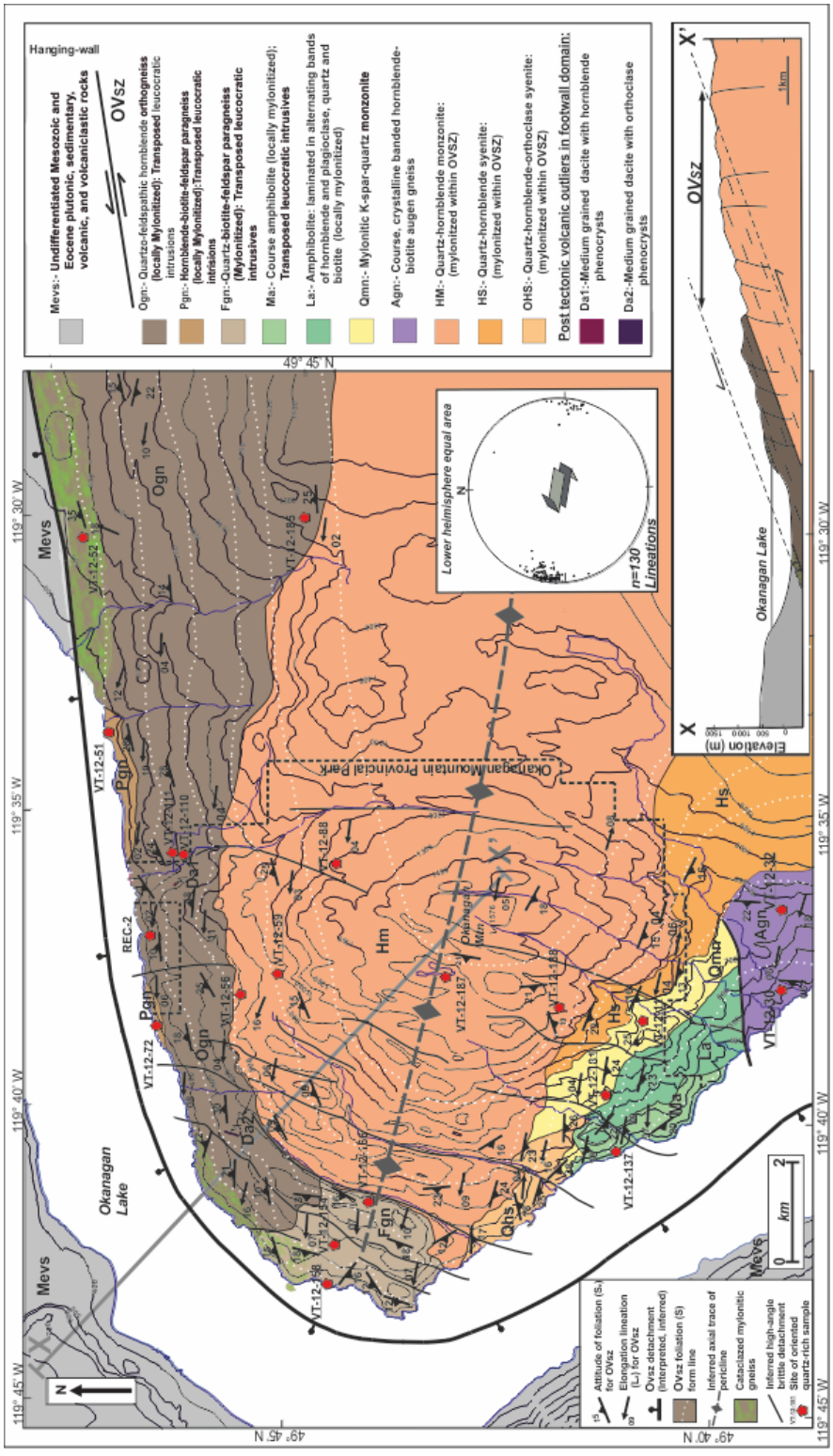

Figure 1.3. Geologic map of the study area in the vicinity of the Okanagan mountain provincial Park

Foliation form lines (S) highlight the corrugated nature of the shear zone. Geologic cross-section X-X' showing the shallow-dipping Okanagan Valley shear zone (OVsz). Inset; Lower hemisphere equal area projection of penetrative mineral elongation lineations (mean plunge 05˚ toward 279°).

Many studies cite the exhumation of the Shuswap metamorphic complex as a type-example of post-convergent gravitational collapse of an overthickened crust (Tempelman-Kluit and Parkinson, 1986; Parrish et al., 1988; Vanderhaeghe and Teyssier, 2001; Price and Monger, 2003; Rey et al., 2009). These studies argue that overthickened crust produced by Mesozoic contraction within the Cordilleran hinterland became gravitationally unstable due to a reduction in mid- to lower crustal viscosity and a reduction in the convergence rate owing to the onset of regional transtension in the Eocene (Fig 1.4A; Price and Monger, 1986; Tempelman-Kluit and Parkinson, 1986; Parrish et al., 1988). The crust is therefore interpreted to have spread laterally during the Eocene via deep-seated crustal extension aided by the formation of extensional crustal shear zones, including the OVsz and oppositely directed Columbia River fault (Fig. 1.4A,B; Tempelman-Kluit and Parkinson, 1986, Parrish et al., 1988; Vanderhaeghe and Teyssier, 2001).

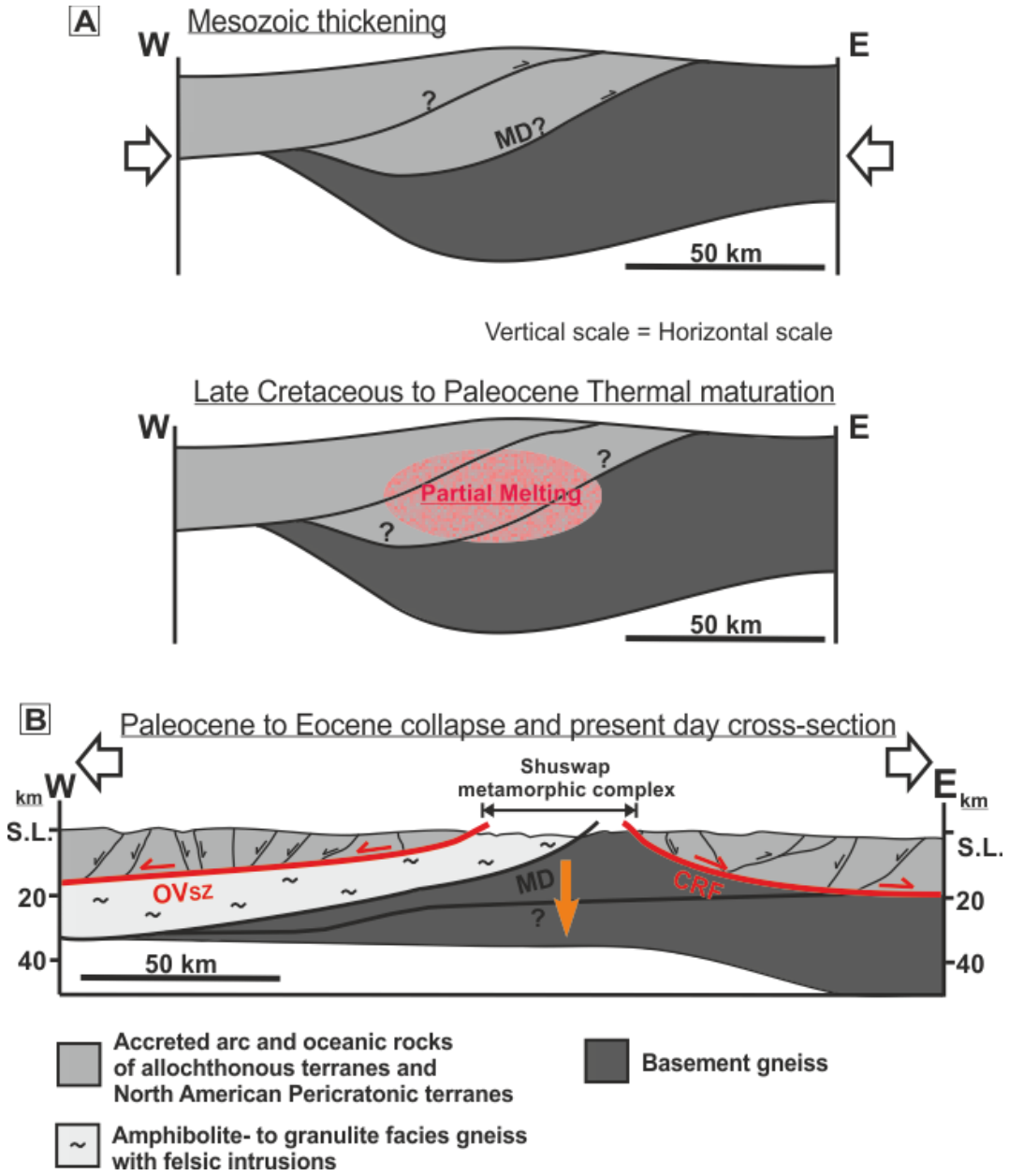

Figure 1.4. Conceptualized model showing gravitational collapse as a mode of exhumation of the Shuswap metamorphic complex.

(A) Crustal thickening during W-E compression in the Mesozoic resulted in significant crustal thickening in the Cordilleran hinterland. (B) With time, partial melting ensues in the mid-crust and W-E compression eases during Late Cretaceous to Paleocene time. (C) Post-compressional gravitational collapse (peach arrow) of the overthickened crust is initiated during the Paleocene to Eocene with oppositely verging, extensional, low-angle detachments, including the Okanagan Valley shear zone, facilitating exhumation of the mid-lower crust.

In contrast, several studies have interpreted the OVsz to represent the high strain upper boundary of a channelized mid-crustal ductile flow zone (Fig.1.4; Johnston et al., 2000; Brown and Gibson, 2006; Glombick et al., 2006; Gervais and Brown, 2011). The channel flow model involves lateral flow of a relatively low viscosity, weak crustal layer between stronger bounding layers (Godin et al., 2006; Grujic, 2006). East of the OVsz, within the Shuswap metamorphic complex, orogen-normal Poiseuille flow (i.e. where flow in a layer is fastest in the middle and decreases towards the margins; see Godin et al., 2006) is interpreted to have operated in a ~10 km-thick channel that was decoupled contemporaneously from its lid, the hanging wall of the OVsz, and base, the footwall of the thrust-sense Monashee décollement (Fig. 1.4; Brown and Gibson, 2006). The OVsz has therefore been interpreted to represent the normal-sense top of a Cretaceous to early Paleogene mid-crustal channel, reactivated during Eocene extension (Fig. 1.4; Brown and Gibson, 2006; Gervais and Brown, 2011). The coeval development of sub-parallel opposite-sense structures at the top and bottom of the channel is required by the channel flow model (Grujic, 2006). Previous studies have documented 55–49 Ma east-propagating contractional structures in the lower levels of the Shuswap metamorphic and Monashee complexes (i.e., base of channel) and similarly-aged top-to-the-west extensional structures within the OVsz, the inferred upper boundary of the channel (Johnson and Brown, 1996; Brown and Gibson, 2006).

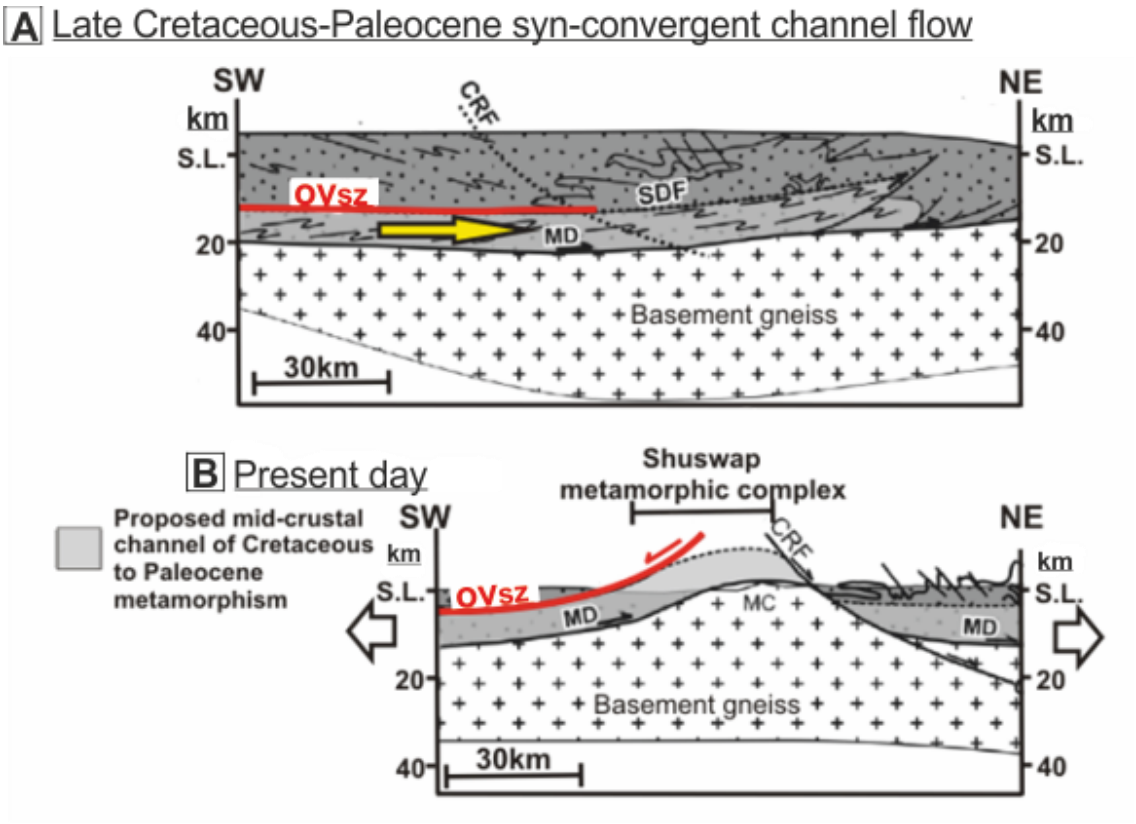

Figure 1.5. Generalized cross-sections of the southern Canadian Cordillera demonstrating potential mid-crustal flow

(A) A potential Late Cretaceous–Paleocene configuration of mid-crustal channel prior to extensional faulting and (B), the present-day geometry. The middle-crustal layer is interpreted to have been a zone of channel flow in the Late Cretaceous to early Paleogene with the OVsz (highlighted in red) and the Monashee décollement (MD) acting as the upper and lower boundaries, respectively. CRF, Columbia River fault; MC, Monashee complex; SDF, Selkirk detachment fault (Modified from Brown and Gibson 2006).

Regardless of whether or not channel flow was involved, most workers agree that the OVsz is a crustal-scale detachment facilitating tens of kilometres of displacement. Tempelman-Kluit and Parkinson (1986) estimated 60-90 km of horizontal extension based on correlation of Eocene volcanic outliers in the hanging wall with their inferred Eocene “plutonic root”, the Coryell syenite, in the footwall. Bardoux (1993) used palinspastically-restored cross sections to determine 45-70 km of displacement in the Kelowna area. Farther north, Johnson

and Brown (1996) estimated ~32 km of displacement also using palinspastic restoration. Brown et al. (2012) estimated 64-89 km of displacement based on geometric and thermobarometric arguments.

Conversely, the hypothesis that the OVsz is a major crustal-scale detachment has been challenged by studies in the Vernon area (Fig. 1.1; Thompson and Unterschutz 2004; Glombick et al., 2006a). Middle Eocene volcanic and sedimentary hanging wall rocks have been mapped across the trace of the OVsz and are interpreted to sit unconformably on the high-grade metamorphic footwall rocks of the Shuswap metamorphic complex in a series of semi-continuous Eocene outliers (Glombick et al., 2006a). The continuity of hanging wall stratigraphy across the trace of the shear zone is interpreted to suggest that the Shuswap metamorphic complex was not exhumed by crustal-scale detachments (Glombick et al., 2006a). An alternative channel flow model is proposed by Glombick et al. whereby partial melting of the middle crust in the Late Cretaceous to early Paleogene resulted in the development of a channel of ductile flow that was underthrust by a crustal-scale ramp and exhumed from depths of 20–30 km by vertical thinning. Consequently, a substantial attenuation of metamorphic isograds across low-angle detachments such as the OVsz resulted. However, this model does not factor in the open, upright, km-scale corrugations found along the trace of the OVsz (Fig. 1.1; Brown, 2010). These structures plunge at about 15° to the west-northwest parallel to the previously inferred stretching direction and are interpreted to have formed syn-extension rather than during a later folding event (Christie, 1973; Ross, 1981; Bardoux, 1993; Brown, 2010). These corrugations are common in extensional shear zones (Whitney et al., 2013) and are strongly correlated with occurrences of metamorphic core complexes, suggesting a genetic link between the two (Singleton, 2012). The corrugations model can explain the semi-continuous nature of hanging wall units across the shear zone, in that they are preserved as 'islands' on top of the footwall domain within synformal keels of the corrugations.

Many questions remain regarding the deformational processes associated with the development of the OVsz and its overall role in the exhumation of the Shuswap metamorphic complex. In particular, no work has been done that documents the deformation mechanisms and the style of flow that characterize different structural levels of the OVsz and its three-dimensional strain geometry, which is the focus of this study.

1.4. Research Objectives

This study aims to elucidate the thermo-kinematic evolution of the OVsz in the vicinity of Okanagan Mountain Provincial Park in southeastern British Columbia where the complete thickness of the shear zone is exposed. This research focuses on the following questions:

1. What is the strain state and temperature of deformation of the OVsz in the study area?

2. Are there variations in deformation temperature, shear strain deformation mechanisms down structural succession of the shear zone?

3. Can the data contribute to our understanding of the deformation processes involved with the exhumation of rocks from mid- to lower crustal depths along low angle extensional shear zones such as the OVsz?

These questions are addressed through detailed 1:10 000 scale mapping of lithology and structures across the OVsz in the vicinity of the Okanagan Mountain Provincial Park (Fig.1.3). Field mapping was carried out over a period of two months during the summer of 2012. A representative suite of quartz-rich oriented samples was collected throughout the field area across the entire structural section of the OVsz. The geological map and structural measurements serve as the framework to establish the 3-dimensional macro- to microstructural

characterization of the shear zone. Deformation temperatures, strain geometry, and the style of strain across the OVsz within study area are constrained using quartz microstructures and petrofabrics acquired across the entire thickness of the shear zone. Thin sections orientated perpendicular to the foliation and parallel to the lineation were examined to investigate mineral assemblages, deformational fabrics, shear sense indicators and quartz and applicable feldspar recrystallization mechanisms. Quartz crystallographic preferred orientations (CPO) in several thin sections were analysed using a combination of the Fabric Analyser (FA) technique (e.g. Wilson et al., 2003; 2007) and Electron backscatter diffraction analyses (EBSD) (e.g. Prior et al., 1999; 2009) using a scanning electron microscope at Colgate University, New York.

Results, interpretations, conclusions and outstanding issues related to this study are presented in Chapter 2 and Appendices A through E. Chapter 2 describes the geology and kinematics of the OVsz in the study area and is written with the intent to be submitted as a stand-alone manuscript to the *Journal of Structural Geology*. This chapter also integrates the results and conclusions from this thesis with previous studies to formulate a regional tectonic model for the OVsz. Chapter 3 presents a brief summary of the conclusions derived from this study.

Chapter 2.

Quartz microstructures and petrofabrics of the Okanagan Valley shear zone: Insights into its progressive exhumation from the middle crust

2.1. Abstract

Quartz recrystallization mechanisms and quartz crystallographic preferred orientations (CPOs) are used to examine the thermo-kinematic evolution of a mylonite zone associated with the extensional Okanagan Valley shear zone (OVsz) in the southern Canadian Cordillera. The north-south striking, <30° west-dipping OVsz forms the southwestern margin of the Shuswap metamorphic complex, which consists of variably mylonitized orthogneiss and paragneiss, and transposed leucocratic intrusions over an approximate 1-1.5 km thick structural section. The ductile fabric is partially overprinted by brittle fractures towards the structural top of the shear zone as the footwall was progressively exhumed during Eocene extension. A top-to-the-WNW sense of shear is interpreted from both meso- and micro-shear-sense indicators. Quartz a-axis patterns suggest plane strain deformation with slight constriction in the upper 150 m of the structural section. Quartz microstructures and quartz c-axis fabric data suggest deformation temperatures progressively and rapidly increase downward from ~280°C to >650 °C over the 1-1.5 km of structural section. A simplified geometric particle path model demonstrates how penetrative non-coaxial flow along detachment-parallel flow planes in predominantly plane strain deformation could

result in this significant telescoping of originally horizontal isotherms during progressive exhumation. This model involves a scenario where deformation fabrics in structurally lower rocks with originally higher deformation temperatures were 'locked-in' as they migrated out of the active zone of deformation during exhumation of the footwall to upper crustal levels. These locked-in higher temperature fabrics were passively exhumed along an ESE trajectory that resulted in their progressive juxtaposition beneath lower temperature fabrics that were being generated in the narrowing active part of the WNW-directed shear zone in higher crustal levels.

2.2. Introduction

Microstructures and petrofabric textures in plastically deformed quartz can be utilized to interpret deformation temperatures, strain rate, non-coaxiality of flow and distortional strain geometry in exhumed shear zones (Lister, 1978; Law, 1990; Stipp et al, 2002a,b; Law et al., 2004; Toy et al., 2008; Barth et al., 2010; Sullivan and Beane, 2010; Law et al., 2010). The quartzo-feldspathic mylonites in the immediate footwall of the Okanagan Valley shear zone (OVsz; Brown et al. 2012) provide an opportunity to constrain deformation parameters by combining analysis of dynamic recrystallization mechanisms and crystallographic preferred orientations (CPOs) of quartz. The OVsz is a north-south striking, 1-2 km-thick, shallow west-dipping, ductile to brittle shear zone interpreted to have played a significant role in the Eocene exhumation of the southern Shuswap metamorphic complex in the southeastern Canadian Cordillera (Parkinson, 1985; Tempelman-Kluit and Parkinson, 1986; Parrish et al., 1988; Bardoux, 1993; Johnson and Brown, 1996; Brown et al., 2012).

Previous studies of the OVsz have focused on mapping of rock units and structures, and constraining the pressure temperature-time (P-T-t) path of the shear zone utilizing U-Pb age analysis and conventional $^{40}Ar/^{39}Ar$

geothermobarometry (Tempelman-Kluit and Parkinson, 1986; Parrish et al., 1988; Bardoux, 1993; Johnson and Brown, 1996; Glombick et al. 2006a; Brown et al., 2012). However, a rigorous quantitative three-dimensional strain analysis has yet to be carried out on the OVsz. Such a study can provide constraints on the rheological evolution and finite strain development of the shear zone. Acquisition of such data may also help determine possible deformation processes that operated during the evolution and exhumation of the OVsz from mid-crust. In turn, these insights can be applied to other similar crustal-scale shear zones.

In this study, quartz recrystallization mechanisms and CPO patterns are analysed in terms of dislocations at the atomic-scale, with the latter based on the activation of different intracrystalline slip systems (Passchier and Trouw, 2005). These features are sensitive to variations in temperature, imposed strain path or kinematic framework, and magnitude and symmetry of finite strain (Schmid and Casey 1986; Law, 1990; Passchier and Trouw, 2005). Consequently, these methods are commonly utilized in characterizing the thermo-kinematic evolution of exhumed shear zones (e.g. Xypolias and Koukouvelas, 2001; Law et al., 2004; 2010; 2011; 2013; Sullivan and Law, 2007; Toy et al., 2008; Barth et al., 2010). For example, an observed quartz recrystallization and CPO temperature increase down the structural succession of the OVsz may be indicative of a simple, evolving extensional shear zone model proposed in several metamorphic core complexes in the North American Cordillera (Reynolds 1982, Lister & Davis 1983, Lister et al., 1984a.b, Wernicke 1985). In such a model, mylonites that formed at relatively deeper crustal levels move structurally upward during tectonic denudation and are overprinted by lower temperature fabrics and recrystallization mechanisms. Alternatively, Toy et al. (2008) argue that preservation of relatively-high temperature CPO fabrics towards the structural top of a shear zone may imply intense localization of shear strain at deeper crustal depths. If this were the case, intense strain localization could result in

preservation of higher temperature fabrics despite being exhumed through cooler parts of the crust as few grains would be suitably orientated for lower temperature fabrics to develop. Farther from this localized zone, where shear strain was less intense, fabrics would be more likely to be modified at shallower crustal levels during exhumation.

In this paper, new data are presented that constrain the deformation temperatures and strain within the OVsz. The data were collected in and around the vicinity of the Okanagan Mountain Provincial Park in southern British Columbia, where a complete three-dimensional exposure of the OVsz facilitates detailed structural and lithological mapping of the shear zone. Deformation temperatures are inferred from quartz microstructures and quartz c-axis fabrics derived from electron backscatter diffraction (EBSD) and fabric analysis (FA). Strain geometry is interpreted from quartz a-axis fabrics provided by EBSD analysis. The data were used to investigate the deformation conditions and type of flow during exhumation of the OVsz using a simplified geometric particle path model. These new data provide an opportunity to investigate the flow process that occurred during the development and exhumation of the OVsz.

2.3. Geological setting

The Shuswap metamorphic complex is the largest core complex in the North American Cordillera, representing a large part of the exhumed metamorphic core of the southern Canadian Cordillera (Coney, 1980; Coney and Harms, 1984; Okulitch, 1984, Parrish et al., 1988, Vanderhaeghe et al., 2003; Gibson et al., 2008). The Shuswap metamorphic complex consists of a series of domal culminations that expose penetratively-deformed amphibolites- to granulite-facies gneisses and granitic intrusions within southern British Columbia and northeastern Washington (Fig. 2.1, Ewing, 1980; Armstrong, 1982; Okulitch, 1984; Brown and Carr, 1990; Brown et al., 2012). The metamorphic peak of the

Shuswap metamorphic complex corresponds to a period of crustal thickening in excess of 55 km in the southern Canadian Cordillera during the Mesozoic and earliest Paleogene (Price and Mountjoy, 1970; Brown et al., 1986; Parrish et al., 1988; Brown and Gibson, 2006; Gibson et al., 2008). This crustal thickening was in part due to the accretion and obduction of arc and oceanic terranes along the ancestral western margin of North America coincident with the westward migration of the continent (Monger et al., 1982; Monger and Price, 2002). Deeply buried parts of the Shuswap metamorphic complex were exhumed to upper crustal levels during the Eocene (Tempelman-Kluit and Parkinson, 1986; Parrish et al., 1988; Parrish 1995) in response to a change from transpression to transtension between the North American and Pacific plates during the Paleogene (Ewing, 1980; Price and Carmichael, 1986; Monger and Price, 2002).

Eocene crustal extension accommodated by structures such as the OVsz juxtaposed the high grade rocks of the Shuswap metamorphic complex to the east with lower metamorphic grade arc-related terranes to the west (Ewing, 1980; Tempelman-Kluit and Parkinson, 1986; Parrish et al., 1988; Bardoux, 1993; Johnson and Brown, 1996; Johnson 2006; Brown et al., 2012). The OVsz is part of a ~300 km north-south striking, brittle-ductile crustal detachment (Fig. 2.1), and is characterized by moderately to intensely mylonitized orthogneiss and paragneiss intruded by felsic sheets that are moderately to intensely mylonitized within the footwall domain of the OVsz. The shear zone displays prominent west-northwest trending elongation lineations with shear-sense indicators consistently indicative of relative westward displacement of the hanging wall (Bardoux, 1985, 1993; Parkinson, 1985; Journeay and Brown, 1986; Tempelman-Kluit and Parkinson, 1986; Brown et al., 2012; this study). U-Pb zircon crystallization ages confirm that the mylonitic gneiss within the OVsz developed during Eocene metamorphism and deformation that accompanied motion along the shear zone (Parrish et al., 1988; Johnson and Brown, 1996; Brown et al., 2012). The orthogneiss is interpreted to have been derived from multiple intrusions, including

Late Jurassic to Eocene granodiorite plutons (Tempelman-Kluit and Parkinson, 1986), whereas the paragneiss units are interpreted to represent Paleozoic to Early Jurassic sedimentary protoliths (Brown et al., 2012). The sinuous surface trace of the shear zone reflects its shallow and corrugated geometry along strike. The OVsz is further characterized by open, west-northwest trending, upright, multi-scale folds. The trend of the hinge of these folds parallels the interpreted finite Eocene extension direction (Fig. 2.1; Ross, 1981; Brown, 2010). At intervals of 50-100 km, hanging wall rocks appear as semi-continuous outliers intersecting the N-S trace of the OVsz where they occur in the structural lows of synformal keels, whereas gneissic rocks of the footwall domain are exposed in the adjacent antiformal highs (Fig. 2.1).

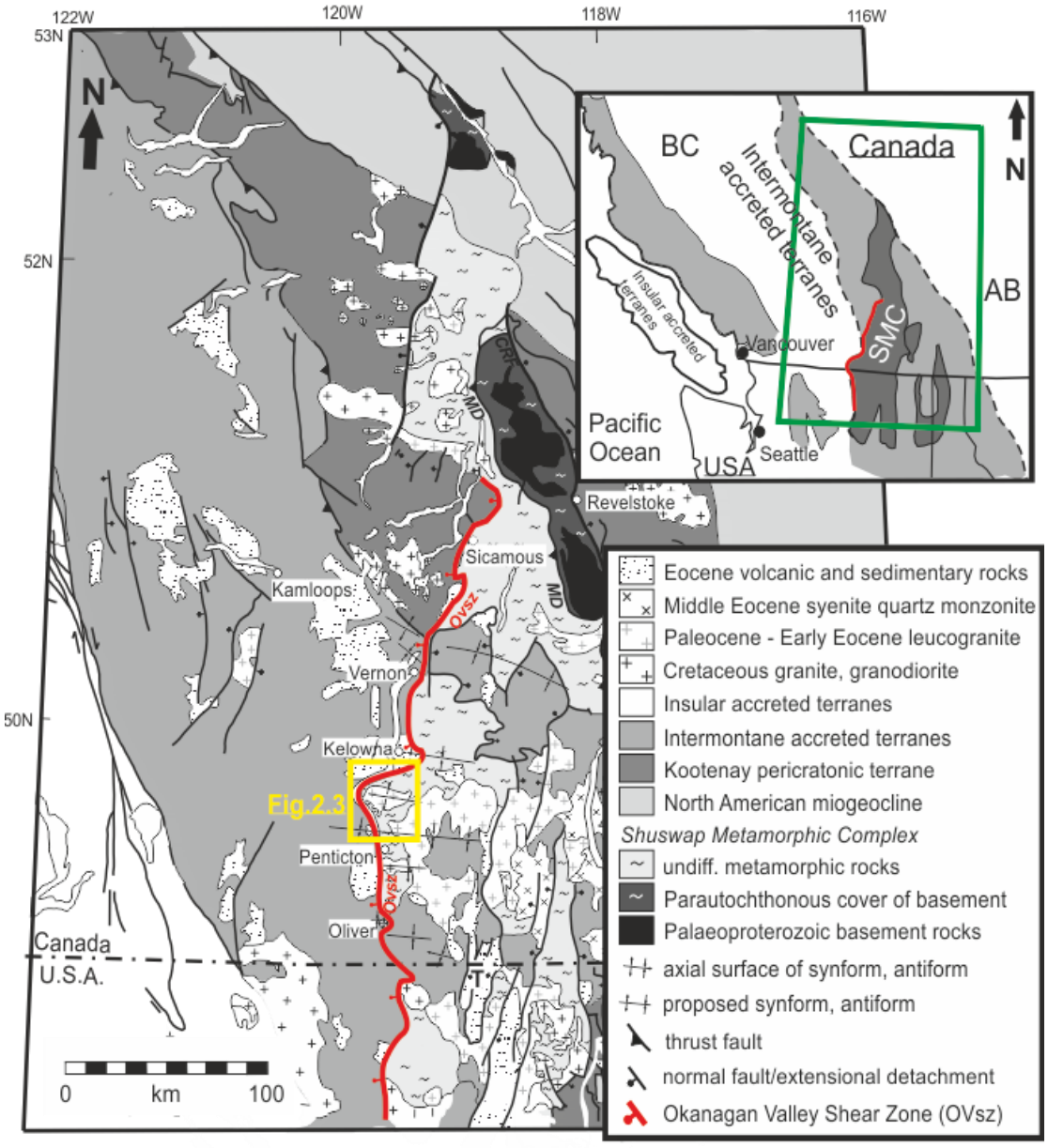

Figure 2.1. Generalized geological map of the southern Canadian Cordillera

Inset figure: Simplified map of the southern Canadian and northwestern US Cordillera, highlighting the accreted terranes and high-grade metamorphic and plutonic belts and the outline of the Shuswap metamorphic complex (Modified from Brown et al., 2012). Yellow inset shows the location of the study area, which is shown in Fig. 2.3. Okanagan Valley shear zone (OVsz); MD, Monashee décollement; CRF, Columbia River fault (Modified from Johnson, 2006).

Additional evidence supporting the interpretation that the OVsz is a crustal-scale detachment that help facilitate the exhumation of the Shuswap metamorphic complex from mid-crustal depths includes the break in metamorphic grade across the shear zone (Brown et al., 2012). Zeolite- to greenschist-facies rocks of the hanging wall are juxtaposed against mylonitic amphibolite- to granulite-facies footwall rocks of the Shuswap metamorphic complex (Fig. 2.1; Brown and Journey, 1987; Parrish et al., 1988; Brown et al., 2012). The immediate hanging wall is affected by localised brecciation, chloritization and silicification (Bardoux, 1993), and is dissected by high-angle normal faults. Eocene syn-extensional half graben basins formed in response to movement on these faults and were subsequently filled with local detritus including Eocene volcanogenic sedimentary rocks, as well as gneissic clasts from the exhuming footwall (McClaughry and Gaylord, 2005). The extension and filling of the hanging wall basins was approximately coeval with anatectic melting and amphibolite-facies metamorphism recorded in the footwall domain, which implies rapid exhumation of mid-crustal rocks to the near-surface. This exhumation was achieved through lithospheric stretching focused along extensional detachments such as the OVsz (Tempelman-Kluit and Parkinson, 1986; Parrish et al., 1988; Bardoux, 1993; McClaughry and Gaylord, 2005). This evidence is in line with other studies that show the footwall of the OVsz was rapidly exhumed from at least 20 km depth to shallow levels in the crust (<3 km) during the Eocene (ca.56–48 Ma). This understanding is based on overlapping K-Ar and $^{40}Ar/^{39}Ar$ cooling ages for hornblende, biotite and muscovite and modal fission-track ages of apatite and sphene with U-Pb zircon and monazite ages from the high grade gneisses and anatectically-derived granitoid rocks (Baadsgaard et al., 1961; Ross, 1974; Medford, 1975; Wanless et al., 1978; Mathews, 1981; Stevens et al., 1982; Archibald et al., 1984; Parrish et al., 1988; Armstrong et al., 1991; Bardoux, 1993; Johnson and Brown, 1996; Kruckenberg

et al., 2008; Toraman et al., 2011; Brown et al., 2012). Exhumation and cooling are interpreted to be contemporaneous with axatexis and emplacement of syntectonic intrusions since cooling from zircon and monazite crystallization to argon closure temperatures occurred within a few million years (Hansen and Goodge, 1988; Kruckenberg et al., 2008; Kruckenberg and Whitney, 2011; Brown et al., 2012).

In contrast, K-Ar and $^{40}Ar/^{39}Ar$ analyses indicate that large portions of the hanging wall remained below 280 °C ($\leq$ 9km) since the late Mesozoic, as many plutonic rocks yield Jurassic to Early Cretaceous cooling ages (White et al., 1968; Roddick et al., 1972; Medford, 1975; Fox et al., 1976; Parrish et al., 1988). The sharp contrast in the isotopic cooling ages across the OVsz further suggests that the OVsz accommodated regional crustal-scale extension during the Eocene (Bardoux, 1993).

Rapid exhumation of the OVsz is also indicated by the pressure-temperature data from upper amphibolites-facies garnetiferous schist that were at, or above, the wet granite solidus within the OVsz (Bardoux, 1993; Laberge and Pattison, 2007; Brown et al., 2012). Garnet porphyroblasts show little evidence of retrograde re-equilibration related to exhumation (Bardoux, 1993; Brown et al., 2012). Similar geochronological, thermochronological and themobarometric data have been documented in footwall rocks farther to the east, which also argue for rapid Eocene exhumation of the Shuswap metamorphic complex (e.g. Vanderhaeghe et al., 1999; Teyssier et al., 2005; Rey et al., 2009).

Estimates of displacement along the OVsz vary considerably along strike, from <2 km to >90 km, (Parkinson, 1985; Tempelman-Kluit and Parkinson, 1986; Parrish et al., 1988; Bardoux, 1993; Bardoux, and Mareschal, 1994; Glombick et al., 2006; Johnson and Brown, 1996; Brown et al., 2012). The variations in the estimated amount of displacement have led to differences in the interpreted role

played by the OVsz in the exhumation of the Shuswap metamorphic complex. Several models of have been proposed that involve post-convergence, extensional gravitational collapse of an overthickened crust (e.g. Fig. 2.2A; Tempelman-Kluit and Parkinson, 1986; Brown and Journeay, 1987; Parrish et al., 1988; Vanderhaeghe and Teyssier, 2001; Price and Monger, 2003; Rey et al., 2009). In these models, the OVsz facilitated Eocene lateral spreading of the gravitationally unstable, overthickened orogen with lowered viscosity in the mid- to lower crust due to partial melting. This collapse coincided with a change in plate kinematics and a reduction in convergence rate along the western plate margin (Ewing, 1980; Price and Carmichael, 1986; Monger and Price, 2002). Alternatively, the OVsz has been interpreted to represent the shallow west-dipping, normal-sense top of a syn-convergent, ductile mid-crustal channel during Cretaceous to Paleocene, subsequently reactivated during Eocene extension (Fig. 2.2B; Brown and Gibson, 2006; Glombick et al., 2006; Gervais and Brown, 2011). In this model, the OVsz may have played a significant role in localizing orogen-normal Poiseuille flow in the channel (i.e. where flow in a layer is fastest in the middle and decreases towards the margins; see Godin et al., 2006) within the Shuswap metamorphic complex (Fig. 2.2B; Brown and Gibson, 2006; Gervais and Brown, 2011). Although Brown and Gibson (2006) and Gervais and Brown (2011) do not dispute that the OVsz played a major role in the Eocene collapse of the orogen by the OVsz, Glombick et al. (2006) argued otherwise. They contended that the channel was underthrust by a crustal-scale ramp and exhumed from depths of 20–30 km by vertical ductile thinning, requiring <2km of actual displacement along the OVsz.

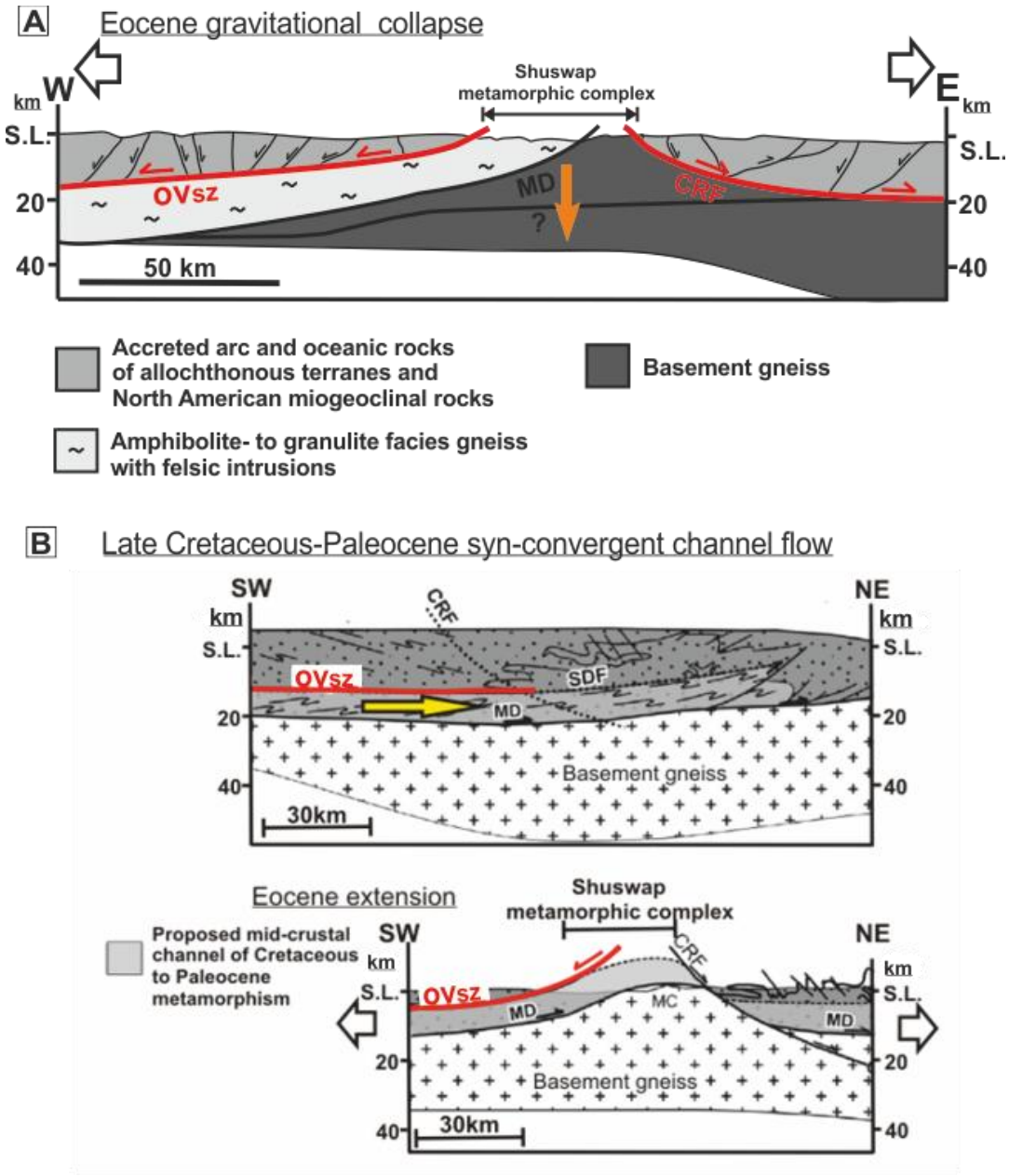

Figure 2.2. Cross-sections of the southern Canadian Cordillera showing potential exhumation modes of the Shuswap metamorphic complex.

(A) Post compressional gravitational collapse, highlighted with the orange arrow, was facilitated by oppositely directed, extensional, low-angle detachments (highlighted in red) including the Okanagan Valley shear zone (Modified from Vanderhaeghe and Teyssier, 2001). (B) Mid-crustal ductile channel formed from the Late Cretaceous-Paleocene flowing towards the NE (yellow arrow). The Okanagan Valley shear zone (highlighted in red) and the Monashee décollement (MD) acting as the upper and lower boundaries, respectively (Modified from Brown and Gibson 2006). Abbreviations: CRF, Columbia River fault; MC, Monashee complex.

2.4. Geology of the Okanagan Valley shear zone in the vicinity of the Okanagan Mountain Provincial Park

The OVsz exposed in the Okanagan Mountain Provincial Park is a gently to moderately west-dipping brittle-ductile shear zone that transitions downward from cataclastic ultramylonitic to mylonitic gneiss and felsic intrusive rocks to mylonitic amphibolite-facies gneiss and felsic intrusive rocks, to a weakly- to non-deformed syntectonic granitoid pluton at the base (Figs. 2.2; 2.3; 2.4). Within the study area, the OVsz is warped by a west-northwest trending, kilometre-scale, open, antiform that is defined by the variation in attitude of the foliation that dips gently (~03° to 25°) across the field area (Fig. 2.3). The antiform is interpreted to be one of the corrugations that characterize the overall OVsz geometry (Brown, 2010). Shear-sense indicators such as S-C fabrics, asymmetric porphyroclast and pressure shadows consistently indicate top-down-to-the-WNW sense of shear. Aligned quartz, feldspar and elongated hornblende define a penetrative elongation lineation trending 279° (Fig. 2.3). The mean trend of the penetrative elongation lineation, which is primarily defined by the alignment of quartz, feldspar and elongated hornblende, is 279 ° (Fig. 2.3). The hinge line of the antiformal corrugation is broadly parallel to the mean mineral elongation direction (Fig. 2.3). A series of steeply dipping, north striking, top-down-to-the-WNW brittle faults cut the OVsz (Figs. 2.3; 2.4A). Although these structures appear to locally offset the mylonitic foliation on a <5 metre scale, they do not significantly affect the overall inferred structural succession of the OVsz.

The top of the OVsz is bounded by a brittle detachment surface marking the break between the penetratively deformed high grade metamorphic rocks within the shear zone and the low grade metamorphic to unmetamorphosed volcanic and sedimentary rocks of the hanging wall to the west (Fig. 2.3). Previous studies described the detachment system as a ductile shear zone overprinted by a brittle detachment (i.e. Okanagan Valley crustal shear of Tempelman-Kluit and Parkinson, 1986; Okanagan Valley fault of Parrish et al.,

1988, and Johnson and Brown, 1996). This study uses the terminology of Brown et al. (2012), who referred to the detachment system as the Okanagan Valley shear zone, in order to account for the distributed nature of the shear zone that includes both the brittle and ductile components.

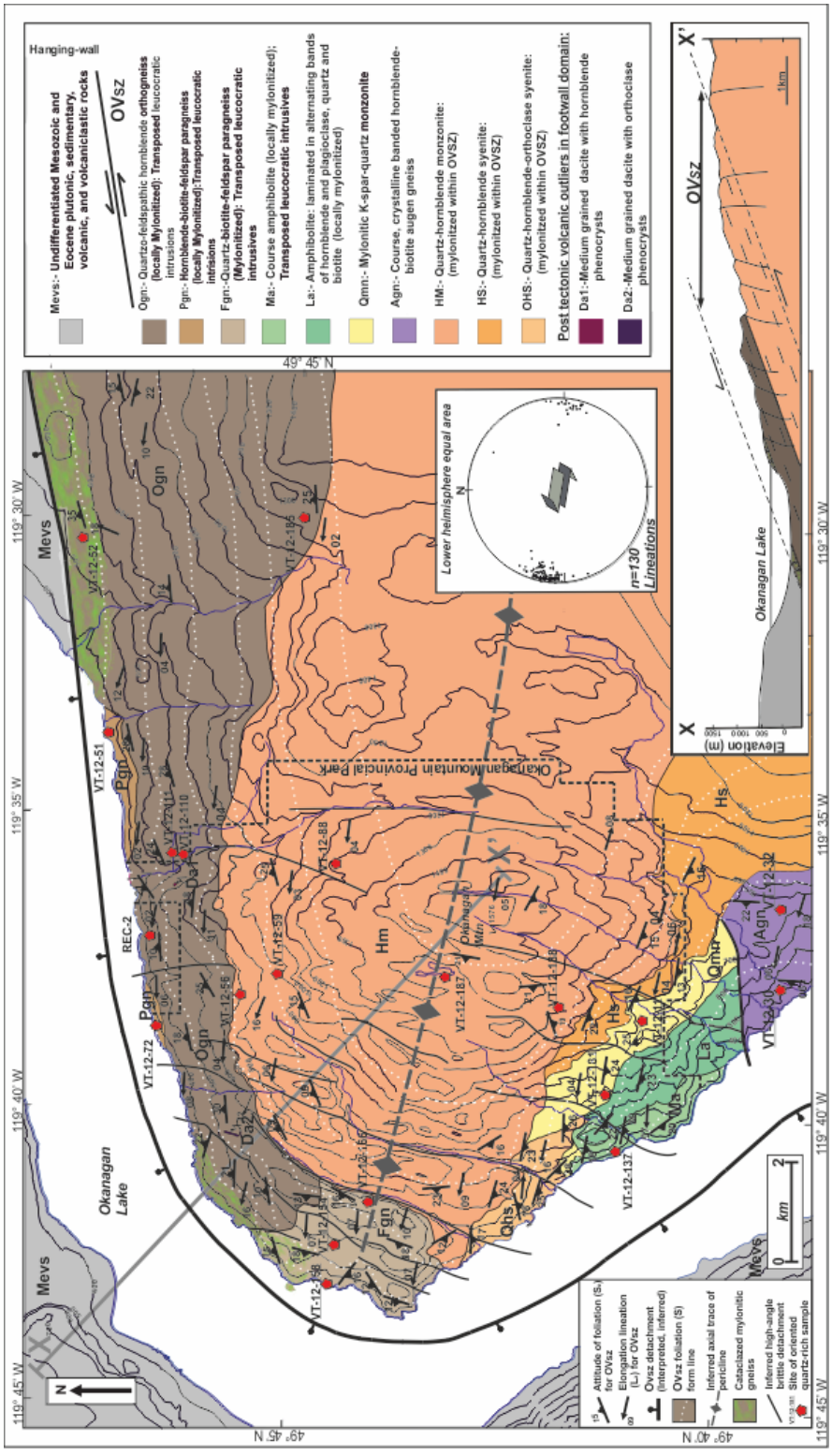

Figure 2.3. Geologic map of the Okanagan Valley shear zone in the vicinity of the Okanagan Mountain Provincial Park.

Foliation form lines (S) highlight the antiformal corrugation that defines the shear zone in the study area. Simplified geologic cross-section X-X' showing the shallow-dipping OVsz. Inset of lower hemisphere equal area show projection of elongation lineations with a mean trend of ~279°. Sample locations in this study are also highlighted.

The northern limb of the antiform is defined by a sequence of mixed mafic and felsic orthogneiss with thin bands of paragneissic units (Figs. 2.3; 2.4). Centimetre-scale hornblende-rich and hornblende-poor- layers characterize the mafic orthogneiss. Orthoclase-quartz-hornblende±biotite with orthoclase porphyroclasts delineate the more felsic orthogneiss (Fig. 2.4C.E). The paragneissic units comprise transposed layers of finely banded quartz-K-feldspar-biotite±hornblende (Fig.2.4C). Numerous boudinaged centimetre-scale ultramafic and amphibolite veins intrude the paragneiss.

The southern limb of the antiformal pericline consists of a penetratively to weakly mylonitized amphibolitic gneiss containing an abundance of small, rootless isoclinal folds (Fig.2.5A), structurally underlain by laminated amphibolite gneiss (Fig. 2.5B) and mylonitic felsic orthogneiss (Fig. 2.5C). The southern limb of the pericline terminates at a north-south striking, banded quartz-feldspar-orthoclase-hornblende±biotite-chlorite gneiss containing distinctive augen orthoclase clasts (Fig. 2.3; 2.5F). All units across the study area contain transposed syntectonic leucosome and pegmatitic sheets (e.g. Fig 2.4).

The core of the antiformal pericline is dominated by a quartz-hornblende monzonite to quartz-hornblende syenite based on the modal percentages of the constituent mineral (Figs. 2.3; 2.4I; 2.5D), contrary to the granodiorite interpretation of Medford (1975) and Tempelman-Kluit (1989). The quartz-hornblende monzonite unit dominates the northern exposures of the pluton with the syenite unit restricted to the south. $^{40}Ar/^{39}Ar$ cooling ages from hornblende and micas suggest these units were at a temperature above 500 °C at ~51 Ma, cooling rapidly to <280 °C at ~48 Ma (Medford 1975; Mathews 1981; Parkinson 1985). The monzonite and syenite units are dominated by feldspar megacrysts

that parallel a penetrative mineral lineation (e.g. Fig. 2.4D). The base of the shear zone is broadly defined by non-foliated monzonite and syenite units transitioning structurally upward from the base into progressively more foliated units, and eventually into mylonitized felsic orthogneiss interlayered with mafic orthogneiss and paragneiss (Figs 2.4; 2.5). Within this mixed region, boudins of the plutonic units are intercalated, transposed, and interfolded with enclaves of mafic orthogneiss, becoming progressively concordant with the mylonitized gneissic layering towards the structural top of the OVsz (Figs 2.4; 2.5). This mixed region is interpreted as an irregular intrusive contact possibly affected by syntectonic deformation.

Two post-kinematic dacitic outliers are mapped in northern limb of the pericline where dikes that feed into the outliers cut through the mylonitic gneiss (Fig. 2.3) (see Appendix E). These outliers are tentatively correlated with the Marama Formation based on previous mapping of similar felsic volcanics within and west of the OVsz where cooling ages from volcanic rocks of these formations range from 48.4 Ma (whole rock) to 53.1 Ma (K/Ar-biotite) (Church 1973; 1985; Bardoux, 1993). The cooling ages of these regional volcanic outliers are coeval with the ages of tectonized leucosome, dikes and plutons interpreted to have been generated and deformed at mid-crustal depths (Bardoux, 1993; Brown et al., 2011). These relationships suggest that ductile deformation lower in the structural succession may have still been on-going while the mid-lower section of the OVsz was at or near the surface.

2.4.1. Structural and kinematic framework of the Okanagan Valley shear zone in the vicinity of the Okanagan Mountain Provincial Park

The approximate 1-1.5 km structural thickness of the OVsz observed in the Okanagan Mountain Provincial Park is broadly divided into three lithostructural domains (Figs. 2.3, 2.4) that transition structurally downward from:

(i) Domain 1: cataclasite grading downwards into ultramylonite that is locally overprinted by brittle features;

(ii) Domain 2: moderately mylonitized greenschist to amphibolites-facies ortho- and paragneiss and transposed syntectonic felsic intrusions;

(iii) Domain 3: moderately to weakly foliated ortho- and paragneiss rocks interlayered with a weakly- to non-deformed plutonic rock at the base of the shear zone.

The gradation of brittle to ductile structural features down the structural column is in agreement with previous studies along strike of the OVsz (e.g. Parkinson, 1985; Tempelman-Kluit and Parkinson, 1986; Bardoux, 1993; Brown et al., 2012).

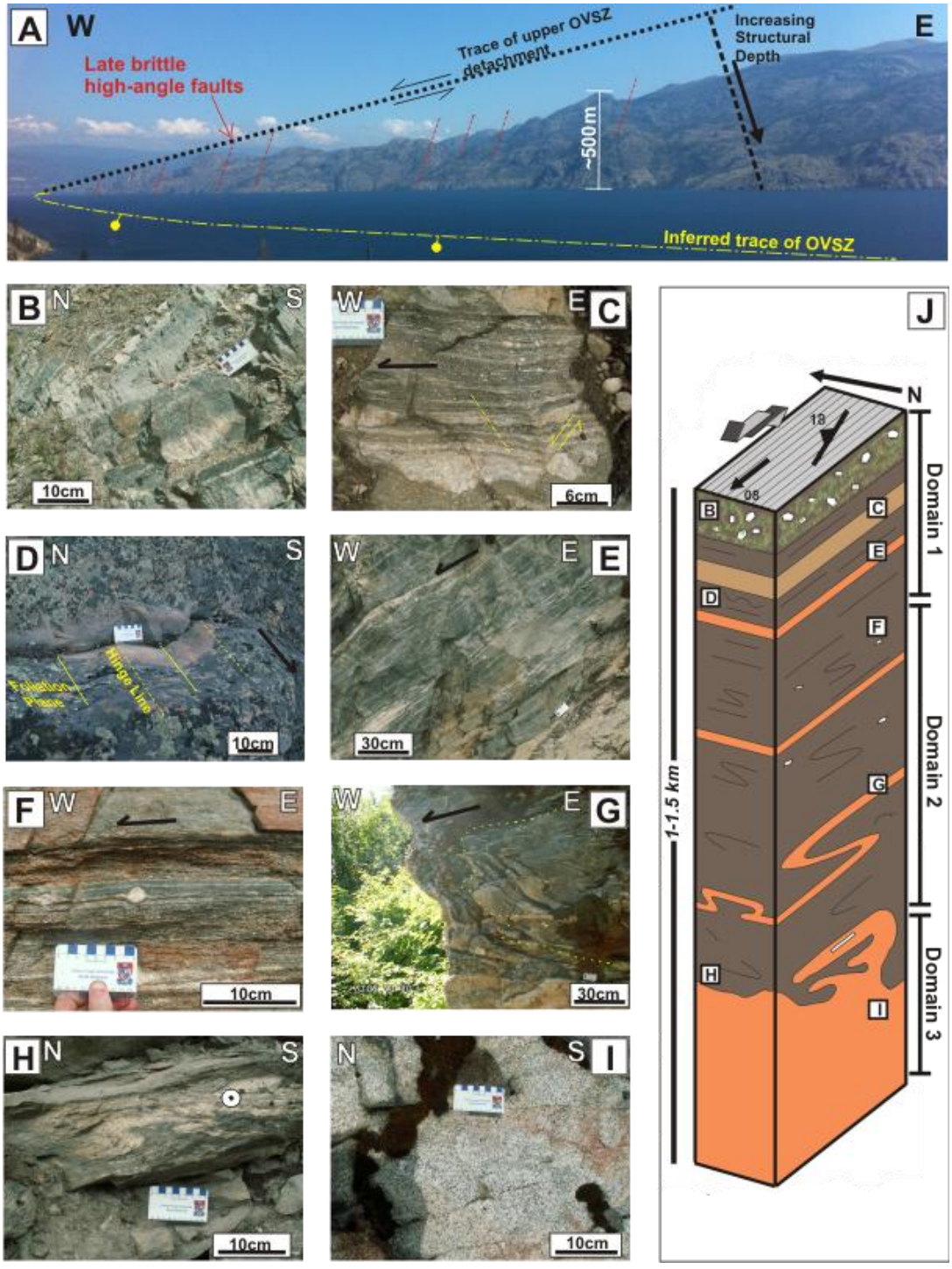

Figure 2.4. Outcrop photos down structural succession in the northern limb

(A) View of the Okanagan Mountain Provincial Park from the south showing the inferred trace of the upper boundary of the Okanagan Valley shear zone in the westernmost part of the study area. The dashed red lines represent inferred late, high-angle, brittle faults. (B) Example of cataclasite with mylonitized gneissic fragments at the top of the structural section. (C) Ultramylonitic paragneiss overprinted by conjugate brittle faults. (D) Open folds interpreted to be corrugations with centimetre- to metre-scale wavelengths that have hinge lines parallel to the penetrative elongation lineation. (E) Transposed leucocratic intrusive sills and melt wisps within hornblende-rich mylonitic orthogneiss at the base of Domain 1. (F) Domain 2 mylonite containing a delta feldspar porphyroclast recording top-to-the-WNW sense of shear (G) and (H) Recumbent sheath folds with axial surfaces parallel to the layering and foliation in Domain 2. (I) Quartz hornblende monzonite near the base of the shear zone with euhedral feldspar clasts free of internal deformation. (J) Schematic vertical section of the northern limb of the antiform showing approximate structural depths of Figs 2.3B-I (grey arrows indicate inferred shear sense).

The upper 50–100 m portion of Domain 1 is characterized by the superposition of fractures around brecciated and chloritized lenses of ductile fabrics near the top of the mylonitic front (Figs. 2.2; 2.4B). Cataclasite gradually transitions structurally downward into the less fractured, locally brecciated, chloritized and silicified ultramylonite (Fig. 2.3C). Domain 1 appears absent in the southern limb, apparently cropping out only in the northern antiformal limb.

The ultramylonite gradually loses the prevalent brittle overprint structurally downward, where it preferentially preserves solid-state deformation features characteristic of the lithostructural Domain 2 mylonite. In Domain 2, the mylonitic fabric in the gneissic and intrusive units is characterized by a centimetre to metre-scale, discontinuous, laterally transposed, compositionally layered foliation (e.g. Figs. 2.4E, F; 2.5B), and ubiquitous elongation lineation trending 279° (Fig. 2.2). The elongation lineation is defined by the alignment of hornblende, biotite and ribboned quartz. Pervasive Type I S-C fabrics (Lister and Snoke, 1984) are defined by the S-surfaces of the aligned long axes of hornblende. Quartz ribbons also indicate top-to-the-WNW sense of shear and commomly anastomose around rotated feldspar aggregates in the intrusive units. Sigma- and delta-type asymmetric pressure shadows of porphyroclasts also indicate top-to-the-WNW sense of shear (Fig. 2.4F). The leucocratic intrusions become progressively transposed parallel to the gneissic layering higher in the structural section (e.g.

2.4E & F). Lower in the structural section, near the middle of Domain 2 (~>500m), planar fabric elements, intrusions and foliations are ubiquitously re-folded, forming isoclinal, rootless and recumbent sheath folds with axial planes parallel to the penetrative foliation (e.g. Fig 2.4H & J).

Folds with centimetre- to metre-scale wavelengths and hinges that parallel the pervasive elongation lineation locally appear in the upper 500m of the OVsz where the mylonitic foliation is folded (Fig. 2.4C). These folds are likely to be minor folds related to the kilometre-scale corrugations along the strike of the shear zone and not related to the recumbent, isoclinal and transposed folds present in the gneiss. These open, upright folds appear to have not experienced the same degree of flattening as the isoclinals folds within the gneiss and are nearly concentric with straight hinge lines parallel to the extensional direction.

Domain 3, located ~650 m below the top of the shear zone, consists of moderately to weakly foliated ortho- and paragneiss interlayered with a variably foliated syntectonic leucocratic syenite to monzonite pluton (Fig.2.4G). The pluton becomes progressively less foliated to non-deformed down structural section towards the base of the shear zone. Elongate mafic enclaves within the leucocratic units are preferentially aligned in the direction of the mean elongation lineation direction (Fig. 2.4E). A banded orthoclase gneiss unit containing distinctive augen orthoclase clasts occurs immediately south of the southern limb of the pericline (Fig. 2.2; 2.4F). The foliation orientation indicates either that this gneiss is faulted in place with respect to the structural section of the antiform, or is beyond the inflection point of the southern limb of the antiform(Fig. 2.2). The asymmetry of the augen clasts within the gneiss often displays top-to-the-WNW shear sense. However, the unit is not mylonitized like the gneissic units within Domains 1 and 2, thus it is classified as Domain 3.

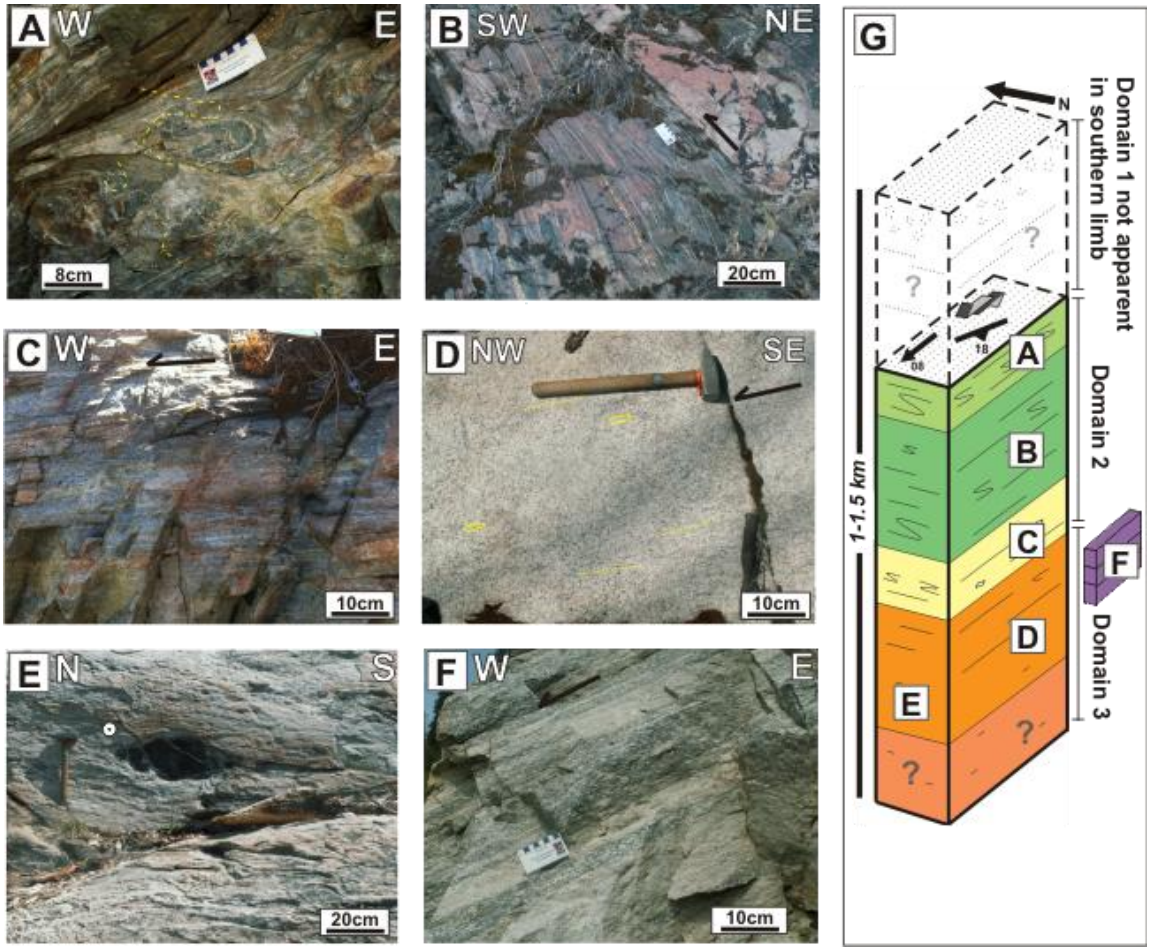

Figure 2.5. Outcrop appearance down structural succession in the southern limb

(A) Rootless folds of an amphibolite lens in the southern periclinal limb. (B) Banded hornblende- and plagioclase-rich amphibolite with top-to-the-WNW shear sense defined by asymmetric tails of feldspar porphyroclasts. (C) Mylonitic felsic orthogneiss. (D) Preferred alignment of long axis of euhedral orthoclase phenocrysts (yellow ellipses) near the base of the shear zone. (E) Preferred alignment of elongate mafic enclaves in the direction of the trend of the mean elongation lineation direction. (F) Banded orthoclase augen gneiss immediately south of the southern limb of the pericline. (G) Schematic vertical section of the southern periclinal limb showing approximate placement of A-E (grey arrows indicate inferred shear sense).

2.5. Methodology of microstructural analysis

Oriented samples of quartz-rich mylonitic gneiss and leucogranite were collected down the entire exposed structural column of the OVsz. The relative positions of the samples were projected into the structural succession of the OVsz by calculating their approximate structural depth below the inferred upper contact of the shear zone assuming the dip of the OVsz is constant throughout the section. Because the dip of the detachment ranges from 3˚ to 25°, the estimated structural depth in this study is interpreted within 50-100m error. The approximate locations of the structural sections are based on their relative position with respect to the hinge and limbs of the antiform that controls the map-scale geometry the OVsz in the study area.

Twenty representative samples with appropriate modal quartz mineral assemblages from either transposed leucocratic intrusions or gneissic country rock were chosen for microstructural analysis using a petrographic microscope to ascertain the dominant dynamic recrystallization mechanisms at each position within the OVsz. Ten samples were chosen from this group for CPO analysis, with eight of these selected down a vertical structural transect within the northern hinge of the antiformal pericline. This vertical transect was chosen to investigate CPO fabrics because it contained a homogenous rock type and the notable variation in mesoscopic-scale deformation structures down the structural section. The remaining two CPO samples were selected from both the middle of the southern limb and the gneissic unit south of the antiform. Representative samples were cut parallel to the X-Z plane of the finite strain ellipsoid, parallel to the elongation lineation and perpendicular to foliation. Consequently, all photomicrographs utilized for quartz microstructural and CPO analysis in this study are viewed approximately towards the north-northeast at right angles to the inferred transport direction.

2.5.1. Quartz recrystallization mechanisms

Dynamic recrystallization mechanisms of quartz and where applicable, feldspar (Pryer, 1993), were used as an estimate of temperature conditions during deformation (Hirth and Tullis, 1992; Stipp et al., 2002a, b). Stipp et al. (2002a, b) combined inferred deformation temperatures of naturally deformed rocks with experimental data of Hirth and Tullis (1992) to constrain the deformation conditions according to the recrystallization mechanisms of deformed quartz grains. These dynamic recrystallization mechanisms are typically the result of the formation and progressive rotation of subgrains and the migration of grain boundaries in response to a change in dislocation density (strain energy) within individual quartz grains (e.g., Guillop and Poirier 1979; Urai et al., 1986). The interaction of these two processes results in three different dynamic recrystallization mechanisms (Regimes) of quartz microstructures based on deformation temperature (Stipp et al., 2002a). Regime 1 is a localised, low temperature grain boundary migration known as bulging recrystallization (BLG), which dominates from approximately 280 to 400 °C. Regime 2 is characterized by concentration of dislocations along grain walls due to a reduction of elastic distortional strain energy resulting in subgrain rotation recrystallization (SGR), which occurs from approximately 400 °C to 500 °C. Regime 3 is a strain-induced grain boundary migration recrystallization (GBM) driven by differences in stored strain energy between adjacent grains occurring at temperatures >500 °C (Fig. 2.6C; Stipp et al., 2002a and references therein). Above 650°C, quartz displays chessboard extinction whereby two orthogonal sets of tilt walls define subgrain boundaries indicating relatively higher temperatures (Blumenfeld et al., 1986; Mainprice et al., 1986; Hirth and Tullis, 1992; Stipp et al., 2002a,b). Appendix A provides further information on the theory of quartz recrystallization mechanisms analysis.

2.5.2. Quartz crystallographic preferred orientations

Quartz CPO fabrics were used in conjunction with the identification of dynamic recrystallization mechanisms to assess shear sense, deformation temperatures, and strain symmetry (Fig. 2.6; Lister et al., 1978; Lister and Hobbs, 1980; Law, 1990; Sullivan and Beane, 2010). CPO fabrics are interpreted through a combination of c- and a-axis plots, where different regions of an equal area stereographic plot represent basal <a>, rhomb <a>, prism <a> or prism <c> slip of individually measured quartz crystals (Fig. 2.6; Lister et al. 1977; Schmid and Casey, 1986; Law, 1990). Quartz CPO patterns are assessed according to the definitions of Lister (1977), in which the plane normal to the lineation (Y-Z plane) is defined as the symmetry plane. Fabrics that do not mirror themselves across this plane are described as asymmetric. A summary of the orientation of principal strain axes, active slip systems, fabric geometries in different strain fields, and evolution of CPO patterns during non-coaxial strain at various temperatures is portrayed in Figure 2.6 (see Appendix A for a more extensive review on CPO fabric analysis).

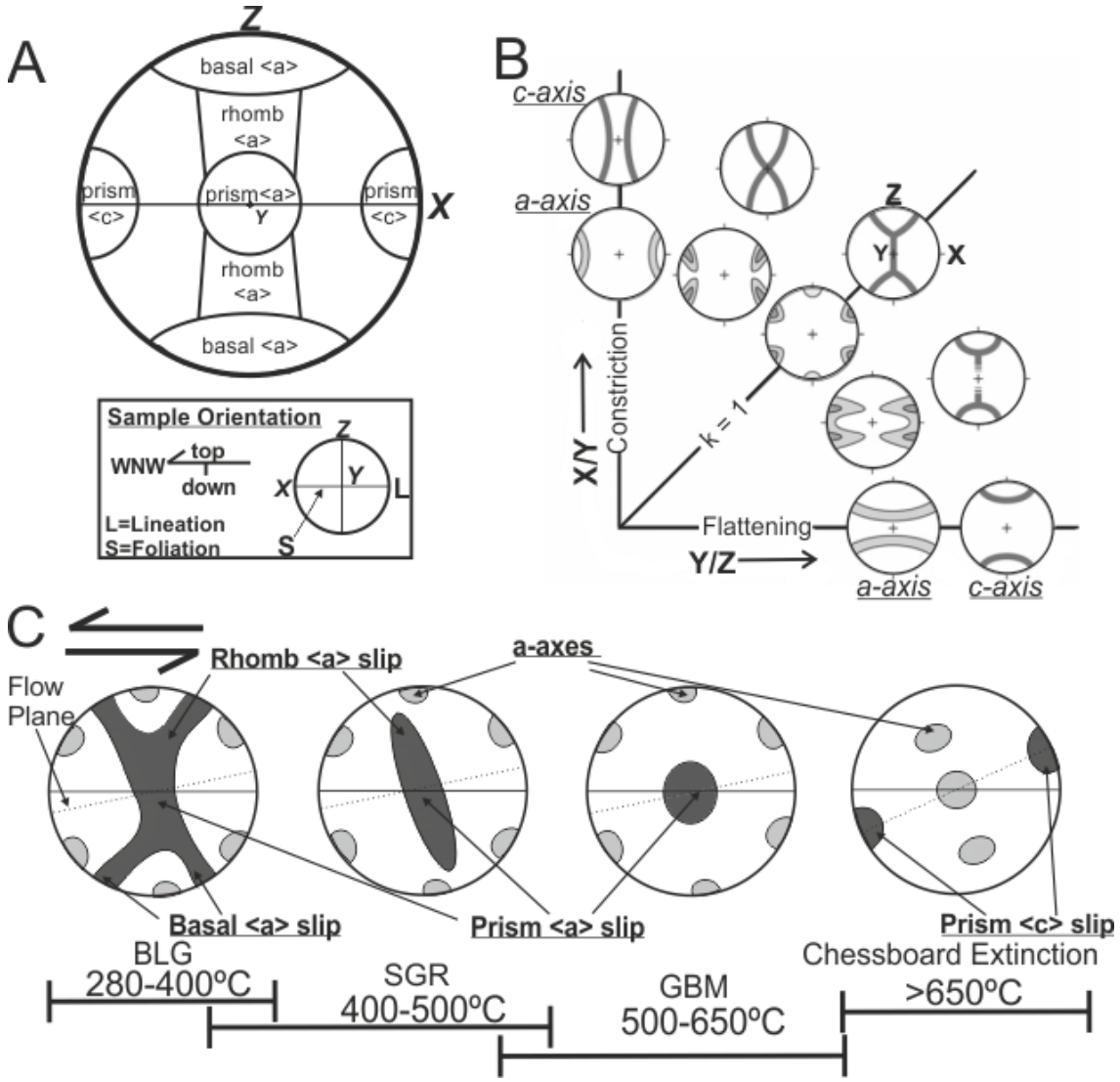

Figure 2.6. Summary of the interpretation and presentation of quartz crystallographic orientations

(A) The location of quartz c-axis peaks and active slip systems in equal area lower hemisphere projection cut parallel to lineation, perpendicular to foliation, based on Schmid and Casey (1986) and adapted from Toy et al. (2008). (B) Flynn plot showing relationships between strain symmetry and quartz c-axis and a-axis fabrics for non-coaxial deformation. C-axis fabrics are represented by fabric skeletons as girdles or point maxima. A-axis represented by contours (after Schmid and Casey, 1986; Law, 1990). (C) Stereonets showing the evolution of c- and a-axis fabrics with increasing temperature for top-to-the-west (sinistral) non–coaxial deformation and plane strain; c-axis shown in dark grey, a-axis shown in light grey. Temperature ranges of dynamic recrystallization mechanisms also shown with respect to CPO fabrics (adapted from Passchier and Trouw, 2005; Langille et al., 2010).

Quartz c- and a- axis CPO fabrics were collected using an electron backscatter diffraction (EBSD) detector mounted on scanning electron microscope at Colgate University, New York. A description of the scanning electron microscope settings and the measurement conditions and setup parameters of the EBSD technique in this study are summarized in Table 2.1. For further description of EBSD techniques and its application to geologic problems, see Prior et al. (1999; 2009).

Table 2.1. Scanning electron microscope settings for electron backscatter diffraction analysis at Colgate University, New York

Scanning electron microscope	JEOL JSM636OLV
Software for scanning electron microscope	Oxford Instruments HKL Channel 5.0
Electron backscatter diffraction detector	Nordlys EBSD detector
Accelerating Voltage	20 kV
Working Distance	10-20 mm
Binning	4X4
Vacuum	High
Bands	6
Step Size	Greater than the average grain size in individual domains of the thin section

Individual data points for quartz collected during automated mapping are established according to the ‘step sizes’ that are deemed appropriate for a given sample. These step sizes are set at increments smaller than the average quartz grain size in an entire thin section, or within a domain of a thin section, to ensure representative sampling of all grains when determining the crystallographic orientation of individual quartz grains by indexing. Post-acquisition data reduction includes the removal of wild data spikes. Clusters of proximal point data with crystallographic misorientations (<10°) are grouped to eliminate any erratic or misindexed orientations. Following this, crystallographic misorientations (>10°) are defined by point grain boundaries. Clusters of similar crystallographic

orientations are then grouped as individual grains and a new data set is created where each grain is represented as a single point.

Quartz c-axis orientations were also collected using the using the fabric analyser (FA) method as a complimentary technique to EBSD analysis using multiple high-resolution digital images acquired simultaneously from several orientations generated with spatial resolution of ~2.8 μm per pixel (Petternell et al., 2010). These images use rotating polarizing filters to create false colour composites of crystal c-axis orientations. Within these images, individual quartz grains are manually selected based on recrystallization properties and prior identification of suitable quartz localities. The c-axis orientations of individual pixels inside the images are evaluated using the 'INVESTIGATOR©' software where gradational shades of colour in these images represent orientations of the c-axes. Data acquisition and reduction related to FA analysis are described in detail by Wilson et al. (2003, 2007) and Peternell et al. (2009). The availability of high-resolution digital images allow for a relatively rapid evaluation of textural heterogeneities in quartz c-axes within an individual thin section (Petternell et al., 2010). Bulk CPO fabrics can be also utilized, as opposed to relying on fabrics within individual quartz-rich domains. This flexibility serves as an effective method to determine deformation partitioning within a thin section and account for heterogeneities of c-axis patterns within the bulk thin section.

2.6. Results

This section describes microstructures of the representative samples from the top of the OVsz to progressively lower structural levels and considered within the context of the three lithostructural domains previously described (see Fig.2.2). The approximate structural depth, rock types, quartz recrystallization mechanisms, CPO fabrics and estimated temperatures of deformation for each sample are summarized in Table 2.

2.6.1. Microstructures and quartz dynamic recrystallization mechanisms

2.6.1.1. Cataclasites and ultramylonites in upper Okanagan Valley shear zone - Domain 1

Brittle deformation features indicative of cataclastic flow and retrogressive processes dominate the upper 50 m of Domain 1, gradually transitioning to ultramylonite in the lower part of the Domain (Fig. 2.7B, C). In thin section, angular broken fragments of mylonitic gneiss and felsic intrusive rocks are embedded in a matrix of quartz, feldspar and chlorite (Fig. 2.7A). Small often conjugate fractures are offset from a few millimetres to centimetres and are infilled with quartz, chlorite and possibly calcite (Fig.2.7A). Limited evidence of ductile deformation is provided by patchy undulose extinction of quartz in the groundmass and by the lobate contacts inferred to be due to low temperature grain boundary migration (BLG) indicative of relict ductile quartz deformation (Fig. 2.7A).

Table 2.2. Summary of the 20 samples selected for quartz microstructural and petrofabric analysis

Sample Number	UTM co-ordinate	Approximate structural depth (m)	Rock type (Mylonitized, unless stated with *)	Mesoscopic shear sense	Dominant quartz micro-structures	Quartz c-axis fabric	Temp.of deform-ation (°C)
		Northern limb					
VT-12-52	U 0319864-5518647	<50	Cataclazed orthogneiss	na	Brittle	na	<280
VT-12-158	U 0304259-5513370	~50	leucocratic intrusion	t-t-WNW	Semi-Brittle	na	<280-400
VT-12-154	U 0305044-5513407	~50-100	leucocratic intrusion	t-t-WNW	Semi-Brittle	basal/rhomb/prism <a>	<280-400
VT-12-72	U 0309818-5517046	~100-150	leucocratic intrusion	t-t-WNW	SGR	basal/rhomb/prism <a>	280-400
VT-12-51	U 0315672-5518045	~100-150	Hbl-Kfs-Qtz Paragneiss	t-t-WNW	SGR	na	400-500
REC_2	U 0312269-5517328	~150-200	leucocratic intrusion	t-t-WNW	SGR	rhomb/prism <a>	400-500
VT-12-110	U 0313046-5516363	~200-300	leucocratic intrusion	t-t-WNW	SGR	na	400-500
VT-12-111	U 0313288-5516143	~300-400	leucocratic intrusion	t-t-WNW	SGR	rhomb/prism <a>	400-500
VT-12-56	U 0310130-5515312	~400-500	Qtz-Hbl monzonite	t-t-WNW	SGR	minor rhomb/prism <a>	500-650
VT-12-166	U 0305956-5518647	~500-600	leucocratic intrusion	t-t-WNW	GBM	minor rhomb/prism <a>	500-650
VT-12-59	U 0310438-5514505	~600-700	leucocratic intrusion	t-t-WNW	GBM	weak fabric	500-650
VT-12-88	U 0313143-5513252	~700-800	leucocratic intrusion	t-t-WNW	GBM	na	500-650
VT-12-185	U 0320092-5513922	>1000	leucocratic intrusion	t-t-WNW	GBM	weak fabric/prism <c>	500->650
		Southern limb					
VT-12-137	U 0306962-5507359	~300-400	leucocratic intrusion	t-t-WNW	SGR	na	400-500
VT-12-11	U 0309731-5506537	~450-550	Kfs-Qtz monzonite	t-t-WNW	SGR	prism <a>	400-500
VT-12-181	U 0308154-5507519	~600-700	Kfs-Qtz monzonite	t-t-WNW	SGR/GBM	na	500-650
VT-12-188	U 0310009-5508472	~1000-1000	Qtz-Hbl monzonite	t-t-ESE	GBM	a	500-650
VT-12-187	U 0310737-5510890	~1500	Qtz-Hbl monzonite	t-t-WNW	GBM	na	500-650
VT-12-30†	U 0310484-5503777	~500-600	Hbl-Bt augen gneiss*	t-t-WNW	GBM	prism <a>	500-650
VT-12-32†	U 0311998-5505749	~700-800	Hbl-Bt augen gneiss*	t-t-WNW	GBM	na	500-650

Note. †; not interpreted to be within the inferred antiformal limbs. Localities of samples are shown in Fig. 2.2.

Extensional shear bands within feldspar porphyroclasts record top-to-the-WNW shear sense (Fig.2.7B, C). Tension gashes and microfractures within these porphyroclasts are filled with recrystallized quartz and are generally oriented perpendicular to the long dimension of the porphyroclasts. Lower in the ultramylonitic part of Domain 1, feldspar porphyroclasts are often asymmetric, reduced in size and exhibit elongated ovoid shapes with their long dimension seemingly tilted parallel to the YZ plane with evidence suggesting onset of core-mantle structures (Fig. 2.7D). The onset of ductile deformation of quartz is evident within the upper ultramylonitic zone (~50-100m) with possible evidence of BLG recrystallization. Due to the highly fractured nature of the rocks towards the structural top of Domain 1 however, these ductile fabrics could also be relict ductile deformation. Overall the features are indicative of deformation temperatures ranging from <280°C to 400 °C.

The onset of SGR recrystallization at ~100 m down the structural succession is generally indicated by elongated quartz ribbons oriented in the direction of instantaneous stretch consistent with top-to-the-WNW sense of shear (Fig. 2.7D). These elongated ribbons become more distinct with increasing structural depth, and coupled with the first appearance of core-mantle structures of feldspars indicate deformation temperatures >400°C (e.g. Passchier and Trouw, 2005) (Fig. 2.7E). These microstructures appear exclusively in the northern limb of the antiform with no apparent evidence for sub-400 °C plastic deformation of quartz in the southern limb (Figs. 2.7; 2.8).

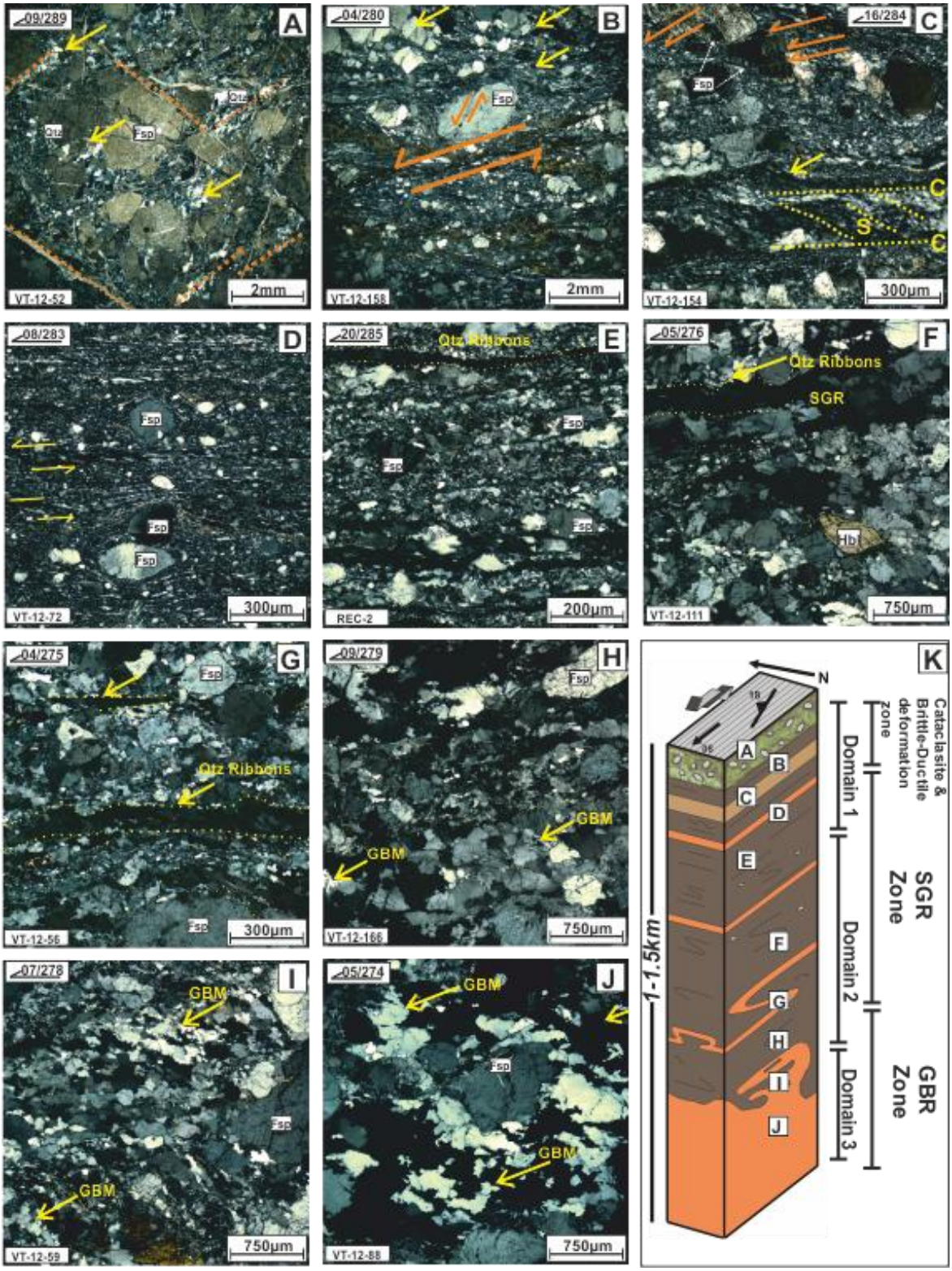

Figure 2.7. Photomicrographs of microstructures of increasing structural depth in the northern limb of the antiform.

(A) Fractured angular fragments within cataclasites with evidence of grain size reduction. Fragments are offset by conjugate shear fractures (orange dashes). Relict ductily-deformed quartz with patchy undulose extinction and serrated grain boundaries are evident (yellow arrows). (B) Shear band offsets in brittlely-deformed feldspar porphyroclasts and quartzo-feldspathic matrix indicating top-to-the-WNW shear sense (orange arrows). (C) Onset of SGR recrystallization shown by elongated quartz ribbons and systematic shear band offsets in feldspar porphyroclasts highlighted by orange arrows. (D,E) SGR recrystallization indicating deformation temperatures of 400-500 °C and core-mantle structures in feldspar porphyroclasts in the lower section of Domain 1. (F,G) Elongated quartz ribbons indicative of SGR at the top of Domain 2. (H) Amoeboid quartz grains with serrated boundaries indicate GBM recrystallization (>500 °C) at the base of Domain 2. (I, J) Quartz exhibiting GBR in syntectonic pluton towards the base of the shear zone which shows increasing grain size down the structural column. (K) Schematic vertical section of the northern antiformal limb showing approximate locations with respect to their approximate structural depth in the Okanagan Valley shear zone. Mineral abbreviations (after Whitney and Evans, 2010): Qtz, quartz; Fsp, feldspar; Hbl, hornblende; Bt, biotite. Estimated structural depths of samples are listed in Table 2.2. All photos are viewed towards the NNE under crossed polarized light.

2.6.1.2. Quartz recrystallization mechanisms and microstructures in middle section of the Okanagan Valley shear zone - Domain 2

Elongated quartz ribbons and S-C fabrics indicate a top-to-the-WNW sense of shear and a discontinuous increase in size in recrystallized quartz grains in the upper section of Domain 2 (~300-500m) (Figs 2.7F,G; 2.8A,D). These features are common in the northern limb and appear at the lowest structural section in the southern limb of the pericline. Feldspar porphyroclasts in Domain 2 generally show core-mantle structures with slight onset of asymmetric pressures shadows in the form of sigma- and delta-type clasts indicating top-to-the-WNW shear sense with a deformation temperature range of ~400-500 °C in this part of the shear zone.

A discreet SGR to GBM transition occurs ~500-600m down structural section indicating deformation temperatures of ~500 °C. Amoeboid grains with relatively large recrystallized grain sizes and distinct lobate and inter fingered serrated grain boundaries are observed, coupled with undulose extinction and

SGR along grain boundaries (Figs 2.7H; 2.8C). Further down section, amoeboid quartz grains with generally larger recrystallized grain sizes and GBM suggest deformation temperatures ranging from ~500°C to 650°C.

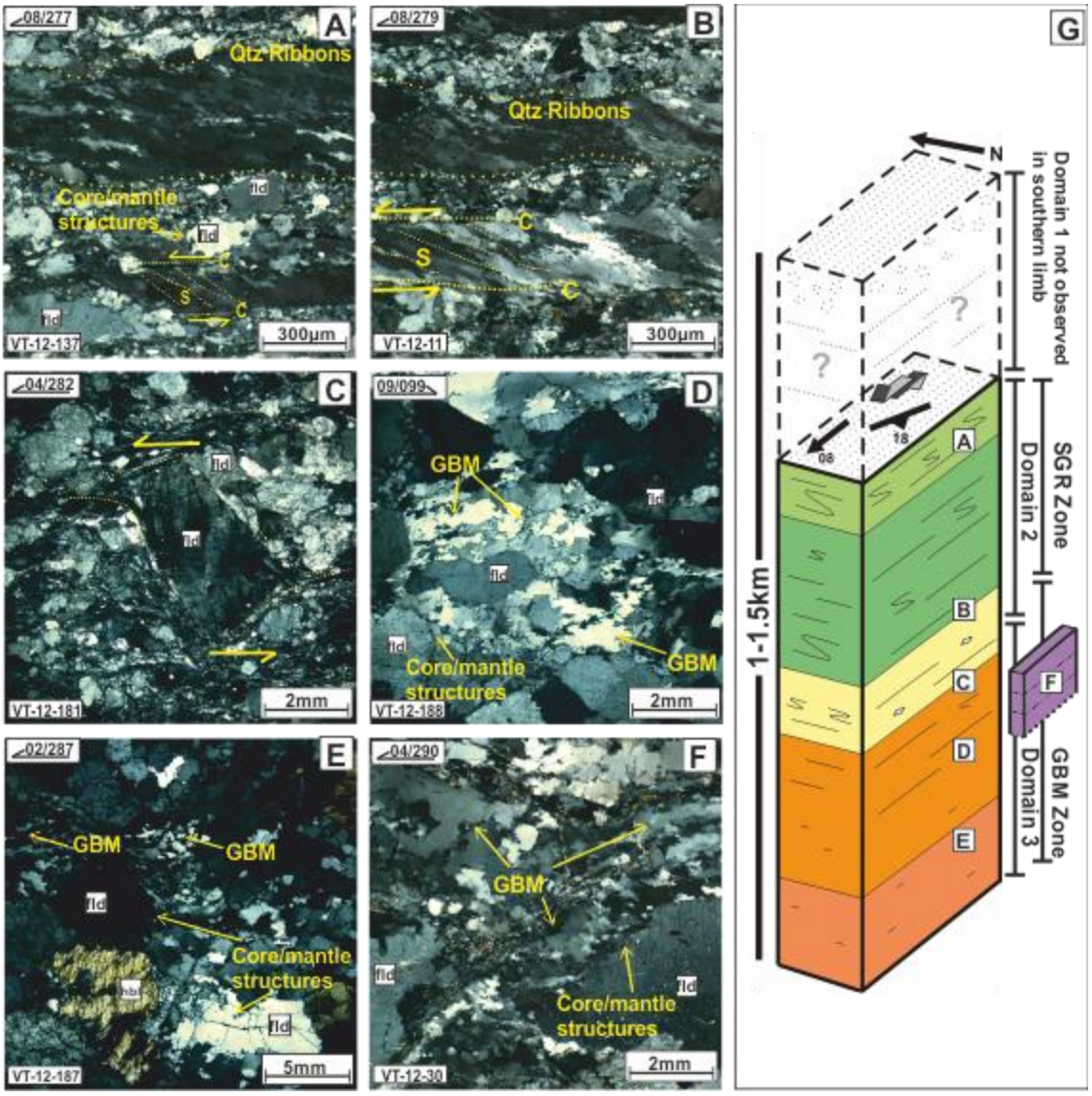

Figure 2.8. Photomicrographs of microstructures in order of increasing structural depth in the southern limb of the antiform.

(A) SGR within elongated quartz ribbons and core-mantle structures of feldspar porphyroclasts. (B) SGR within elongated quartz ribbons accompanied by increased recrystallized grain size with increasing structural depth. (C) SGR to GBM transition indicating ~500°C temperature of deformation; also includes sigma-type feldspar porphyroclast within elongated quartz ribbons. (D,E) GBR recrystallization within the syntectonic intrusive plutons indicating deformation temperatures of 500-650°C. Deformed symmetric feldspars make it difficult to determine a shear sense. There is a broad distribution of recrystallized grain size and core-mantle structures in feldspar porphyroclsasts. (F) GBM deformation of quartz in banded gneiss immediately south of the southern limb of the pericline. (G) Schematic vertical section of the southern antiformal limb showing approximate locations with respect to their approximate structural depth in the Okanagan Valley shear zone. All photos are viewed towards the NNE under crossed polarized light.

2.6.1.3. Quartz recrystallization mechanisms and microstructures near the base of the Okanagan Valley shear zone - Domain 3

Both the host gneiss and intrusive plutonic units towards the base of the OVsz are characterized almost exclusively by GBM recrystallization and core-mantle structures of feldspar porphyroclasts (e.g. Figs 2.8I, J; 2.9D,E; 2.12). Quartz displays distinctive lobate, ameoboid texture indicative of deformation temperatures ranging from 500-650°C.

Despite the overall increase in grain size, there appears to be a broader distribution of recrystallized quartz grain size (e.g., Figs 2.7I; 2.8E). The relatively smaller grains may be “island grains” (e.g., Stipp et al., 2002a) formed by an increase in the size of lobate structures and interfingering, thus becoming isolated from the remainder of the irregular crystal boundary. The absence of chessboard extinction within quartz suggests the temperature of deformation did not exceed 650°C. The gneissic units south of the southern antiformal limb show primarily GBM recrystallization (Fig. 2.8F). This coupled with the core-mantle structures and slight asymmetric delta-type porphyroclasts of the ‘augen’ feldspar clasts indicate top-to-the-WNW shear sense with deformation temperatures of 500-650°C (Fig. 2.8F).

2.6.2. Quartz crystallographic preferred orientation analysis

2.6.2.1. Quartz crystallographic preferred orientations in the upper section of the Okanagan Valley shear zone -Domain 1

Towards the structural top of the OVsz (~50-150m), quartz c-axis fabrics show asymmetric single girdles of basal <a>, rhomb <a> and prism <a> slip, sinistrally inclined <15° with respect to the Y-Z plane (e.g. VT-12-154 and VT-12-72; Fig. 2.9a, b), indicating top-to-west-northwest sense of shear and deformation temperatures of 280-400 °C (Fig. 2.6) . The a-axis fabrics suggest a deviation from plane strain towards constrictional strain near the structural top of the OVsz (Fig. 2.9A, B). Further down the structural section of Domain 1, a weakly developed top-to-the-WNW rhomb <a> and prism <a> fabric is observed (e.g. Rec_2), suggestive of deformation temperatures of 400-500 °C (Fig. 2.9C). This transition also corresponds to the possible onset of a weak six point maxima of <a> axis fabrics bounding the stereoplot suggesting an onset of plane strain conditions.

2.6.2.2. Quartz CPO fabrics in the middle section of the Okanagan Valley shear zone -Domain 2

Domain 2 is characterized by rhomb <a> and prism <a> slips suggesting temperatures in the range of 400-500 °C (e.g.VT-12-111; Fig. 2.9D). It is difficult to determine a sense of symmetry from most of the CPO fabrics in Domain 2 with the exception of the top-to-the-ESE sense of shear observed for the FA fabric in VT-12-166 (~500-600m down structural section). From ~400-600 m down structural section, CPO patterns appear to indicate prism <a> slip, *Y*-axis maxima with a temperature range of 500-650 °C (Figs. 2.9E, F; 2.10A). Generally, the <a> axes across Domain 2 in both the northern and southern

limbs show point maxima suggesting plane strain deformation conditions (Figs. 2.9; 2.10).

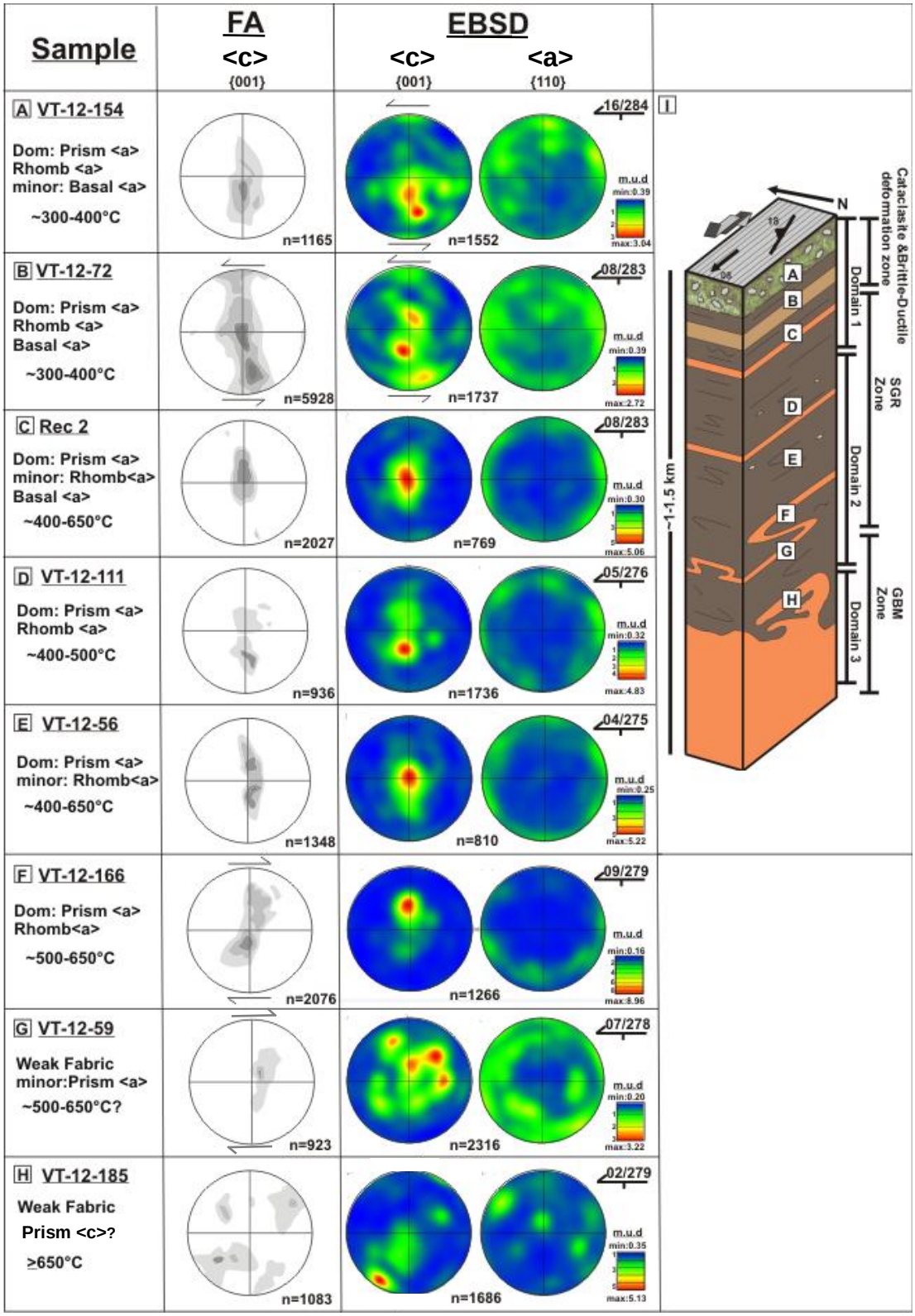

Figure 2.9. Electron backscatter diffraction and Fabric Analyser quartz c- and a-axis orientations in the northern limb

Fabrics shown in equal area lower hemisphere projections presented in order of increasing structural depth in the northern limb of the antiformal pericline. The c- and a-axis orientations are shown with respect {001} and {110} plane of the Miller index, respectively. Contouring of stereoplots is based on the mean uniform density (m.u.d.) with designated maximum and minimum values. (A-H) Quartz c-axis fabrics show a systematic progression of increasing temperature with increasing depth based on the active slip systems. The a-axes show a dominance of plane strain in the middle structural succession of the OVsz with a possible deviation towards constriction in the upper 200m of the structural succession. (I) Schematic vertical section of the northern antiformal limb showing approximate locations of Figs. 2.9A-H with respect to structural depth in the Okanagan Valley shear zone.

2.6.2.3. Quartz crystallographic preferred orientations in the lower section of the OVsz - Domain 3

The CPO fabric from the upper part of Domain 3 (~600-700m below the top of the section) shows a distribution around the Y-pole of the stereoplot (Fig. 2.9G). This fabric occurs near the structural top of the quartz monzonite pluton around the gradational contact with the host gneiss (e.g. VT-12-59) (Fig. 2.9I). The weak EBSD fabric is difficult to interpret, but the FA fabric defines an asymmetric top-the-the-ESE single girdle. The weak prism <a> with slight onset of rhomb <a> slip may indicate deformation temperatures in the range of 400-500 °C, which appears to contradict the GBM recrystallization mechanism in the sample. The weak a-axes orientations makes it difficult to determine a definitive strain geometry.

The CPO fabric from a transposed leucocratic dike (VT-12-185) within the gneiss near the base of the shear zone (>1000m) has a clear top-to-the-ESE sense of shear (Fig. 2.9H). This could be interpreted as an asymmetric single girdle of basal <a>, rhomb <a> and prism <a> slip indicating deformation temperatures of 280-400 °C. Alternatively, the distribution of the c-axis plot could also be interpreted to represent prism <c> slip with deformation temperatures >650 °C. This is supported by the distribution of the a-axis plot, which suggests plane strain conditions during prism <c> slip (see Fig. 2.6C).

Immediately south of the southern antiformal limb, the measured CPO fabric (VT-12-30) indicates a strong prism <a> slip with a minor component of rhomb <a> slip (Fig. 2.10B). The resultant asymmetric single girdle shows a top-to-the-ESE fabric (Fig. 2.10B). This contradicts the mesoscopic kinematic indicators, which indicate a top-to-the-WNW sense of shear (See Fig. 2.4F). The a-axis plot suggests plane strain conditions (Fig. 2.10B). The c-axis orientation is interpreted to indicate a temperature range of 400 to >500 °C.

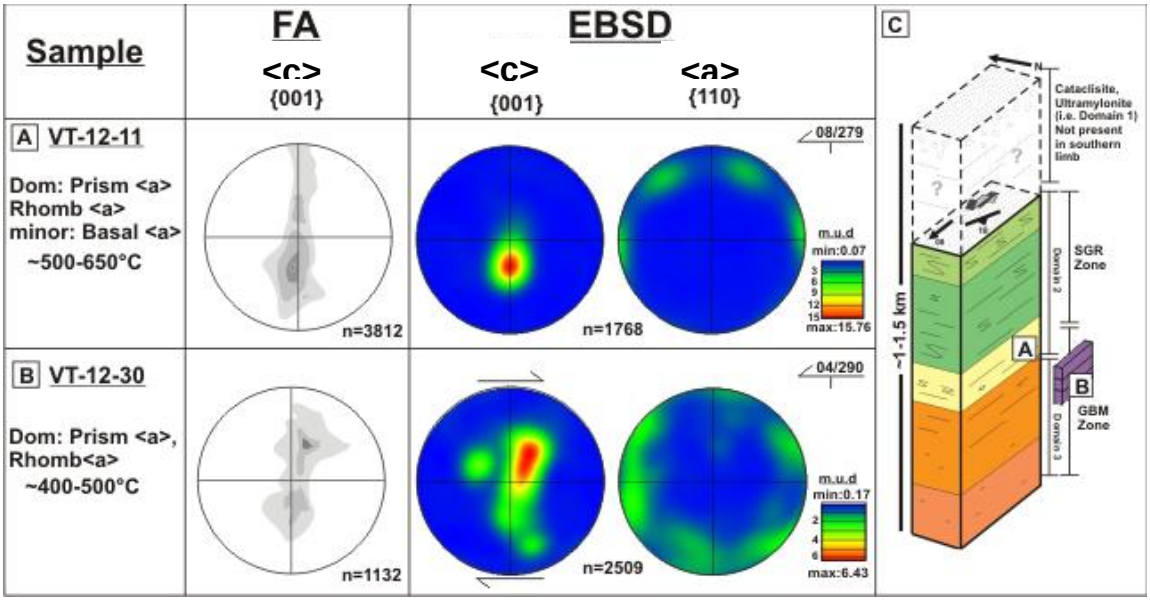

Figure 2.10. Electron backscatter diffraction and Fabric Analyser quartz c- and a-axis orientations in order of increasing structural depth in the southern limb.

The c- and a-axis orientations are shown with respect {001} and {110} plane of the Miller index, respectively. Contouring of stereoplots based on the mean uniform density (m.u.d.) with designated maximum and minimum values. (A) CPO in the middle structural succession displays prism <a> slip, Y-axis maxima (500-650 °C). (B) Prism <a>, Y-maxima slip with a minor rhomb <a> component (400 to >500 °C). (C) Schematic vertical section of the southern antiformal limb showing approximate locations of Figs 2.10A-B with respect to their approximate structural depth in the OVsz.

2.6.2.4. Heterogeneity of crystallographic preferred orientations heterogeneities in microstructural domains

High-resolution images acquired from the FA analysis facilitate testing of fabric homogeneity between microscale domains within a single thin section (Fig. 2.11). Measurements collected on a raster area across VT-12-72 primarily display an asymmetric single girdle, yet also suggest the presence of prism <c> slip (Fig. 2.11C). This heterogeneity can also be found within an individual microscale domain (Fig.2.11E). This is the only analysed sample where this microscale heterogeneity occurs. It is uncertain whether other microscale heterogeneities occur throughout the shear zone.

The CPO data presented in Figures 2.9 and 2.10 were collected in several quartz rich domains within individual thin sections, and therefore can be thought of as representing a bulk CPO fabric for each thin section. Although these bulk CPO fabrics are easier to interpret, they may not accurately reflect the CPOs within individual quartz domains or the overall fabric heterogeneities at the thin section scale. For instance, the bulk CPO fabric for VT-12-72 is interpreted as an asymmetric sinistral single girdle with inferred deformation temperatures ranging from 280 °C to 400 °C (Fig. 2.9B; 2.11). In contrast, an individual microscale CPO domain appears to contain dominantly prism <c> slip with inferred deformation temperatures >650 °C. This domain occurs within an inferred transposed leucocratic intrusion (Fig. 2.11). The process responsible for the formation of this microstructural domain is uncertain requiring further investigation; particularly pertaining to the nature of the transposed intrusive rocks with respect to the overall CPO fabric of the sample.

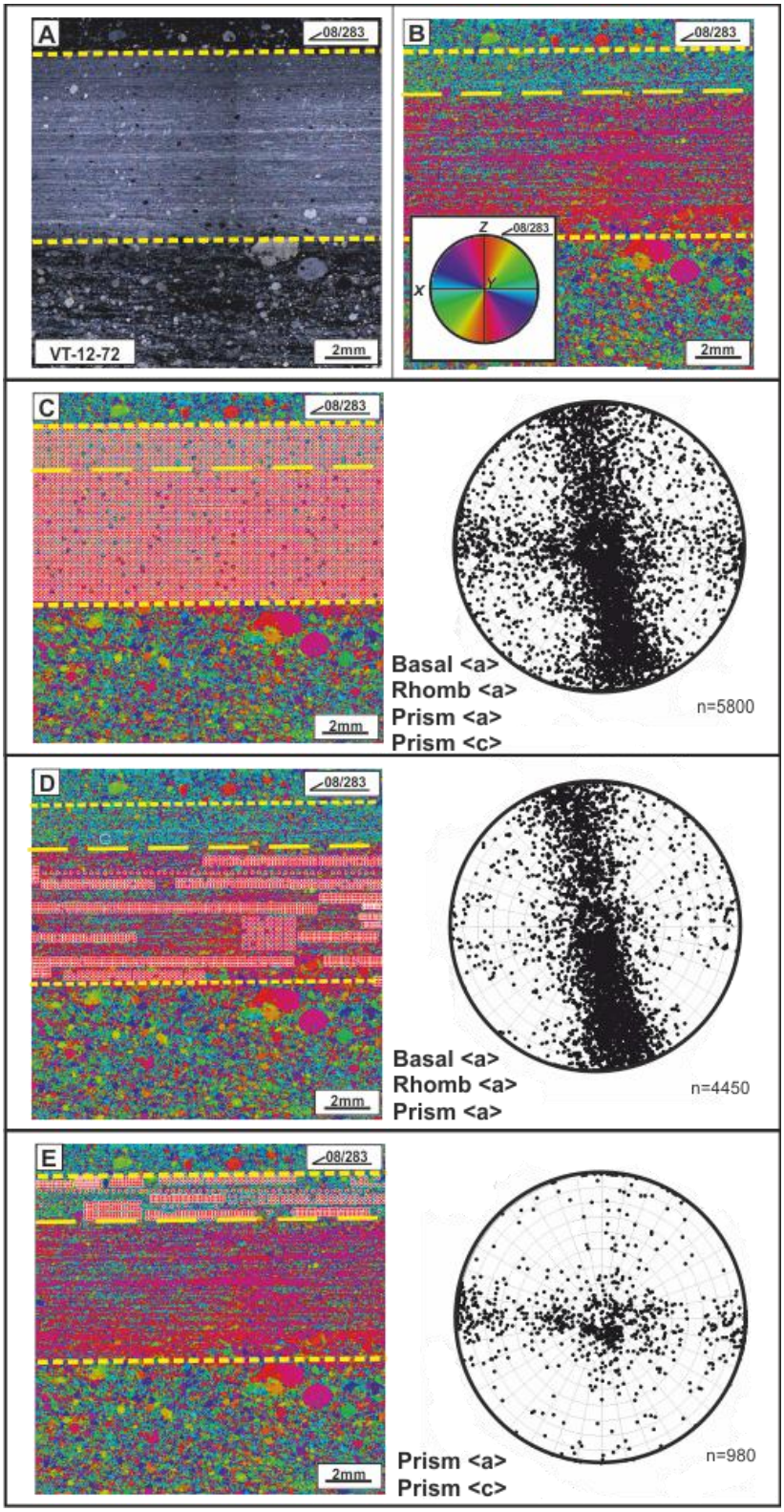

Figure 2.11. Individual microscale domains of quartz c-axis fabrics identified within VT-12-72 acquired using a Fabric Analyser.

(A) Plane polarized image of transposed felsic intrusive in which quartz CPO fabrics were measured. (B) High resolution false-colour digital image showing the variation in orientation of the main fabrics of all grains in the unit (assignment of false colours are based on a coloured stereogram shown in the bottom left corner). (C) Bulk raster of a selected section of this section showing a lower hemisphere projection of c-axis fabric with basal <a>, rhomb <a> and prism <a> in an asymmetric single girdle and a prism <c> girdle. (D) Basal <a>, rhomb <a> and prism <a> asymmetric single girdle restricted to lower domain based on random point accumulation. (E) Prism <c> girdle from quartz CPOs localized in upper domain based on random point accumulation.

2.6.2.5. Comparison between Electron backscatter diffraction and Fabric Analysis

In most samples both EBSD and FA yield similar results with minor differences in the pole figures for several samples in the middle of the shear zone within Domain 2 (e.g. VT-12-11 and VT-12-56). EBSD fabrics record Y-axis maxima with minor rhomb <a> slip as opposed to more pronounced asymmetric single girdles of prism <a> and rhomb <a> obtained by the FA in these samples. This may be attributed to the EBSD data reduction and FA quality indices. Additionally, the FA may negatively bias against prism <a> fabrics, since INVESTIGATOR© may assign a low geometric and retardation quality for vertical quartz crystals (Peternell et al., 2010). Because the grains in FA are manually selected, this bias has been limited, as shown by numerous FA plots with a good density of Y-maxima grains. This problem appears more pronounced when using a general raster box in the automated mode.

2.7. Discussion

2.7.1. Three-dimensional distribution of deformation temperatures and strain in the Okanagan Valley shear zone

2.7.1.1. Variations in deformation temperatures with structural depth

Deformation temperatures indicated by quartz microstructures and c-axis fabrics range from ~280°C to >650°C, increasing non-linearly with structural depth beneath the inferred upper detachment surface of the OVsz (Figs 2.7; 2.8; 2.9; 2.10; 2.12). The progression of deformation temperatures obtained from dynamic recrystallization mechanisms on the microstructural scale is broadly compatible with deformation temperatures estimated from the c-axis fabrics down the structural succession (Fig. 2.12). Isothermal surfaces have subsequently been created based on the distribution of deformation temperature data across the field area, which give an apparent geothermal gradient between 300-400 °C km^{-1} across the OVsz.

The interpreted deformation temperature increases from <280°C to 400°C in the upper 200 m of the shear zone, to up to ~400-500 °C 500 m down the structural section (Fig. 2.12). Below a structural depth of 500 m, deformation temperatures of 500-650 °C are recorded (Fig. 2.12). At a depth of ~1-1.5 km, deformation temperatures appear to remain constant at <650 °C (Fig. 2.12). This may be ascribed to a gradual reduction of the strain of the shear zone towards its base, with a transition to a more conventional geothermal gradient (e.g. 25°C km^{-1}) below it. However, the prism <c> fabric of sample VT-12-185 (Fig. 2.9H) does suggest the temperature of deformation in the OVsz at that location may have exceeded 650°C. Another exception to the general pattern described above is found within the southern limb of the antiform. Here, the lack of microstructural evidence for deformation temperatures below 400 °C is in agreement with

mesostructural observations that demonstrate an absence of ultramylonites and cataclasized mylonitic units that characterize Domain 1 where the relatively low temperature fabrics are found. The lack of sufficient data makes it difficult to provide an adequate explanation for the absence of Domain 1 in this limb. Notably, throughout the study area there is no evidence of thermally-induced static annealing across the OVsz. The lack of any recorded polygonal quartz crystals with straight boundaries and 120° triple junctions due to grain boundary area reduction (e.g. Passchier and Trouw, 2005) suggest that there was no significant thermal relaxation of the shear zone during or after deformation.

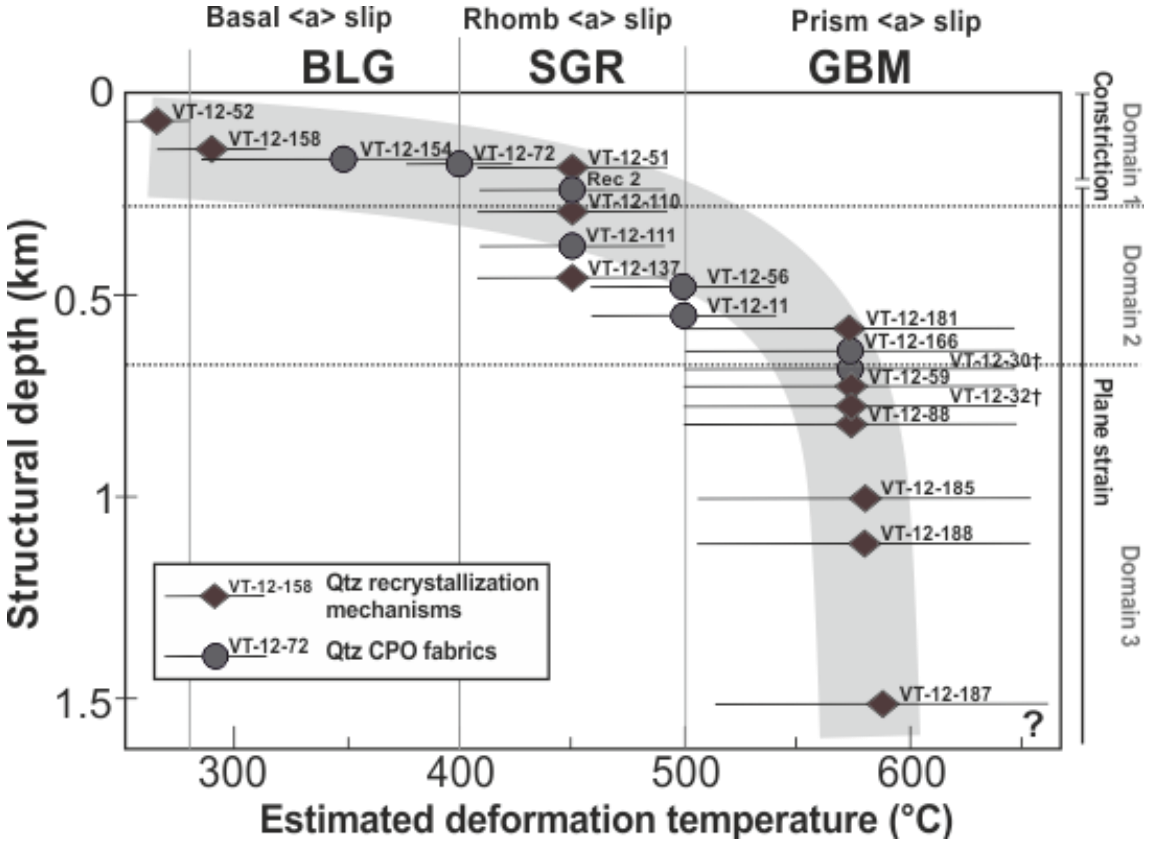

Figure 2.12. Schematic diagram showing the apparent relationship between deformation temperatures with respect to structural depth

The data suggest an apparent geothermal gradient within the shear zone of approximately 300-400 °C km^{-1} over a vertical distance of ~1 km. † - samples not interpreted to be within antiformal limbs upon which structural depths are based.

Deformation temperatures indicated by c-axis fabrics and quartz recrystallization mechanisms in samples from transposed leucocratic intrusive dikes throughout the structural section appear to yield similar results (e.g samples Rec-2; VT-12-111; VT-12-154; VT-12-166). These samples also appear to yield similar deformation temperatures acquired from quartz-rich country rock samples at similar structural levels (e.g. Rec-2 and VT-12-51), suggesting that these transposed intrusions cooled to ambient background temperatures prior to the cessation of penetrative deformation in the OVsz.

The observed individual microscale domain of prism <c> slip within a leucocratic intrusion in VT-12-72 indicates deformation temperatures of >650 °C, in contrast with the general inferred deformation temperature of ~280-400 °C for the sample (Figs. 2.11; 2.12). The possible relict higher temperature from this domain may be related to the transition from magmatic temperatures to solid-state deformation temperatures in syntectonic intrusions. Lister and Williams (1983) noted how CPO fabrics in quartz-rich samples not only follow trending maxima where the angle of the girdle changes while tracking the finite strain axes, but that the fabric can stay fixed in its relationship to the flow plane. Thus, the magmatic crystallographic fabrics that developed at sub-granitic solidus conditions prior to transposition of the intrusion may be preserved or locked (hardened) into place. In this scenario, the magmatic fabric may pass seamlessly into a >650 °C (prism <c>) solid-state fabric where the pre-existing fabric influences the progressive CPO development during onset of plastic deformation below the granite solidus.

Alternatively, domains with higher deformation temperatures in syntectonic leucocratic intrusions could suggest the intrusions remained at higher temperatures than the wall rocks when plastic deformation of quartz ceased and fabrics were ’locked-in’. If so, these intrusions could have been emplaced during a relatively late stage of penetrative deformation associated with the OVsz.

2.7.1.2. Interpretation of strain geometry variation with structural depth

A-axis fabrics generally suggest plane strain deformation across the OVsz with a deviation towards constriction in the upper ~150m of the structural succession (i.e. within Domain 1 in the northern antiformal limb) (e.g. Fig. 2.9). Plane strain in general shear occurs where stretching in one direction is compensated by flattening at right angles to the stretching direction, with Y = 1 and X > Y > Z with respect to the strain ellipsoid (Fossen, 2010). Sullivan (2013) postulated that near plane strain progressive simple shear can create L-S tectonites where the foliation occupies the direction of flattening perpendiular to X on the X-Y plane. This arrangement is compensated by constriction accommodated by the elongation lineations forming parallel to the X direction. Within the study area, L-S tectonites predominate across the OVsz with L tectonites becoming more pronounced towards the top of the section and weakening towards the base (See section 2.4). For plane strain deformation conditions, the active slip system typically controls the location of the fabric maxima on the stereoplot, which in turn is diagnostic of deformation temperature (Lister 1981, Sullivan and Beane, 2010). Therefore, the data in this study indicate that deformation at mid-crustal amphibolite-facies occurred primarily under plane-strain deformation conditions. There is an indication of possible slight constrictional deformation that developed during progressive exhumation to upper-crustal, greenschist- to sub greenschist-facies deformation (i.e. Domain 1) as described in the northern limb.

2.7.1.3. Interpretation of shear sense from c-axis fabrics

The consistent top-to-the-WNW asymmetry of the c-axis fabric girdles in the upper 400 m of the structural section (e.g. VT-12-72; VT-12-154) is compatible with the mesoscopic shear-sense indicators. However, several of the c-axis fabrics deeper in the structural section suggest top-to-the-ESE sense of

shear (e.g. VT-12-11; VT-12-30; VT-12-166). It is unclear what their significance is with respect to the penetrative deformation in the OVsz. These fabrics could represent preserved penetrative deformation linked with the northeast-directed compressional phase of the Shuswap metamorphic complex either preceding or synchronous with top-to-the-WNW deformation higher up in the shear zone. A similar switch in asymmetry was documented by Johnson and Brown (1996) farther north along a transect between Sicamous and Revelstoke, British Columbia. Johnson and Brown (1996) noted a kinematic reversal from W-direct to NE-directed shear sense occurred within deeper levels of OVsz footwall domain at ~ 2 km depth. Alternatively, the opposing shear sense documented in this study could be attributed to non-coaxial deformation with a significant pure shear component in plane strain that resulted in coeval, oppositely directed fabrics that formed as conjugates oblique to the principal strain axes. However, there is no evidence in the data of this study that supports this explanation, aside from the reversal in shear sense.

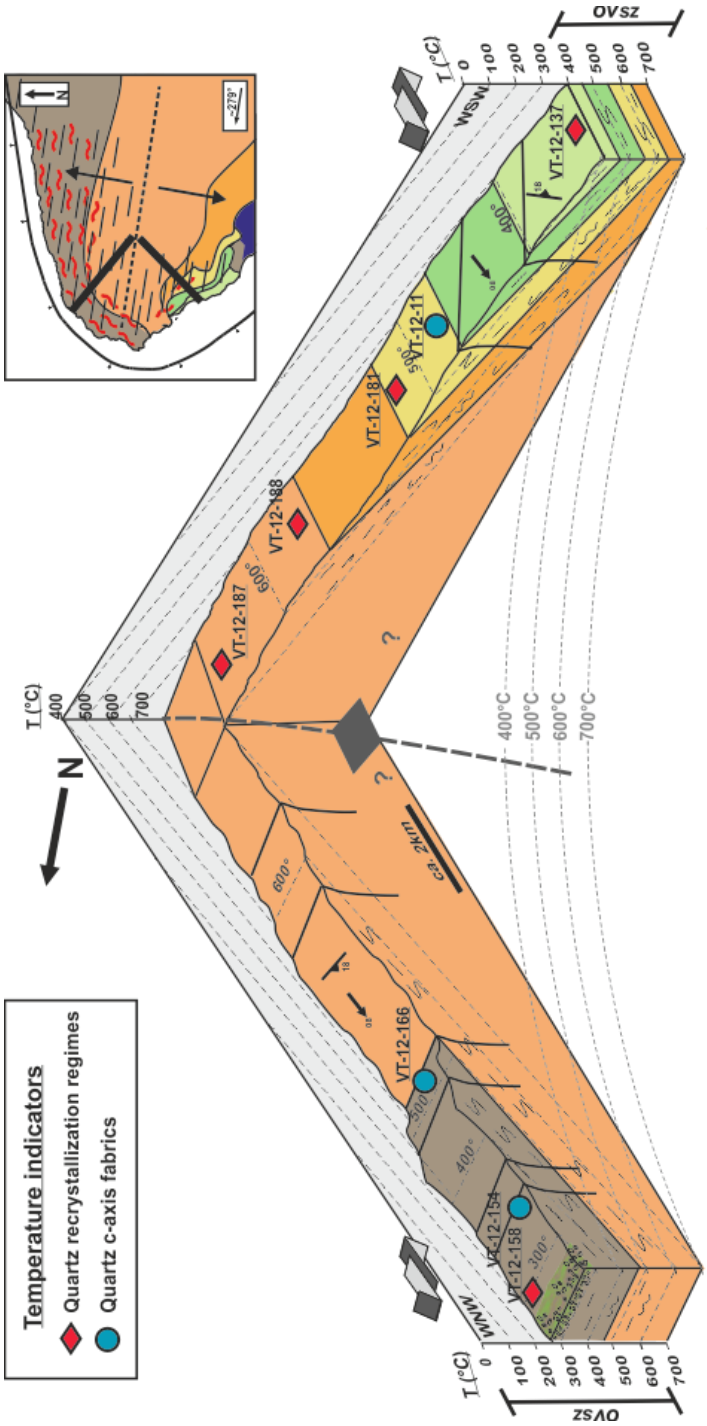

Figure 2.13. Model showing inferred paleo-isotherms within the study area

Cross sections are based on the approximate dip of the foliation and by the location of interpreted quartz recrystallization regimes and quartz c-axis fabrics of samples projected from close proximity to the cross-sections (See inset map for approximate location of cross sections).

2.7.2. Inferred minimum ages of the quartz deformation structures during exhumation

The quartz microstructures and CPO fabrics are interpreted to be mostly Eocene in age, constrained with U-Pb zircon crystallization and $^{40}Ar/^{39}Ar$ cooling ages from the gneissic and intrusive rocks within the OVsz from previous studies (Medford, 1975; Bardoux, 1993; Parrish et al., 1988; Johnson and Brown, 1996; Brown et al., 2012). Deformation temperature estimates from this study are in agreement with the closure temperature range for K/Ar and $^{40}Ar/^{39}Ar$ cooling ages obtained on rocks within the OVsz that track its Eocene exhumation within and around the study area (Medford, 1975; Bardoux, 1993). Hornblende samples typically cooled below 550°C (McDougall and Harrison, 1999) between ~53 and 48.5 Ma (Medford, 1975; Bardoux, 1993). Muscovite ages indicate the OVsz cooled below 350 °C at ~50 Ma and biotite below 280 °C (McDougall and Harrison, 1999) at 48.7 Ma. Apatite and titanite fission-track ages within the cataclasite rocks suggest the carapace was near surface by at least ~47±1 Ma (Medford, 1975; Bardoux, 1993). The overlap between the hornblende and mica cooling ages suggests rapid exhumation of the footwall by ductile shearing along the OVsz at an average rate of 4 km/Myr between 54 Ma and 48 Ma while cooling from ~650°C to <280°C (Bardoux, 1993).

Bardoux (1993) dated intrusive felsic bodies within the OVsz immediately north of the study area, which indicate shearing may have started as early as 56 Ma. Immediately south of the study area, Brown et al. (2012) obtained zircon crystallization ages of ~53-50 Ma for syntectonic felsic intrusives and anatectic leucosome interpreted to have formed at >20 km depth. The overlap in time of the $^{40}Ar/^{39}Ar$ cooling ages of Bardoux (1993) and of the zircon crystallisation of Brown et al. (2012) is consistent with the rapid exhumation facilitated by the OVsz.

The apparent overlap of zircon crystallization and $^{40}Ar/^{39}Ar$ cooling ages summarized above may also imply that higher temperature, mid-crustal ductile deformation and upper-crustal lower temperature brittle-ductile deformation occurred simultaneously. However, this hypothesis does not fully explain the apparent elevated geothermal gradient in the OVsz of ~300-400 °C km^{-1} in a vertical distance of ~1-1.5 km (Figs. 2.12; 2.13). Deformation with a significant component of pure shear or vertical shortening may account for the apparent telescoping of isotherms in the immediate footwall of the OVsz during exhumation. This scenario, along with other possible mechanisms, is discussed below.

The bulk of quartz microstructures and CPO fabrics presented in this study are interpreted to have formed during exhumation of the OVsz from the mid-crust to progressively shallower crustal levels during WNW-ESE-directed extension. This progression is supported by the apparent decrease in metamorphic grade towards the structural top of the shear zone. Deformation temperatures deeper in the structural section (i.e. Domain 3) demonstrate amphibolite-facies deformation and metamorphism, compatible with exhumation from the mid-crust. To the south, within the OVSZ, geothermobarometric data suggest exhumation from at least ~17-23 km depth during Eocene deformation (c.f. Fig. 4; Brown et al., 2012). Deformation temperatures progressively decrease up structural section with greenschist-facies deformation (i.e. upper Domain 2 and Domain 1) overprinting amphibolite-facies structures, followed by brittle deformation overprinting ductile fabrics towards the structural top of Domain 1. The microstructural and metamorphic gradation suggests mid-crustal ductile fabrics may have been capped by lower temperature structures that formed progressively nearer to the surface as the detachment evolved and its deeper levels were progressively exhumed to shallower levels.

2.7.3. Geometrical criteria and flow associated with telescoping of isotherms and exhumation in the immediate footwall of the Okanagan Valley shear zone

The inferred telescoping of isotherms that define an apparent geothermal gradient of ~300-400 °C km^{-1} in the OVsz during the Eocene (Fig. 2.13) is possibly the result of several geometric and tectonic factors either working singularly or in unison. Pressure-temperature estimates from Bardoux (1993) and Brown et al. (2012) indicate paragneissic domains within the OVsz equilibrated in the early Eocene at 670 °C ± 50 °C and 6 ± 1 kbar, equivalent to ~17-23 km depth. Based on these estimates, the initial Eocene geothermal gradient is estimated to lie between 30-39 °C km^{-1} (See Appendix D for calculations). Below, we discuss how several parameters such as the coaxiality, magnitude and velocity of flow in principally plane strain deformation could explain the intense telescoping of isotherms. These parameters are incorporated into a conceptual model which proposes how isotherms ranging within ~280 °C to >650 °C were telescoped from their original vertical separation of ~9-15 km to a final separation of 1-1.5 km during exhumation (See Appendix D for calculations).

Shear-sense indicators from both field and microstructural analysis indicate that penetrative deformation within the OVsz involves non-coaxial deformation. Therefore, a simplified two-dimensional particle displacement model for exhumation with a non-coaxial component is adopted (e.g. Law et al., 2011) to account for the telescoping of the ~280 °C to >650 °C isotherms to a final separation of 1-1.5 km (Figs. 2.12; Fig. 2.13; See Appendix D). This model is based on the premise that particles move along different parallel paths in the shear zone with the orientation of the flow planes parallel to the foliation planes, with differential transport-parallel motion between the particles (Fig.2.14; Law et al., 2011). For the sake of simplicity, the isotherms are assumed to be originally horizontal, inclined to the detachment surface at an angle equal to the detachment dip (Fig. 2.14). Several other geometric variables include the dip

angle of the detachment and the original vertical spacing between isotherms for which we assume a prevailing linear geothermal gradient (Fig. 2.14; Law et al., 2011). A component of shortening from the observed non-coaxial shear is likely to have reduced both the original angle between the detachment and isotherms and the vertical spacing between the original isotherms, although it is unlikely to have been a sufficient amount to explain the observed telescoping of the isotherms vertical shortening of ~85-92% (see Appendix D). Simultaneously, however, the transport parallel stretching produced by this shortening contributes to the shear plane-parallel displacements, thereby lengthening the particle path in primarily plane strain conditions. It should be stressed that this model is solely geometric with no account of thermal processes such as chilling of the hotter footwall against the cooler hanging wall, thermal relaxation, or the influence of syntectonic plutonic activity. Furthermore, the potential role of circulating fluids on the geothermal gradient during deformation is not factored in this model. For instance, any influence on an elevated transient geotherm during deformation from a potential influx of cool surface fluids into the shear zone is not considered (e.g. Gottardi et al., 2011).

Quartz microstructures and CPO fabrics used to infer deformation temperatures are interpreted to be the product of exhumation-related shearing and cooling, with the recorded fabrics for individual particles being ’locked-in’ at progressively higher levels and cooler temperatures as the shear zone manoeuvres during exhumation. Therefore, assuming that the original metamorphic mineral assemblages, microstructures, and CPO fabrics were not reset at lower temperatures after movement along their respective exhumation paths, the telescoping of the isotherms indicated by these thermometers would result in steeper apparent thermal gradients (Fig. 2.14).

Although the OVsz is interpreted to have rapidly exhumed to the upper crust during the Eocene, there is little definitive data on the absolute timing for when the individual observed microstructures and CPO fabrics either

commenced, or were ’locked-in’ during exhumation. It is difficult to decipher whether penetrative deformation down the exposed structural section could have been simultaneously active or occurred diachronously throughout the shear zone. Based on the observations in this study, It is most likely diachronous, but over a very short range of geologic time.

We therefore propose a model whereby the active zone of penetrative deformation became narrower up structural section near the Earth’s surface (Fig. 2.14). This progression would result in microstructures and CPO fabrics in structurally lower rocks with originally higher deformation temperatures to be ‘locked-in’ as they migrated out of the active zone of deformation during exhumation of the footwall to upper crustal levels (Fig. 2.14). Once locked in, these higher temperature fabrics were passively exhumed along a trajectory that resulted in their progressive juxtaposition against lower temperature fabrics that were being generated in the active part of the shear zone (Fig. 2.14). There is a component of overprinting of the lower temperature fabrics on the higher temperature fabrics but this was confined to structurally higher levels where the shear zone narrowed approaching the surface. Thus, the deepest level fabrics remained relatively unscathed during exhumation. The progressive increase in the inferred deformation temperatures down structural section in this study supports this model.

Furthermore, similar to the low-angle South Tibetan Detachment System in the Himalayas, progressive accretion of relatively cooler rocks during exhumation would result in progressive telescoping and translation of rocks deformed at different crustal depths and temperatures (Cottle et al., 2011). This juxtaposition of rocks from progressively deeper structural levels would result in the formation of a condensed section with an apparent smooth gradient in deformation temperatures.

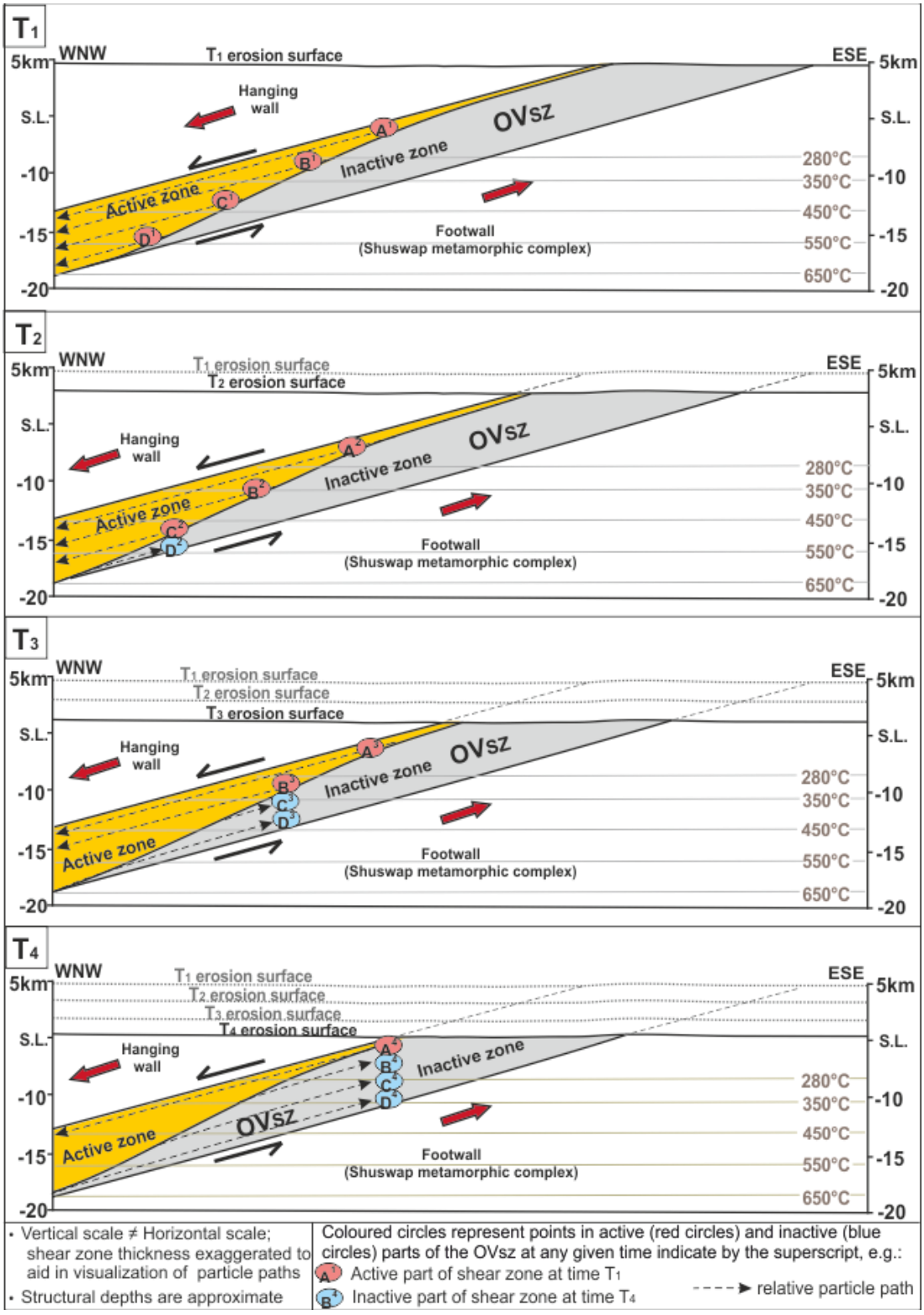

Figure 2.14. Particle displacement model showing the possible progressive kinematic evolution of the Okanagan Valley shear zone during exhumation

Simplified cross sections depicting the proposed kinematic evolution of the Okanagan Valley shear zone in this study. The yellow part of the shear zone represents the active part of the shear zone during particular snapshots in time chronologically in order from T1 to T4 with the black dashed arrows indicating the relative particle trajectories. Microstructures and fabrics created in the structurally deeper and originally hotter parts of the shear zone are progressively 'locked-in' in as they migrated out of the active zone of deformation during exhumation. These locked-in higher temperature fabrics were passively exhumed along an ESE trajectory (black dashed arrows) in the quenched 'inactive zone' (grey area) that resulted in their continuous juxtaposition against lower temperature fabrics that were being generated in the progressively narrowing active part of the WNW-directed shear zone. The isotherms were calculated assuming initial geothermal gradient: 30-39 °C km^{-1}.

2.7.4. Implications for exhumation of the Shuswap metamorphic complex and the Channel Flow model

Given the relatively small structural section and the limitation of the data in this study, we cannot with certainty derive the role of the OVsz within a broader tectonic framework accountable for the exhumation of the Shuswap metamorphic complex. However, several observations in this study support certain modes of exhumation particularly pertaining to the flow type during ductile deformation. For instance, some workers have argued that a significant portion of the exhumation path occurred during syn-convergent ductile extrusion and channel flow from the Late Cretaceous to Paleocene (e.g. Brown and Gibson, 2006; Glombick et al, 2006; Gervais and Brown, 2011).

Unfortunately, this thesis does not provide any definitive evidence for pre-Eocene ductile deformation, either compressional or extensional. Therefore, this study cannot be fully utilized to aid the evaluation of pre-Eocene (~100-60 Ma) mid-crustal channel flow models where the OVsz is inferred to be the normal-sense, high strain, upper detachment of the ductile channel (Brown and Gibson, 2006; Gervais and Brown, 2011). However, quartz c-axis fabrics in the higher temperature, structurally lower part of the shear zone that display apparent top-to-the-ESE sense of shear, which contradict the mesoscopic kinematic indicators (e.g. VT-12-30; VT-12-166; VT-12-185; Figs. 2.9; 2.10) may be an indication of preserved older eastward flow of the Shuswap metamorphic complex in a

proposed Late Cretaceous to Paleocene viscous channel. This would, in turn, predict that the quartz microstructures towards the base of the shear zone in the country rock may be preserving pre-Eocene fabrics. If so, these fabrics may have formed during relatively higher flow velocities under a significant component of pure shear, telescoping the isotherms prior to Eocene exhumation (Fig. 2.16). Nonetheless, the top-to-the-ESE fabric could still be further telescoped during Eocene exhumation. The greater component of pure shear under plane strain deformation conditions towards the base of the OVsz may have resulted in oppositely flowing, top-to-the-ESE shear as a result of simultaneous transport-parallel stretching. Local and thermal anomalies are also not factored in this last hypothesis. Clearly, further thermo-kinematic and geochronological analyses are required along the entire structural section of the Shuswap metamorphic complex from the OVsz to the immediate hanging wall of the Monashee décollement to decipher the flow profile associated with deformation and exhumation.

2.7.5. Implications regarding discrepancies along strike of the OVsz

The affirmation of the OVsz as a crustal-scale extensional detachment in this thesis appears incompatible with studies around the vicinity of Vernon and Osoyoos (Fig. 2.17; Okulitch, 1979, 1987; Thompson and Unterschutz, 2004; Glombick et al., 2004; Glombick et al., 2006a,b; Massey and Duffy, 2007). Several of these studies have questioned the significance of the OVsz as a major crustal-scale detachment (e.g. Thompson and Unterschutz 2004; Glombick et al., 2006a,b). Hanging wall rocks mapped in a series of semi-continuous unconformable outliers across the trace of the OVsz within its footwall domain are used as evidence to suggest the footwall was not exhumed by a km-scale crustal detachment (e.g. Glombick et al., 2006a). A zone of northeast-directed channelized ductile flow between the overlying superstructure, including hanging

wall rocks of the OVsz, and the underthrusting of a crystalline basement crustal-scale ramp is interpreted to have developed in the Late Cretaceous to early Paleogene (Glombick et al., 2006a). Furthermore, the observation that non-coaxial mylonites are not continuously exposed along the entire strike of the OVsz, but appear in "pockets", further complicates interpretation of the OVsz as a crustal-scale detachment (Glombick et al., 2006a).

Alternatively, the discrepancies mentioned above may due to the formation of displacement parallel, syn-extensional open, upright, multi-scale folds, referred to as corrugations, which affect the map-scale geometry of the OVsz (Fig. 2.17; Brown, 2010). Syn-extensional corrugations such as these are inherent features commonly observed within extensional shear zones flanking core complexes, with hinges that parallel the direction of extensional displacement (Spencer, 1999; Singleton & Mosher, 2012). The corrugations that affect the OVsz are defined by the change in direction of the dip of the average contoured foliation and may explain the changes in lithology and shear zone angle along strike (Christie, 1973; Ryan 1973; Ross, 1981; Brown, 2010; this study). Hanging wall units that encroach into the footwall domain of the OVsz occur in synformal lows where the fault dip is shallow (Christie 1973; Ryan 1973; Ross 1981; Bardoux, 1993; Brown, 2010). In contrast, granitoid units and the high-grade gneiss of the footwall occur in antiformal highs where the shear zone arches over them at a higher angle (Christie, 1973; Ryan 1973; Ross, 1981; Brown, 2010; this study).

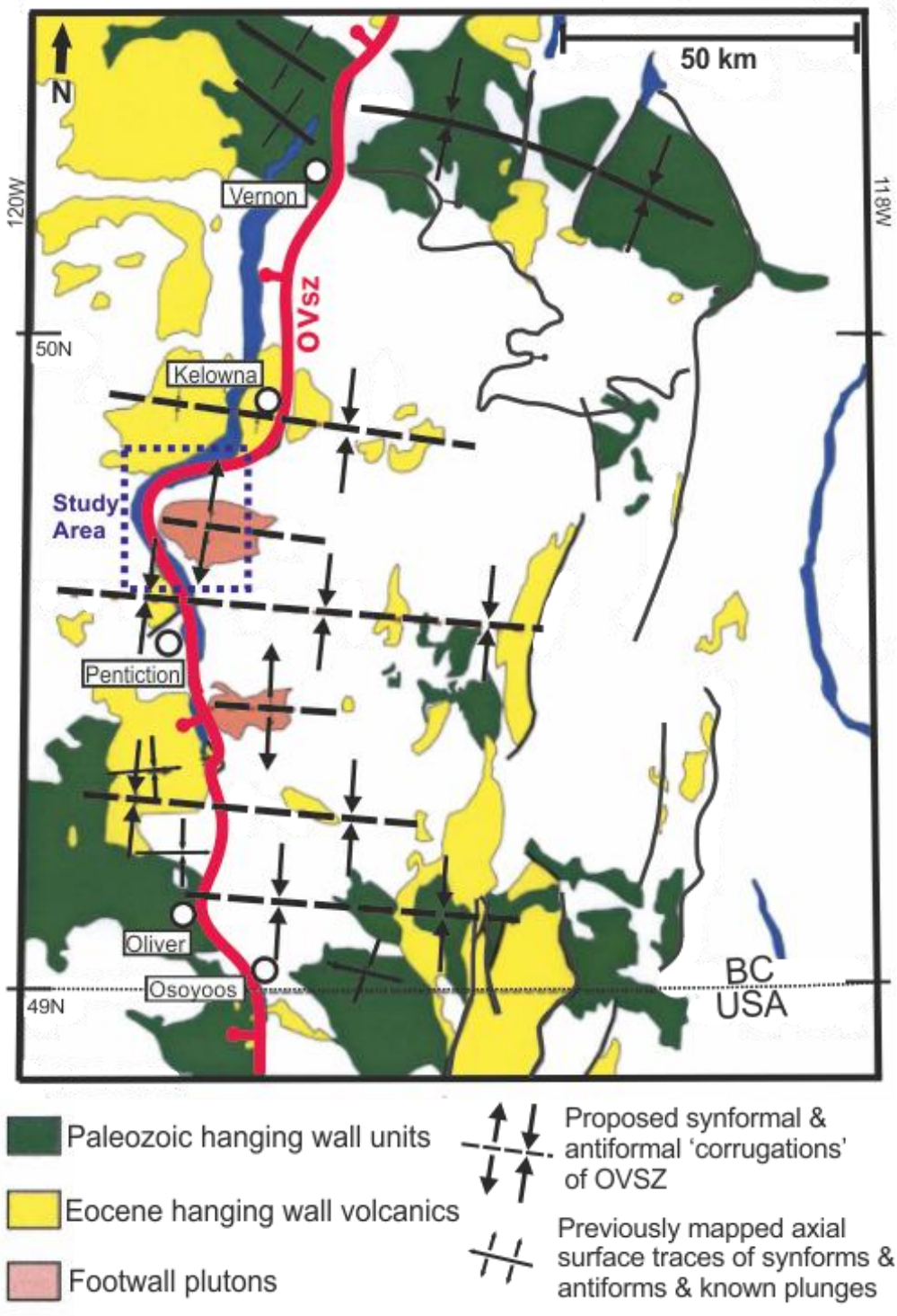

Figure 2.15. Simplified geology map highlighting the inferred corrugations in the footwall

Note how the 'semi-continuous' hanging wall stratigraphy crosses the Okanagan Valley shear zone within synformal keels (Modified after Okulitch, 1987; Brown, 2010).

Lithological mapping in this study appears compatible with this hypothesis. The attitude of the foliation of the mylonitic gneiss in the study area defines a west-northwest trending, kilometre-scale, open, upright, antiform cored by a monzonitic to syenitic pluton (see Chapter 2). This antiform is interpreted to belong to one of a series of kilometre-scale antiformal corrugations (Brown, 2010; Fig. 3.2). The augen gneissic unit in the south end of the study area (see section 2.4.1) may be beyond the inflection point of the antiform, representing the outer northern limb of a synformal keel.

The OVsz is interpreted to have developed in a transtensional regime (e.g. Price and Carmichael, 1986; Harms and Price, 1992). As alluded to above, in similar tectonic settings, the occurrences of warped or corrugated detachments are commonly observed (Bartley et al., 1990; Chauvet and Seranne, 1994; Kurz and Neubauer, 1996; Spencer, 1999; Singleton, 2013). The observation that the fold axes are parallel to the inferred extensional direction, coupled with the minimal deflection of the metamorphic isograd surfaces, suggests these undulations are syn-extensional rather than forming during a later folding event (Christie 1973; Ryan 1973; Ross 1981; Bardoux, 1993; Brown, 2010; this study).

To further test the corrugations hypothesis, future projects could collect microstructural and petrofabric data along strike of the OVsz to check for variations that could be attributable to antiformal or synformal corrugations. For instance, quartz recrystallization mechanisms and petrofabrics in this study were collected on the limbs of an antiformal pericline with samples selected based on their approximate structural depth. These limbs were prioritized due to the apparent ease of approximating their location within the structural section and to maintain lithological consistency between the samples. Future mapping projects may utilize similarly styled structural transects and sampling strategies in individual antiformal and synformal corrugations. Transects could compare kinematic data from limb to hinge to limb to decipher how non-coaxiality of flow, strain geometry, sense of shear and deformation temperatures vary across a folded surface of the OVsz. Additionally, this system could be utilized to compare

the thermo-kinematic data of the exposed antiformal periclines with adjacent synformal keels along strike of the OVsz.

2.7.6. Formation of late, high angle faults within footwall domain

Along-strike warping of the detachment is possibly a late stage feature owing to rapid exhumation (vertical transport) and doming of the lower plate (i.e., a nascent metamorphic core complex), and is often synchronous with, or postdates, the formation of extension-parallel folds (Spencer, 1982; Buck, 1988; Wernicke and Axen, 1988; Bartley et al., 1990; Spencer and Reynolds, 1991). The axis of doming of the detachment is inferred to be transient (i.e. rolling hinge; Buck, 1988), so that all of the detachment and hanging wall are warped to some degree before the upper plate is eventually breached to form an exposed metamorphic core complex. The final stage of this warping is possibly seen in the study area by the high-angle, brittle fractures striking perpendicular to the direction of extension attributed to isostatic bending stresses related to footwall rollover as the gneisses and plutonic rocks (footwall of the OVsz) were exhumed to the surface (Tucholke et al., 1998).

2.8. Conclusions

1. Detailed structural and bedrock mapping coupled with quartz recrystallization mechanisms and crystallographic preferred orientation (CPO) analysis corroborates the OVsz as a major, crustal-scale extensional detachment that exhumed rocks from the middle crust that were metamorphosed at amphibolite-facies conditions.

2. Three lithostructural domains are defined within the OVsz that grade structurally downward from: the upper 200 m of the vertical structural section consisting of cataclasite and ultramylonite (Domain 1); to greenschist and amphibolites-facies mylonites from ~200-600 m (Domain 2); and at 600-1500 m, weakly to moderately developed mylonites interfingered with a weakly- to undeformed pluton (Domain 3). The relatively lower deformation temperatures and brittle overprint of Domain 1 are localized in the northwestern part of the study area where the attitude of the foliation defines the northern limb of an antiform that warps the shear zone.

3. Meso- to microstructural kinematic indicators down the structural section are characterized by a consistent top-to-the WNW sense of shear with a few quartz c-axis fabrics deeper in the shear zone indicating a top-to-the ENE shear sense.

4. The bulk of quartz a-axis patterns suggest general plane strain conditions across the shear zone with slight onset of constrictional strain towards the structural top of Domain 1.

5. Deformation temperatures indicated by quartz recrystallization mechanisms and quartz c-axis fabrics range from ~280 to >650 °C and progressively increase with respect to structural depth beneath the inferred upper surface of the detachment. Estimated isothermal surfaces are projected within the study area and are broadly parallel to the dip of the penetrative foliation planes. The observed telescoping of ~280-650 °C isotherms within a ~1-1.5 km vertical structural section suggests an elevated geotherm in the range of 300-400 °C/km in the immediate footwall of the OVsz.

6. We propose a model whereby microstructures and CPO fabrics in structurally lower rocks with originally higher deformation temperatures to be ‘locked-in’ as they migrated out of the active zone of deformation during exhumation of the footwall to upper crustal levels. These locked-in higher temperature fabrics were passively exhumed along an ESE trajectory that resulted in their continuous juxtaposition against lower temperature fabrics that were being generated in the progressively narrowing active part of the WNW-directed shear zone. The component of overprinting of the lower temperature fabrics on the higher temperature fabrics was confined to structurally higher levels where the shear zone narrowed approaching the surface with the deepest level fabrics remained relatively unscathed during exhumation.

Chapter 3.

Conclusions

The Shuswap metamorphic complex in the southern Canadian Cordillera formed in response to a period of crustal thickening in excess of 55 km following a compressional phase during the Mesozoic and Paleogene (Brown et al., 1986; Parrish et al., 1988; Price and Monger, 2002; Brown and Gibson, 2006; Gibson et al., 2008). Deeply buried parts of the complex were exhumed to upper crustal levels during the Eocene (Tempelman-Kluit and Parkinson, 1986; Parrish et al., 1988; Parrish 1995) in response to a change from transpression to transtension between the North American and Pacific plates during the Paleogene (Ewing, 1980; Price and Carmichael, 1986). Eocene exhumation of the southern Shuswap metamorphic complex was, in part, facilitated by crustal-scale extension along the Okanagan Valley shear zone (OVsz) (Tempelman-Kluit and Parkinson, 1986; Parrish et al., 1988; Bardoux, 1993; Johnson and Brown, 1996; Johnson 2006; Brown et al., 2012). The shear zone marks the western-most, and structurally-highest margin of the Shuswap metamorphic complex exhibiting a major metamorphic and thermochronological offset, juxtaposing the penetratively deformed amphibolite to granulite-facies rocks of the Shuswap metamorphic complex in the footwall to the east with greenschist-facies to unmetamorphosed hanging wall rocks to the west (Tempelman-Kluit and Parkinson, 1986; Parrish et al., 1988; Bardoux, 1993; Johnson and Brown, 1996; Johnson 2006; Brown et al., 2012). The OVsz is characterized by a < 30° west-dipping, 1-2 km-thick, ductile shear zone capped by a brittle detachment surface. The OVsz includes prominent west-northwest trending elongation lineations with fabrics consistently indicative of relative WNW displacement of the hanging wall (Parkinson, 1985;

Journeay and Brown, 1986; Tempelman-Kluit and Parkinson, 1986; Bardoux, 1993; Brown et al., 2012; this study).

The OVsz in the vicinity of the Okanagan Mountain Provincial Park in southern BC is warped by a west-northwest trending, kilometre-scale, open, antiform that is interpreted to be one of the antiformal corrugations that characterize the OVsz (Brown, 2010). Here, the OVsz grades upwards from a non- to weakly mylonitized syntectonic pluton, to mylonitic to ultramylonitic ortho- and paragneiss and tectonized felsic intrusions, with a thin band of cataclasite at the top of the section. Deformation temperatures indicated by quartz recrystallization mechanisms and quartz c-axis fabrics from these rocks range from ~280 to >650 °C, and progressively increase with respect to structural depth beneath the inferred upper detachment. Quartz a-axis patterns suggest deformation occurred primarily under general plane strain conditions with slight onset of constrictional strain towards the structural top of the shear zone. Inferred isothermal surfaces are broadly parallel to the dip of the penetrative foliation planes. The observed telescoping of the ~280 to 650 °C isotherms within a ~1-1.5 km vertical structural section suggests an elevated geotherm in the range of 300-400 °C per km in the immediate footwall of the OVsz.

This intense telescoping of isotherms could have been due to microstructures and CPO fabrics in structurally lower rocks with originally higher deformation temperatures being ‘locked-in’ as they migrated out of the active zone of deformation during exhumation of the footwall to upper crustal levels, These higher temperature fabrics were passively exhumed along a trajectory that resulted in their continuous juxtaposition against lower temperature fabrics that were being generated in the progressively narrowing active part of the shear zone in higher crustal levels. This resulted in an apparent compression of deformation isotherms within the 1-1.5 structural section of the OVsz.

References

Archibald, D.A, Krough, T.E., Armstrong, RL., and Farrar, E. 1984. Geochronology and tectonic implications of magmatism and metamorphism, southern Kootenay arc and neighboring regions, southeastern British Columbia. Part II: mid-Cretaceous to Eocene. Canadian Journal of Earth Sciences 21, 567-583.

Armstrong, R 1982. Cordilleran metamorphic core complexes - from Arizona to southern Canada. Annual Reviews of Earth Planetary Science 10, 129-154.

Armstrong, RL., Parrish, RR, van der Heyden, P., Scott, K., Runkle, D., and Brown, RL. 1991. Early Proterozoic basement exposures in the southern Canadian Cordillera: core gneiss of Frenchman Cap, Unit I of the Grand Forks Gneiss, and the Vaseaux Formation. Canadian Journal of Earth Sciences 28, 1161-1201.

Axen, G.J. 2004.Mechanics of low-angle normal faults: in Karner, G. , Taylor, B., Driscoll, N., and Kohlstedt, D.L. (eds.) Rheology and Deformation in the Lithosphere at Continental Margins, Columbia University Press, 46-91.

Bardoux, M. 1993. The Okanagan Valley normal fault from Penticton to Enderby-Southcentral British Columbia. Ph.D. Dissertation, Carleton University, Ottawa, Ontario, 292 p.

Bardoux, M., Mareschal, J.-C., 1994. Extension in south-central British Columbia; mechanical and thermal controls. Tectonophysics, 238(1-4): 451-470.

Barth, N.C., Hacker, B.R., Seward, G.G.E., Walsh, E.O., Young, D., Johnston, S., 2010. Strain within the ultrahigh-pressure western Gneiss region of Norway recorded by quartz CPOs. In: Law, R., Butler, R., Holdsworth, R., Krabbendam, M., Strachan, R. (Eds.), Continental Tectonics and Mountain Building: The Legacy of Peach and Horne. Geological Society, London, Special Publication.

Bartley, J. M., Fletcher, J. M., and Glazner, A. F. 1990. Tertiary extension and contraction of lower-plate rocks in the central Mojave metamorphic core complex, southern California. Tectonics 9, 521- 534.

Beaumont, C., Jamieson, R.A., Nguyen, M.H., and Lee, B. 2001. Himalayan tectonics explained by extrusion of a low-viscosity crustal channel coupled to focused surface denudation. Nature 414, 738-742.

Beaumont, C., Jamieson, R.A., Nguyen, M.H., and Medvedev, S. 2004. Crustal channel flows: 1. Numerical models with applications to the tectonics of the Himalayan-Tibetan orogen. Journal of Geophysical Research 109.

Beranek, L. P., Mortensen J. K., Orchard, M.J., and Ullrich, T. 2010. Provenance of North American Triassic strata from west-central and southeastern Yukon; correlations with coeval strata in the Western Canada Sedimentary Basin and Canadian Arctic Islands. Canadian Journal of Earth Sciences 47(1): 53-73.

Blumenfeld, P., Mainprice, D. and Bouchez, J.L., 1986. C-slip in quartz from subsolidus deformed granite. Tectonophysics 127, pp. 97-115.

Brown, R. L. and J. M. Journeay 1987. Tectonic denudation of the Shuswap metamorphic terrane of southeastern British Columbia, Geology 15(2), 142-146.

Brown, RL. and Carr, S.D. 1990. Lithospheric thickening and orogenic collapse within the Canadian Cordillera. In Proceedings, Pacific Rim Congress 90, University of Queensland,Brisbane, Australia 2, 1-10.

Brown, R.L., Gibson, H.D., 2006. An argument for channel flow in the southern Canadian Cordillera and comparison with Himalayan tectonics. In: Law, R.R., Searle, M.P., Godin, L. (Eds.), Channel flow, ductile extrusion and exhumation in continental collision zones. Geological Society special publication. Geological Society, London, pp. 543-559.

Brown, S.R., 2010. Geology and Geochronology of the Southern Okanagan Valley Shear Zone, Southern Canadian Cordillera, British Columbia, Simon Fraser University, Burnaby, 320 pp.

Brown, S. R., Gibson, H. D., Andrews, G.D.M., Thorkelson, D.J., Marshall, D.D., Vervoort, J.D., Rayner N., 2012. New constraints on Eocene extension within the Canadian Cordillera and identification of Phanerozoic protoliths for footwall gneisses of the Okanagan Valley shear zone. Lithosphere 4, 354-377.

Brown, R. L. Journeay, J. M. Lane, L. S. Murphy,D. C. Rees, C. J. 1986. Obduction, backfolding and piggyback thrusting in the metamorphic hinterland of the southeastern Canadian Cordillera, Journal of Structural Geology 8, 255-268, doi:10.1016/0191-8141(86)90047-7.

Buck, W.R 1988. Flexural rotation of normal faults. Tectonics 7, 959-973.

Chauvet, A, and Seranne, M. 1994. Extension-parallel folding in the Scandinavian Caledonides: implications for late-orogenic processes. Tectonophysics 238, 31-54.

Christie, J.S., 1973. Geology of the Vaseaux Lake Area, University of British Columbia, 139 pp.

Church, B.N. 1973. Geology of the White Lake Basin, British Columbia. Department of Mines and Petroleum Resources, Bulletin 61, 3-141.

Church, B.N. 1985. Volcanology and structure of Tertiary outliers in south-central BritishColumbia. Field Trip Guidebook, B.C. Ministry of Energy. Mines, and Petroleum Resources, 46p.

Colpron, M. Warren, M. J. Price, R. A. 1998. Selkirk fan structure, southeastern Canadian Cordillera: Tectonic wedging against an inherited basement ramp, Geol. Soc. Am. Bull. 110, 1060– 1074, doi:10.1130/0016-7606(1998)110<1060.

Colpron, M., Nelson, J.L., and Murphy, D.C. 2007. Northern Cordilleran terranes and their interactions through time. Geological Society of America Today 17, 4-10.

Coney, P.J. 1980. Cordilleran metamorphic core complexes: An overview. In Cordilleran metamorphic core complexes. Edited by M. Crittenden, P. Coney, P. and G. Davis, G. Geological Society of America Memoir, 153: 7-31.

Coney, P.J., Jones, D.L. and Monger, J.W.H. 1980. Cordilleran suspect terranes. Nature 288, 329-333.

Coney, P.I., Harms, T.A 1984. Cordilleran metamorphic core complexes: Cenozoic extensional relics of Mesozoic compression. Geology, 12: 550-554.

Cook, F.A, Green, AG., Simony, P.S., Price, RA, Parrish, RR, Mike eit, B., Gordy, P.L., Brown, RL., Coflin, KC., and Patenaude, C. 1988. Lithoprobe seismic refection structure of the southeastern Canadian Cordillera: initial results. Tectonics 7, 157-180.

Cook, F.A., Varsek, J.L., Clowes, R.M., Kanasewich, E.R., Spencer, C.S., Parrish, R.R., Brown, R.L., Carr, S.D., Johnson, B.J., Price, R.A., 1992. Lithoprobe crustal reflection cross section of the southern Canadian Cordillera, 1. Foreland thrust and fold belt to Fraser River fault. Tectonics 11, 12–35.

Davis, G. A., Monger, J.W.H., Burchfiel, B. C., 1978, Mesozoic construction of the Cordilleran 'collage,' central British Columbia to central California, in Howell, D. G., and McDougall, K. A., eds., Mesozoicpaleogeography of the western United States: Society of Economic Paleontologists and Mineralogists, Pacific Section,Pacific Coast Paleogeography Symposium 2, 1-32.

Engebretson, D.C., Cox, A, Gordon, R.G. 1984. Relative motions between oceanic plates of the Pacific Basin. Journal of Geophysical 89, 10291-10310.

Ewing, T.E. 1980. Paleogene tectonic evolution of the Pacific Northwest. Journal of Geology 88, 619-638.

Fossen, H., 2010. Structural Geology. Cambridge University Press, Cambridge.

Fox, K.F., Jr., Rinehart, C.D., Engels, J.c., and Stern, T.W. 1976. Age of emplacement of the Okanogan gneiss dome, north-central Washington. Geological Society ofAmerica Bulletin 87, 1217-1224.

Gervais, F., Brown, R. L., 2011. Testing modes of exhumation in collisional orogens: Synconvergent channel flow in the southeastern Canadian Cordillera,

Gibson, RD., Brown, R.L., Carr, S.D., 2008. Tectonic evolution of the Selkirk fan, southeastern Canadian Cordillera: A composite Middle Jurassic-Cretaceous orogenic structure. Tectonics, 27(6).

Gibson, H. D., Brown, R. L., Carr, S.D., 2005. U/Th- Pb geochronologic constraints on the structuralnevolution of the Selkirk fan, northern Selkirk Mountains, southern Canadian Cordillera, Journal of Structural Geology 27, 1899–192.

Glombick, P., Thompson, R.I., Erdmer, P., Daughtry, K.L., 2006a. A reappraisal of the tectonic significance of early Tertiary low-angle shear zones exposed in the Vernon map area (82 L), Shuswap metamorphic complex, southeastern Canadian Cordillera. Canadian Journal of Earth Sciences 43(2), 245-268.

Glombick, P., Thompson, R., Erdmer, P., Heaman. L., Friedman, M.. Villeneuve, M., Daughtry, K. 2006b. U-Pb constraints on the thermotectonic evolution of the Vernon antiform and the age of the Aberdeen gneiss complex, southeastern Canadian Cordillera. Canadian Journal of Earth Sciences 43(2), 213-244.

Godin, L., Grujic, D., Law, R.D., and Searle, M.P. 2006. Channel flow, ductile extrusion and exhumation in continental collision zones: an introduction. In: Law, R.D., Searle, M.P., and Godin, L. (eds). Channel Flow, Ductile Extrusion and Exhumation in Continental Collision Zones. Geological Society of London Special Publications, 268: 1-23.

Gottardi, R., Teyssier, C., Mulch, A., Vennemann, T.W., Wells M.L, 2011. Preservation of an extreme transient geotherm in the Raft River detachment shear zone, Geology, 39(8), 759-762.

Grujic, D., and Mancktetow, N.S. 1995. Folds with axes parallel to the extension direction: an experimental study. Journal of Structural Geology 17, 279-291.

Guillope M, Poirier J-P 1979 Dynamic recrystallization during creep of single-crystalline halite: an experimental study. Journal of Geophysical Research 84, 5557–5567.

Hansen, V.L., Goodge, J.W., 1988, Metamorphism, structural petrology, and regional evolution of the Okanogan complex, northeastern Washington, *in* Metamorphism and Crustal Evolution of the Western United States, Rubey Colloquium 7, 233–270.

Harms, T.A., Price, R.A., 1992. The Newport fault: Eocene listric normal faulting, mylonitization. and crustal extension in northeast Washington and northwest Idaho. Geological Society of America Bulletin 104, 745-761.

Hanmer, S., Passchier, C., 1991. Shear-Sense Indicators: A Review: Geological Survey of Canada Current Research 90-17, 72 p.

Helwig, J., Ed. (1974). Eugeosynclinal basement and a collage concept of orogenic belts. eds. Dott, R.H., Jr.

Hirth, G., Tullis, J., 1992. Dislocation creep regimes in quartz aggregates. Journal of Structural Geology 14, 145-159.

Hobbs, B. E. 1985. The geological significance of microfabric. In: Preferred Orientation in Deformed Metals and Rocks (edited by Wenk, H.-R.). Academic Press, Orlando.

Johnson, B.J., 1994. Structure and tectonic setting of the Okanagan Valley fault system in the Shuswap Lake area, southern British Columbia. Ph.D. Thesis, Carleton University, 281 pp.

Johnson, B.J., 2006. Extensional shear zones, granitic melts, and linkage of overstepping normal faults bounding the Shuswap metamorphic core complex, British Columbia. GSA Bulletin, 118(3/4): 366-382.

Johnson, B.J., Brown, R.L., 1996. Crustal structure and early Tertiary extensional tectonics of the Omineca belt at 51degrees N latitude, southern Canadian Cordillera. Canadian Journal of Earth Sciences, 33(12): 1596-1611.

Kruckenberg, S.C., and Whitney, D.L., 2011, Metamorphic evolution of sapphirine- and orthoamphibole- cordierite–bearing gneiss, Okanogan Dome, Washington, USA: Journal of Metamorphic Geology 29, 425–449, doi:10.1111/j.1525-1314.2010.00926.x.

Kruckenberg, S.C., Whitney, D.L., Teyssier, c., Fanning, C.M., Dunlap, W.J. 2008.Paleocene-Eocene migmatite crystallization, extension, and exhumation in the interland of the northern Cordillera: Okanogan dome, Washington, USA. Geological SocietyAmerica Bulletin 120, 912-929.

Kruhl, J.H., 1996. Prism- and basal-plane parallel subgrain boundaries in quartz: a microstructural geothermobarometer. Journal of Metamorphic Geology 14, 581-589.

Kruhl, J.H., 1998. Prism- and basal-plane parallel subgrain boundaries in quartz: a microstructural geothermobarometer: Reply. Journal of Metamorphic Geology 16, 142-146.

Kurz, W., and Neubauer, F. 1996. Deformation partitioning during updoming of the Sonnblick area in the Tauern Window (Eastern Alps, Austria). Journal of Structural Geology 18, 1327-1343.

Laberge, J.D., and Pattison, D.R.M., 2007, Geology of the western margin of the Grand Forks complex, southern British Columbia: High-grade Cretaceous metamorphism followed by Early Tertiary extension on the Granby fault: Canadian Journal of Earth Sciences, 44, 199–228.

Langille, J.M., Jessup, M.J., Cottle, J.M., Newell, D., Seward, G., 2010. Kinematic evolution of the Ama Drime Detachment: insights into orogen-parallel extension and exhumation of the Ama Drime Massif, Tibet-Nepal. Journal of Structural Geology 32, 900-919.

Larson, K.P. and Godin, L. 2009. Kinematics of the Greater Himalayan sequence, Dhaulagiri Himalayas: implications for the structural framework of central Nepal. Journal of the Geological Society, London 166, 25-43.

Law, R.D., 1990. Crystallographic fabrics: a selective review of their applications to research in structural geology. In: Knipe, R.J., Rutter, E.H. (Eds.), Deformation Mechanisms, Rheology and Tectonics. Geological Society, London, Special Publication 54, 335-352.

Law, R.D., Searle, M.P., Simpson, R.L., 2004. Strain, deformation temperatures, and flow at the top of the Greater Himalayan Slab, Everest Massif, Tibet. Journal of the Geological Society, London 161, 305-320.

Law, R.D., Mainprice, D., Casey, M., Lloyd, G.E., Knipe, R.J., Cook, B., Thigpen, J.R., 2010. Moine thrust zone mylonites at the stack of Glencoul: I microstructures, strain and influence of recrystallization on quartz crystal fabric development. In: Law, R.D., Butler, R.W.H., Holdsworth, R., Krabbendam, M., Strachan, R.A. (Eds.), 2010. Continental Tectonics and Mountain Building. The Legacy of Peach and Horne, 335. Geological Society, London, Special Publication, 543-577.

Law, R.D., Jessup, M.J., Searle, M.P., Francsis, M.K., Waters, D.J., Cotte, J.M., 2011. Telescoping of isotherms beneath the South Tibetan Detachment System, Mount Everest Massif. Journal of Structural Geology, 33, 1569-1594.

Law, R. D.; Stahr, D. W.; Francsis, M. K.; Ashley, K. T.; Grasemann, B.; Ahmad, T., 2013. Deformation temperatures and flow vorticities near the base of the Greater Himalayan Series, Sutlej Valley and Shimla Klippe, NW India. Journal of Structural Geology, 54, 21-53.

Lister, G.S., 1977. Discussion: Crossed girdle c-axis fabrics in quartzites plastically deformed by plane strain and progressive simple shear. Tectonophysics 39, 51-54.

Lister, G.S., Price, G.P., 1978. Fabric development in a quartz-feldspar mylonite. Tectonophysics 49 (1-2), 37-78.

Lister, G.S., Paterson, M.S., Hobbs, B.E., 1978. The simulation of fabric development in plastic deformation and its application to quartzite: the model. Tectonophysics 45, 107-158.

Lister, G.S., Paterson, M.S., 1979. The simulation of fabric development during plastic deformation and its application to quartzite: fabric transions. Journal of Structural Geology 1 (2), 99-115.

Lister, G.S. Hobbs, B.E., 1980. The simulation of fabric development during plastic deformation and its application to quartzite: the influence of deformation history. Journal of Structural Geology 2, 335-352.

Lister, G.S., Williams, P.F., 1983. The partitioning of deformation in flowing rock masses. Tectonophysics 92,, 1-33.

Lister, G.S., Snoke, A.W., 1984. S-C Mylonites. Journal of Structural Geology 6 (6), 617-638.

Lister, G.S. Davis, G. A. 1989. The origin of metamorphic core complexes and detachment faults during Tertiary continental extension in the northern Colorado River region, USA. Journal of Structural Geology, 11, 65-94.

Massey, N.W.D., Duffy, A., 2007. Boundary Project: N,[cKinney Creek (NTS 82E/03) and Beaverdell (NTS 82FJ06E, 07W, lOW, llW) Areas, South-Central British Columbia. B.e. Ministry of Energy, Mines and Petroleum Resources, Geological Field workPaper 2008-1, p. 99-107.

Mainprice, D., Bouchez, J.L., Blumenfeld, P., Tubia, J.M., 1986. Dominant c-slip in naturally deformed quartz: implications for dramatic plastic softening at high temperature. Journal of Geology 14, 819-822.

Mathews, W. 1981. Early Cenozoic resetting of potassium-argon dates and geothermalhistory of north Okanagan area, British Columbia. Canadian Journal of Earth Sciences 18, 1310-1319, 198.

McClaughry, J.D., Gaylord, D.R., 2005. Middle Eocene sedimentary and volcanic infilling of an evolving supradetachment basin: White Lake Basin, south-central British Columbia. Canadian Journal of Earth Sciences 42, 49-66.

McDougall, I. Harrison, T.M., 1999. Geochronology and thermochronology by the 40Ar/39Ar method: 2nd edition, New York, Oxford University Press, 269 p.

Medford, G.A 1975. K-Ar and fission track geochronometry of an Eocene thermal event in the Kettle River (west half) map area, southern British Columbia. Canadian Journal of Earth Sciences 12, 836-843.

Monger, J., Price, R , 2002. The Canadian Cordillera: Geology and Tectonic Evolution. Canadian Society of Exploration Geophysicists Recorder, 17: 17-36.

Monger, J.W.H., Price, R.A., Tempelman-Kluit, D.J., 1982. Tectonic accretion and the origin of the two major metamorphic and plutonic welts in the Canadian Cordillera. Journal of Geology, 10, 70-75.

Nelson, J.L., Colpron, M., Piercey, S.J., Dusel-Bacon, C., Murphy, D.C., and Roots, C.F. 2006. Paleozoic tectonic and metallogenic evolution of the pericratonic terranes in Yukon, northern British Columbia and eastern Alaska. In Paleozoic evolution and metallogeny of pericratonic terranes at the ancient Pacific margin of North America, Canadian and Alaskan Cordillera. eds.M. Colpron and J.L. Nelson. Geological Association of Canada, Special Paper 45, pp. 323–360.

Okulitch. A.V., 1984. The role of the Shuswap metamorphic complex in Cordilleran tectonism: A review. Canadian Journal of Earth Sciences 21, 1171-1193.

Okulitch, A.V., 1987. Comment on "Extension across the Eocene Okanagan crustal shearin southern British Columbia." Geology 15, 187-188.

Parkinson, D.L., 1985. U-PB geochronometry and regional geology of the southern Okanagan Valley, British Columbia; the western boundary of a metamorphic core complex. MSc Thesis, University of British Columbia.

Parrish, R.R., 1995. Thermal evolution of the southeastern Canadian Cordillera. Canadian Journal of Earth Sciences 32, 1618-1642.

Parrish, R.R., Carr, S.D., Parkinson, D.L., 1988. Eocene extensional tectonics and geochronology of the southern Omineca Belt, British Columbia and Washington. Tectonics, 7(2): 181-212.

Passchier, C.W., Trouw, R.A.J., 2005. Microtectonics, second ed. Springer, Berlin, 366 pp.

Peternell, M., Kohlmann, F., Wilson, C.J.L., Seiler, C., Gleadow, A.J.W., 2009. A new approach to crystallographic orientation measurement for apatite fission track analysis: Effects of crystal morphology and implications for automation. Chemical Geology 265, 527-539.

Peternell, M., Hasalová, P., Wilson, C.J.L., Piazolo, S. and Schulmann, K. 2010. Evaluating quartz crystallographic preferred orientations and the role of deformation partitioning using EBSD and fabric analyser techniques. Journal of Structural Geology 32, 803–817.

Pfiffner, O.A., Ramsay, J.G., 1982. Constraints on geological strain rates, arguments from finite strain states of naturally deformed rocks. Journal of Geophysical Research 87, 311-321.

Price, R.A., 1986. The southeastern Canadian Cordillera: Thrust faulting, tectonic wedging, and delamination of the lithosphere. Journal of Structural Geology 8, 239-254.

Price, R.A., Monger, J.W.H., Roddick, J.A., 1985. Cordilleran cross-section: Calgary to Vancouver. In: Field Guides to Geology and Mineral Deposits in the Southern Canadian Cordillera: GSA Cordilleran Section Meeting, Vancouver, B. C., May '85. D.J. Tempelman-Kluit (ed.). Vancouver, Geological Society of America Cordilleran Section, 371-385.

Price, RA., Carmichael, D.M., 1986. Geometric test for Late Cretaceous-Paleogene intracontinental transform faulting in the Canadian Cordillera. Geology 14, 468-471.

Price, R.A. Mountjoy, E.W., 1970. Geologic structure of the Canadian Rocky Mountains between Bow and Athabasca Rivers: A progress report. In: Structure of the Southern Canadian Cordillera. J.O. Wheeler (ed.). Geological Association of Canada, Special Publication no. 6, 7-25.

Prior, D.J., Boyle, A.P., Brenker, F., Cheadle, M., Day, A., Lopez, G., Peruzzo, L., Potts, G.J., Reddy, S., Spiess, R., Timms, N.E., Trimby, P., Wheeler, J., and Zetterström, L.1999. The application of electron backscatter diffraction and orientation contrast imaging in the SEM to textural problems in rocks. American Mineralogist 84, 1741-1759.

Prior, D.J. 2009. EBSD in the earth sciences: application, common practice and challenges. In: Schwartz, A.J., Kumar, M., Adams, B.L., Field, D.P. (eds.). Electron Backscatter Diffraction in Materials Science. Springer Science and Business Media, New York. 345-360.

Pryer, L.L., 1993. Microstructures in feldspars from a major crustal thrust zone: the Grenville Front, Ontario, Canada. Journal of Structural Geology 15, 21-36.

Read, P.B., Brown, RL., 1981. Columbia River fault zone: Southeastern margin of the Shuswap and Monashee complexes, southern British Columbia. Canadian Journal of Earth Sciences 18, 1127-1145.

Rey, P., Teyssier, C., and Whitney, D.L., 2009, Extension rates, crustal melting, and core complex dynamics,Geology 37, 391–394.

Reynolds, S.J., 1982, Geology and geochronology of the South Mountains, central Arizona (Ph.D. thesis): Tucson, University of Arizona, 220 p.

Roddick, C., Farrar, E., and Procyshyn, E.L. 1972. Potassium-Argon ages of igneous rocks from the area near Hedley, southern British Columbia. Canadian Journal of Earth Sciences 9, 1632-1639.

Ross, J.V. 1974. A Tertiary Thermal Event in South-Central British Columbia. Canadian Journal of Earth Sciences 11, 1116-1122.

Ross, I.V. 1981. A geodynamic model for some structures within and adjacent to the Okanagan Valley, southern British Columbia. Canadian Journal of Earth Sciences 18, 1581-1598.

Ryan, D. 1973. Structural geology and Rb/Sr geochronology of the Anarc ist Mountain area, south-central British Columbia. Ph.D. Dissertation, University of British Columbia, Vancouver, B.C., 256 pp.

Schmid, S.M., Casey, M., 1986. Complete fabric analysis of some commonly observed quartz c-axis patterns. In: Hobbs, B.E., Heard, H.C. (Eds.), Mineral and Rock Deformation: Laboratory StudiesdThe Paterson Volume. American Geophysical Union Monograph, 36. American Geophysical Union, pp. 246-261.

Shaver, R.H. Modern and ancient geosynclinal sedimentation, Society of Economic Paleontologists and Mineralogists Special Publication. v 19, p. 359-380.

Singleton, J.S. 2013. Development of extension-parallel corrugations in the Buckskin-Rawhide metamorphic core complex, west-central Arizona. GSAB, 125, 453-472.

Singleton, J.S., Mosher, S. 2012. Mylonitization in the lower plate of the Buckskin-Rawhide detachment fault, west-central Arizona: Implications for the geometric evolution of metamorphic core complexes. Journal of Structural Geology 39, 180-198.

Spencer, J.E. 1982. Origin of folds in Tertiary low-angle fault surfaces, so theastern California and western Arizona. In Mesozoic- Cenozoic Tectonic Evolution of th Colorad River Region, California, Nevada and Arizona. Edited by E.G. Frost, D.L. Martin, Cordilleran Publishers, San Diego, CA, p. 123-134.

Spencer, J.E. 1999. Geologic continuous casting below continental and deep-sea detachment faults and at the striated extrusion of Sacsayhuamán, Peru. Geology, v. 27, p. 327-330.

Spencer, J.E., and Reynolds, SJ. 1991. Tectonics of mid-Tertiary extens on along a transect through west-central Arizona. Tectonics 10, 1204-1221.

Stevens, R.D., DeLabio, RN., and Lachance, G.R 1982. Age determination and geologic studies: K-Ar isotopic ages. Report 16, Geological Survey of Canada, Paper 82-2, 56p.

Stipp, M., Stünitz, H., Heilbronner, R., Schmid, S.M., 2002a. The eastern Tonale fault zone: a 'natural laboratory' for crystal plastic deformation of quartz over a temperature range from 250 to 700℃. Journal of Structural Geology 24, 1861-1884.

Stipp, M., Stünitz, H., Heilbronner, R., Schmid, S.M., 2002b. Dynamic recrystallization of quartz: correlation between natural and experimental conditions. In: De Meer, S., Brury, M.R., De Brasser, J.H.P., Pennock, G.M. (Eds.), Deformation Mechanisms, Rheology and Tectonics: Current Status and Future Perspectives. Geological Society, London, Special Publication 200, 171-190.

Struik, L.C., 1993. Intersecting intracontinental Tertiary transform fault systems in the North American Cordillera. Canadian Journal of Earth Sciences 30, 1262-1274.

Sullivan, W.A., 2013. L tectonites. Journal of Structural Geology 50, 161-175.

Sullivan, W.A., Beane, R.J. 2010. Asymmetrical quartz crystallographic fabrics produced during constrictional deformation. Journal of Structural Geology 32, 1,430–1,443.

Tempelman-Kluit, D.J., Parkinson, D., 1986. Extension across the Eocene Okanagan crustal shear in southern British Columbia. Journal of Geology 14, 318-321.

Tempelman-Kluit, D.J., 1989. Geology, Penticton, British Columbia. Scale 1:250 000. Geological Survey of Canada,Ottawa.

Thompson, R.I., Unterschutz, J.L.B., 2004. Geology of the Vernon map area, British Columbia (NTS 82 L/06). Geological Survey of Canada, Open File 4375, scale 1:50000.

Toraman, E., Fayon, A., Whitney, D.L., Teyssier, C., Reiners, P.W., Thomson, S.N., and Krucken berg, S.C., 2011, Apatite-zircon U-Th/He and fi ssion-track dating of the Okanogan Dome exhumation (Washington, USA): Geological Society of America Abstract with Programs 43, 5, 654.

Toy, V.G., Prior, D.J., Norris, R.J., 2008. Quartz textures in the Alpine fault mylonites: influence of pre-existing preferred orientations on fabric develop- ment during progressive uplift. Journal of Structural Geology 30, 602–621.

Tucholke, RE., Lin, J., and Kleimock, M. 1998. Megamullions and mullion structure defining oceanic metamorphic core complexes on the Mid-Atlantic Ridge, Journal of Geophysical Research 103, 9857-9866.

Urai, J. L., Means, W. D., Lister, G. S. 1986. Dynamic recrystallization in minerals, in Mineral and Rock Deformation: Laboratory Studies, Geophysical. Monogr. Ser 36, eds. Hobbs B. E.. Heard H.C. 166-199, AGU, Washington, D.C.

Vanderhaeghe, 0., Teyssier., Wysoczanski, R., 1999. Structural and geochronological constraints on the role of partial melting during the formation 0 the Shuswap metamorphic core complex at the latitude of the Thor- Odin dome, British Columbia. Canadian Journal of Earth Sciences 36, 917-943.

Vanderhaeghe O., and Teyssier C., 2001. Crustal-scale rheological transitions during late-orogenic collapse. Tectonophysics 335, 211-228.

Vanderhaeghe, 0., Teyssier, C., McDougall, I., Dunlap, W., 2003. Cooling and exhumation of the Shuswap metamorphic core complex constrained by 40Ar-39Ar thermochronology. Geological Society of America Bulletin 115, 200-216.

Wernicke, B. 1981. Low-angle normal faults in the Basin and Range Province: Nappe tectonics in an extending orogen. Nature 291, 645–648.

Wernicke, B.P., 1985. Uniform-sense normal simple shear of the continental lithosphere, Canadian Journal of Earth Sciences 22, 108-125.

Wernicke, B., Axen, G.J. 1988. On the role of isostasy in the evolution of normal fault systems. Geology 16, 848-851.

Wheeler. J. 0., McFeely, P., (compilers) 1991. Tectonic assemblage map of the Canadian Cordillera and adjacent parts of the United States of America. Geological Survey of Canada, Map) 712A, scale 1: 2 000 000.

White, W.H.. Harakal, lE., and Carter, N.C. 1968. Potassium-Argon ages of some ore deposits inBritish Columbia. Canadian Institute of Mining and Metallurgy Bulletin, 61: 1326-1334.

Whitney, D. L., Paterson, S. R, Schmidt, K. L. Glazner, A. F., Kopf, C. F. 2004. Growth and demise of continental arcs and orogenic plateaux in the North American Cordillera; from Baja to British Columbia. Geological Society Special Publications 227: 167-175.

Wilson, C.J.L., Russell-Head, D.S., and Sim, H.M., 2003. The application of an automated FA system to the textural evolution of folded ice layers in shear zones. Annals of Glaciology 37, 7-17.

Wilson, C.J.L., Russell-Head, D.S., Kunze, K., and Viola, G. 2007. The analysis of quartz c-axis fabrics using a modified optical microscope. Journal of Microscopy 227: 30-41.

Xypolias, P., Koukouvelas, I.K., 2001. Kinematic vorticity and strain rater patterns associated with ductile extrusion in the Chelmos Shear Zone (External Hellenides, Greece). Tectonophysics 338, 59-77.

Appendix A:

Background information on Methodology

Quartz recrystallization mechanisms

Dislocations are atomic-scale mobile defects within crystal lattices. Migration of dislocations on intracrystalline slip planes (e.g. dislocation creep) contributes to intracrystalline deformation (Fossen, 2010). The characterization of dislocation creep systems is based on mechanical data and on recrystallization mechanisms identified by transmission electron microscopy and optical microscope observations (Hirth and Tullis, 1992; Passicher and Trouw, 2005; Fossen, 2010). Hirth & Tullis (1992) have demonstrated that the dominant recrystallization mechanism is a function of the finite deformation conditions including temperature, stress, and strain rate. Thus, dislocation creep microstructures in quartz have proven useful in determining the kinematics of plastically deformed rocks (e.g. Tullis et al. 1973, White 1976).

This study documents the dynamic recrystallization mechanisms of quartz-rich samples spanning vertical sections within the study are complemented by feldspar deformation textures where applicable (Pryer, 1993). Microtextural analysis according to Stipp et al. (2002a,b) was conducted to ascertain the deformation conditions with respect to structural depth. Stipp et al. (2002a,b) combine inferred deformation temperatures of naturally deformed rocks with experimental data of Hirth & Tullis (1992) to constrain the deformation conditions according to the recrystallization mechanisms identified in quartz-rich mylonites from natural shear zones. These dynamic recrystallization mechanisms are usually the result of the formation and progressive rotation of subgrains and the migration of grain boundaries in response to a change in dislocation density (strain energy) within individual quartz grains (e.g. Guillop and Poirier 1979; Urai et al., 1986). The interaction of these two processes is responsible for the occurrence of three different dynamic recrystallization mechanisms of quartz microstructures based on deformation temperature (Stipp et al., 2002a). Regime 1 is a localised, low temperature grain boundary migration known as bulging recrystallization (BLG), which dominates from approximately 280-400 °C. Regime 2 is characterized by concentration of dislocations along grain walls due to a reduction of elastic distortional strain energy resulting in subgrain rotation recrystallization (SGR), which occurs from approximately 400-500 °C. Regime 3 is a strain-induced grain boundary migration recrystallization (GBM) driven by differences in stored strain energy between adjacent grains occurring at temperatures >500°C (Fig. 2.6C; Stipp et al., 2002a and references therein). Above 650°C, quartz displays chessboard extinction (Fig. A.1C; Blumenfeld et al., 1986; Mainprice et al., 1986; Hirth and Tullis, 1992; Stipp et al., 2002a,b).

Microstructural Analysis using crystallographic preferred orientations

Assuming steady-state deformation with respect to finite strain, CPO fabrics can be used in conjunction with the identification of dynamic recrystallization mechanisms to assess shear sense, deformation temperatures, and strain symmetry (Fig. A.1; Lister et al., 1978; Lister and Hobbs, 1980; Law, 1990; Sullivan and Beane, 2010). This is based on the precepts of the Taylor-Bishop-Hill hypothesis, whereby dislocation creep can be accommodated by the movement of dislocations through rigid body rotation of the crystallographic axes until a particular slip system is oriented to allow slip (Lister et al., 1978; Lister and Paterson, 1979). Therefore, if the deformation within a specified crystalline volume is statistically homogeneous, crystallographic lattices can act as an internal reference frame during deformation (Lister and Hobbs, 1980). The lattice rotations are interpreted to develop in a preferential orientation during deformation because the crystallographic structure deforming through the conservative migration of dislocations remains relatively undistorted, whereas the grain itself undergoes significant changes in shape. The movement of dislocations in quartz is along a certain number of lattice planes in a given direction (Burgers vector) with quartz often deforming by slip on up to four slip planes within the uniaxial system, each of which can accommodate a certain amount of incremental strain (Fig. A.1C; Lister et al. 1977; Law, 1990). Together, the orientation of the slip plane and the magnitude and direction of the Burgers vector define a slip system (Lister et al. 1978). To activate these slip systems, the minimum stress required for slip to occur, referred as the Critical Resolved Shear Stress (CRSS), must be exceeded (Lister et al., 1978). The magnitude of the CRSS for a particular orientation is strongly dependent on temperature, as well as strain rate, pressure, and chemical-fluid activity (Hobbs, 1985).

Both quartz c- and a-axis fabric geometries can be related to distortional strain geometry (Sullivan and Beane, 2010). This is achieved using numerical simulations of plastic deformation based on the Taylor-Bishop-Hill model of slip system activation in quartz c-axes (Lister and Hobbs, 1980) and the inferred geometry of a-axis fabrics in naturally deformed quartzite (Schmid and Casey, 1986). These observations are subsequently incorporated into the Flinn plot showing the relationship between the strain symmetry and quartz c- and a-axis fabrics showing deviations from plane strain towards constriction or flattening (Fig. A.1B; Schmid and Casey, 1986).

Assuming natural strain rates and plane strain, temperatures of deformation can be constrained through the following two methods using quartz c-axis fabrics: (1) the evaluation of quartz c-axis opening angles in cross girdled fabric skeletons (e.g. the fabric skeleton of c-axis girdles in Fig. A.1C and Fig. A.1D; Kruhl, 1998; Law et al., 2004), and (2) the interpretation of dominant slip systems active during deformation (e.g. Fig. A.1D; Law, 1990; Toy et al, 2008).

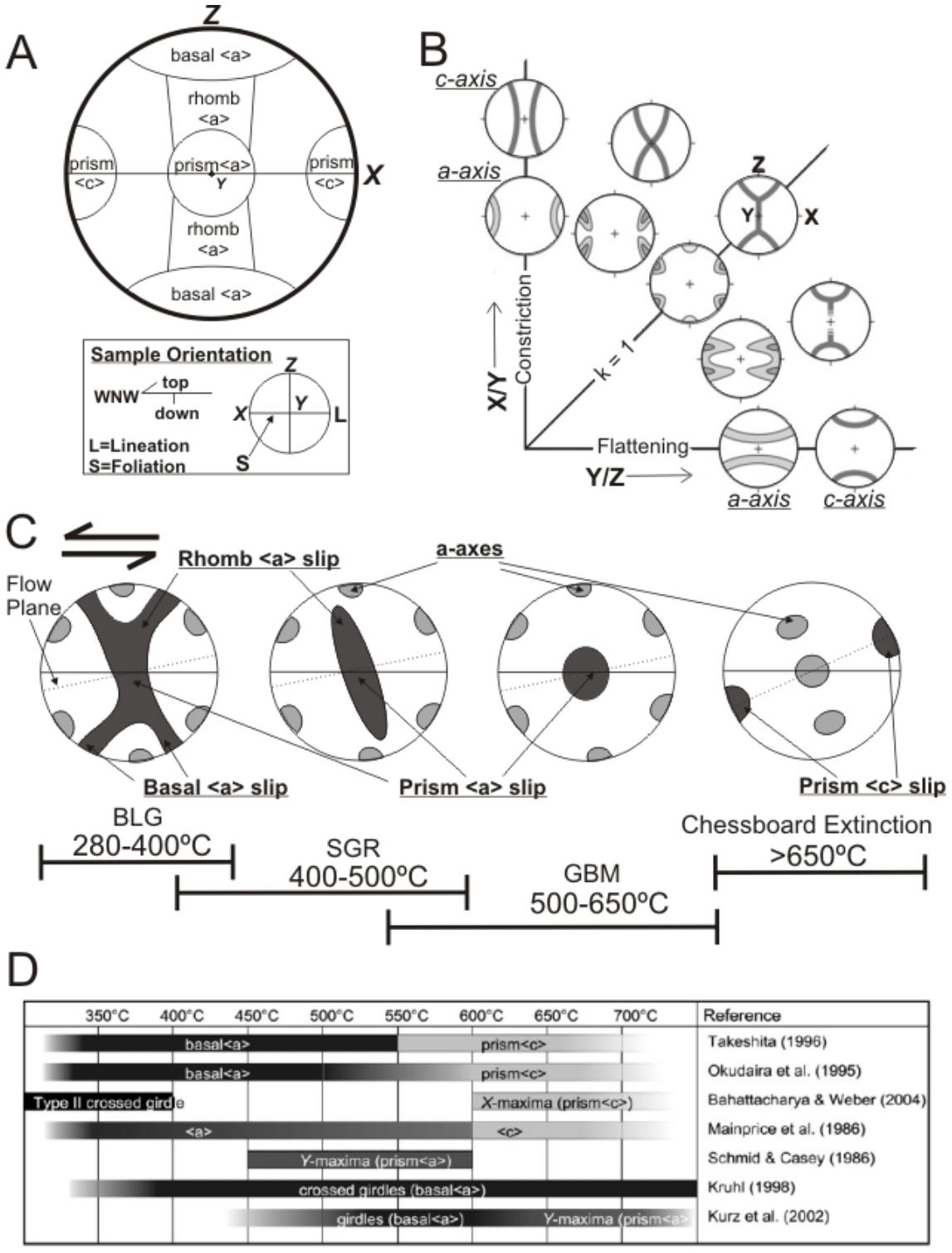

Figure A.1. Summary of the interpretation and presentation quartz CPO fabrics.

(A) the location of quartz c-axis peaks and active slip systems in equal area lower hemisphere projection cut parallel to lineation, perpendicular to foliation, based on Schmid and Casey (1986) and adapted from Toy et al. (2008). (B) Flynn plot showing relationships between strain symmetry and quartz c-axis and a-axis fabrics for coaxial deformation. C-axis fabrics represented by fabric skeletons represented as either girdles or point maximas. A- axis represented by contours (after Schmid and Casey, 1986; Law, 1990). (C) Stereonets showing the evolution of c- and a-axis fabrics with increasing temperature for top-to-the-west (sinistral) non–coaxial deformation and plane strain; c-axisc-axis shown in dark grey, a-axis shown in light grey. Temperature ranges of dynamic recrystallization mechanisms also shown with respect to CPO fabrics (adapted from Passchier and Trouw, 2005; Langille et al., 2010). (D) Summary of previously estimated temperature ranges in which certain quartz slip systems and subsequent quartz c-axes fabrics operate (after Toy et al., 2008 and references therein).

Kruhl (1998) discusses the use of quartz CPO fabrics as a practical geothemometer. He suggests that the transition in dominant dislocation glide with respect to increasing temperature goes from basal <a> to prism <c> slip, caused by the phase transformation from low (α) to high (β) quartz. This depends strongly on temperature and pressure of deformation and equilibration. Blacic (1975) and Linker & Kirby (1981) document that glide is elementary in the <c> direction of synthetic quartz, proposing that the different glide rates in the <a> and <c> directions are related to an anisotropy of diffusion along these directions. Subsequent work of Dennis (1984) and Giletti & Yund (1984) confirmed that oxygen diffusion is much faster in the <c> direction than the <a> direction. Mainprice and Nichols (1989) equate increasing temperature of deformation with an increasing importance of diffusion in the <c> direction, and subsequently, the velocity of dislocation glide in that direction and on planes containing it. This therefore implies that the transition from prism <a> slip to <c> slip is facilitated with increasing temperature. Water may act as a catalyst during deformation and support the formation and migration of lattice defects without being consumed (Kruhl, 1996; 1998). Therefore, Kruhl (1998) suggests that during significant periods of deformation even tiny amounts of water are sufficient to increase the plasticity of quartz and support the development of SGB, which need only low densities of lattice defects to operate.

Therefore, within the limitations of Taylor-Bishop-Hill analysis theory (Lister & Paterson 1979; Lister and Hobbs, 1980) the active slip systems act as a semi-quantitative estimate of deformation temperature. Activation of lattice slip at relatively low temperatures (280-400 °C) is interpreted to be dominantly on the basal plane with single girdle fabrics result from combined Prism <a> and Rhomb <a> slip, progressing to a *Y*-axis maxima fabric perpendicular? to the lineation suggesting dominant prism <a> slip with increasing temperature (500-650 °C) (Fig A.1C; Mainprice et al., 1986; Law, 1990; Tullis and Yund, 1992; Kruhl, 1998; Langille et al., 2010). At temperatures >650 °C, slip of prismatic planes in the

Prism <c> direction are activated (Fig A.1C; Mainprice et al., 1986; Law, 1990; Tullis and Yund, 1992; Kruhl, 1998). Additionally, the asymmetry of the CPO skeleton in a c-axis plot with respect to the kinematic reference frame (foliation and lineation) can be used to determine the sense of shear (Fig. 2.6C; Law, 1990).

The crystallographic orientation of sub-grain boundaries (SGB) in quartz is a useful indicator of the operative slip direction during high temperature plastic deformation (Mainprice, 1986). Preliminary optical fabric data can be acquired by inserting the quarter wavelength retardation plate in the optical microscope to give a quick qualitative 2D analysis of the subgrain boundaries and potential lattice orientation, thus aiding the sample selection for EBSD analysis.

Quartz CPO fabrics are obtained through measuring the crystallographic orientations of an appropriate number of individual recrystallized grains (>300). These fabrics were initially obtained through the use of a universal stage (U-Stage) mounted on an optical microscope (Berek, 1924; Reinhard, 1931). U-stage mounted samples have previously proved an effective and reliable means to gather meaningful quartz c-axes (e.g. Law 1986), but this method has specific limitations. For instance, U-stage analysis is restricted to moderate to coarse-grained samples (low spatial resolution) with data biased to recrystallization regimes associated with larger grain sizes. It is also not possible to measure a-axis fabrics in quartz grains, Furthermore, there is a strong potential to misidentify quartz within quartzo-feldspathic samples during grain identification. As a result, the measurement of CPOs has since evolved to include the use Electron Back Scatter Diffraction (EBSD) detectors mounted to a Scanning Electron Microscope with additional acquisition of c-axes from the Fabric Analyser (FA) technique (Wilson et al., 2003; 2007).

Both Electron backscatter diffraction (EBSD) and Fabric Analyser (FA) techniques allow for the automatic recognition of quartz CPO fabrics where single grain or bulk measurements on a thin section are based on the determination of the orientation of the selected lattice directions (Ullemeyer et al., 2000; Peternell et al., 2010). High-resolution acquisition of CPO data can be acquired from rock-forming mineral grains as small as <1 μm (EBSD) and ~2.8 μm (FA) with automated data acquisition and analysis (Peternell et al., 2010). Both EBSD and FA are ideal for investigating textural heterogeneities within individual thin sections. This enables rapid comparison of statistically significant data from independent methods and allows for analysis of different quartz-rich domains within a sample, which can highlight variations in quartz CPO fabrics within one thin section (e.g. Peternell et al., 2010; Nagy 2012). For a full description of EBSD and FA techniques, and their application to geologic problems, see Prior et al. (1999; 2009) and Wilson et al. (2003; 2007), respectively.

References:

Blacic, J. D. 1975. Plastic deformation mechanisms in quartz: the effect of water. Tectonophysics 27, 271-294.

Blumenfeld, P., Mainprice, D. and Bouchez, J.L., 1986. C-slip in quartz from subsolidus deformed granite. Tectonophysics 127, pp. 97-115.

Fossen, H., 2010. Structural Geology. Cambridge University Press, Cambridge.

Giletti, B. J. & Yund, R. A. 1984. Oxygen diffusion in quartz. Journal of Geophysical Research. 89, 4039-4046.

Guillope M, Poirier J-P 1979 Dynamic recrystallization during creep of single-crystalline halite: an experimental study. Journal of Geophysical Research 84, 5557–5567.

Hirth, G., Tullis, J., 1992. Dislocation creep regimes in quartz aggregates. Journal of Structural Geology 14, 145-159.

Hobbs, B. E. 1985. The geological significance of microfabric. In: Preferred Orientation in Deformed Metals and Rocks (edited by Wenk, H.-R.). Academic Press, Orlando.

Kruhl, J.H., 1996. Prism- and basal-plane parallel subgrain boundaries in quartz: a microstructural geothermobarometer. Journal of Metamorphic Geology 14, 581-589.

Kruhl, J.H., 1998. Prism- and basal-plane parallel subgrain boundaries in quartz: a microstructural geothermobarometer: Reply. Journal of Metamorphic Geology 16, 142-146.

Law, R.D., 1990. Crystallographic fabrics: a selective review of their applications to research in structural geology. In: Knipe, R.J., Rutter, E.H. (Eds.), Deformation Mechanisms, Rheology and Tectonics. Geological Society, London, Special Publication 54, 335-352.

Law, R.D., Searle, M.P., Simpson, R.L., 2004. Strain, deformation temperatures, and flow at the top of the Greater Himalayan Slab, Everest Massif, Tibet. Journal of the Geological Society, London 161, 305-320.

Lister, G.S., 1977. Discussion: Crossed girdle c-axis fabrics in quartzites plastically deformed by plane strain and progressive simple shear. Tectonophysics 39, 51-54.

Lister, G.S. Hobbs, B.E., 1980. The simulation of fabric development during plastic deformation and its application to quartzite: the influence of deformation history. Journal of Structural Geology 2, 335-352.

Lister, G.S., Paterson, M.S., Hobbs, B.E., 1978. The simulation of fabric development in plastic deformation and its application to quartzite: the model. Tectonophysics 45, 107-158.

Lister, G.S., Paterson, M.S., 1979. The simulation of fabric development during plastic deformation and its application to quartzite: fabric transitions. Journal of Structural Geology 1 (2), 99-115.

Lister, G.S., Price, G.P., 1978. Fabric development in a quartz-feldspar mylonite. Tectonophysics 49 (1-2), 37-78.

Mainprice, D. Nicolas, A. 1989. Development of shape and lattice preferred orientations: application to the seismic anisotropy of the lower crust. Journal of Structural Geology 11, 175-189.

Nagy. C. 2012. From cessation of south-directed mid-crust extrusion to onset of orogen-parallel extension, NW Nepal Himalaya. M.Sc.thesis Queen's University Kingston, Ontario, 293 pp.

Passchier, C.W., Trouw, R.A.J., 2005. Microtectonics, second ed. Springer, Berlin, 366 pp.

Peternell, M., Hasalová, P., Wilson, C.J.L., Piazolo, S. and Schulmann, K. 2010. Evaluating quartz crystallographic preferred orientations and the role of deformation partitioning using EBSD and fabric analyser techniques. Journal of Structural Geology 32, 803–817.

Prior, D.J., Boyle, A.P., Brenker, F., Cheadle, M., Day, A., Lopez, G., Peruzzo, L., Potts, G.J., Reddy, S., Spiess, R., Timms, N.E., Trimby, P., Wheeler, J., and Zetterström, L.1999. The application of electron backscatter diffraction and orientation contrast imaging in the SEM to textural problems in rocks. American Mineralogist 84, 1741-1759.

Prior, D.J. 2009. EBSD in the earth sciences: application, common practice and challenges. In: Schwartz, A.J., Kumar, M., Adams, B.L., Field, D.P. (eds.). Electron Backscatter Diffraction in Materials Science. Springer Science and Business Media, New York. 345-360.

Pryer, L.L., 1993. Microstructures in feldspars from a major crustal thrust zone: the Grenville Front, Ontario, Canada. Journal of Structural Geology 15, 21-36.

Schmid, S.M., Casey, M., 1986. Complete fabric analysis of some commonly observed quartz c-axis patterns. In: Hobbs, B.E., Heard, H.C. (Eds.), Mineral and Rock

Deformation: Laboratory StudiesdThe Paterson Volume. American Geophysical Union Monograph, 36. American Geophysical Union, pp. 246-261.

Stipp, M., Stünitz, H., Heilbronner, R., Schmid, S.M., 2002b. Dynamic recrystallization of quartz: correlation between natural and experimental conditions. In: De Meer, S., Brury, M.R., De Brasser, J.H.P., Pennock, G.M. (Eds.), Deformation Mechanisms, Rheology and Tectonics: Current Status and Future Perspectives. Geological Society, London, Special Publication 200, 171-190.

Stipp, M., Tullis, J., 2003. The recrystallized grain size piezometer for quartz. Geophysical Research Letters 2088.

Sullivan, W.A., Beane, R.J. 2010. Asymmetrical quartz crystallographic fabrics produced during constrictional deformation. Journal of Structural Geology 32, 1,430–1,443.

Toy, V.G., Prior, D.J., Norris, R.J., 2008. Quartz textures in the Alpine fault mylonites: influence of pre-existing preferred orientations on fabric development during progressive uplift. Journal of Structural Geology 30, 602–621.

Ullemeyer, K., Braun, G., Dahms, M., Kruhl, J.H., Olesen, N.Ø., Siegesmund, S., 2000.Texture analysis of a muscovite-bearing quartzite: a comparison of some currently used techniques. Journal of Structural Geology 22, 1541-1557.

Urai, J. L., Means, W. D., Lister, G. S. 1986. Dynamic recrystallization in minerals, in Mineral and Rock Deformation: Laboratory Studies, Geophysical. Monogr. Ser 36, eds. Hobbs B. E.. Heard H.C. 166-199, AGU, Washington, D.C.

Wilson, C.J.L., Russell-Head, D.S., and Sim, H.M., 2003. The application of an automated FA system to the textural evolution of folded ice layers in shear zones. Annals of Glaciology 37, 7-17.

Wilson, C.J.L., Russell-Head, D.S., Kunze, K., and Viola, G. 2007. The analysis of quartz c-axis fabrics using a modified optical microscope. Journal of Microscopy 227: 30-41.

Appendix B:

Unprocessed Electron Backscatter Diffraction data

*Thin Section images denote general areas (yellow boxes) on the sample where Electron Backscatter Diffraction data were collected

REC_2

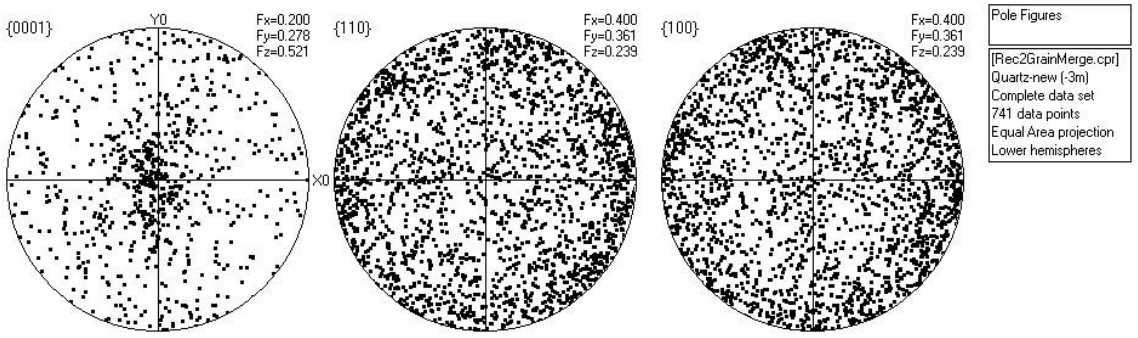

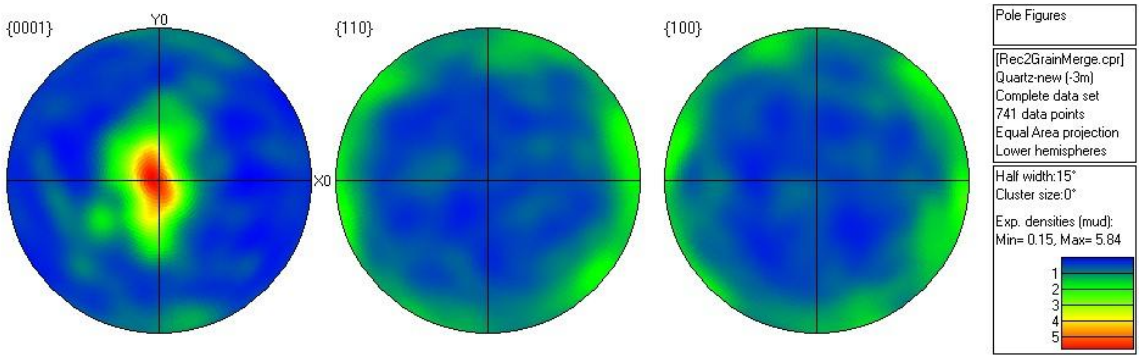

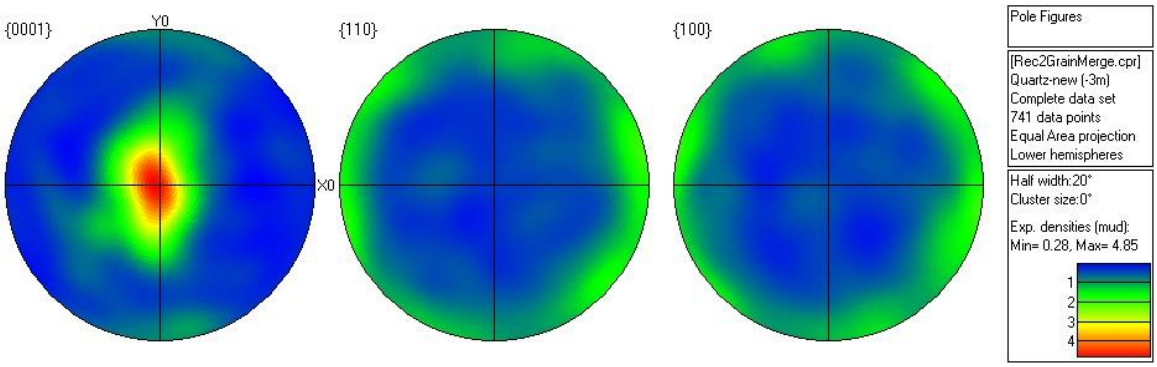
{0001}
Y0
X0
{110}
{100}
Pole Figures
[Rec2GrainMerge.cpr]
Quartz-new (-3m)
Complete data set
741 data points
Equal Area projection
Lower hemispheres
Half width:20°
Cluster size:0°
Exp. densities (mud):
Min= 0.28, Max= 4.85
1
2
3
4

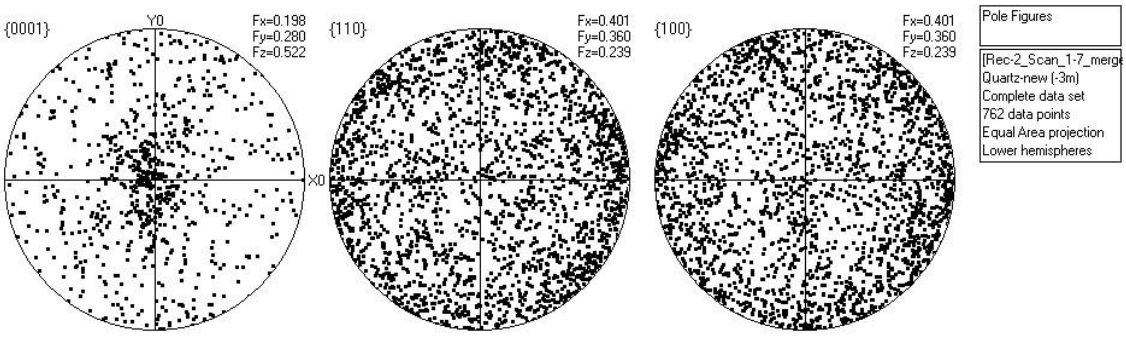
{0001}
Y0
Fx=0.198
Fy=0.280
Fz=0.522
X0
{110}
Fx=0.401
Fy=0.360
Fz=0.239
{100}
Fx=0.401
Fy=0.360
Fz=0.239
Pole Figures
[Rec-2_Scan_1-7_merge
Quartz-new (-3m)
Complete data set
762 data points
Equal Area projection
Lower hemispheres

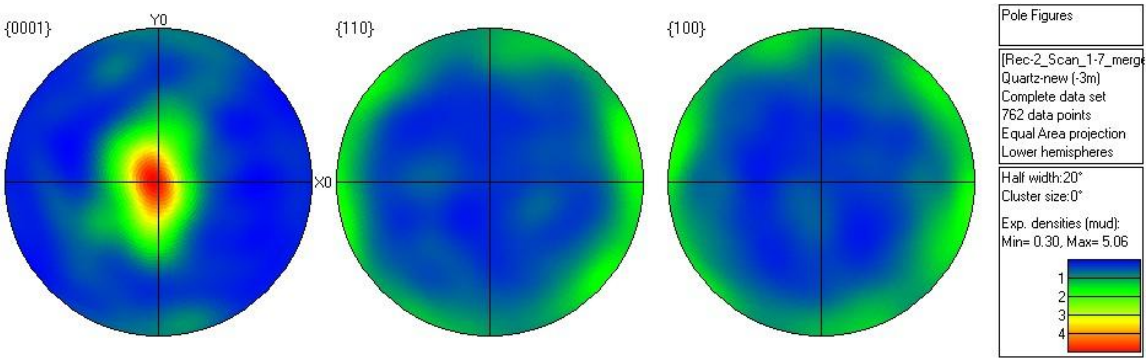
{0001}
Y0
X0
{110}
{100}
Pole Figures
[Rec-2_Scan_1-7_merge
Quartz-new (-3m)
Complete data set
762 data points
Equal Area projection
Lower hemispheres
Half width:20°
Cluster size:0°
Exp. densities (mud):
Min= 0.30, Max= 5.06
1
2
3
4

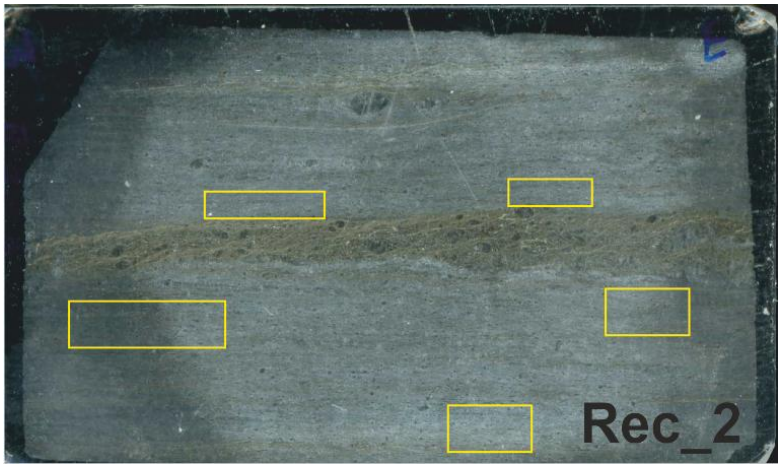
Rec_2

VT-12-11

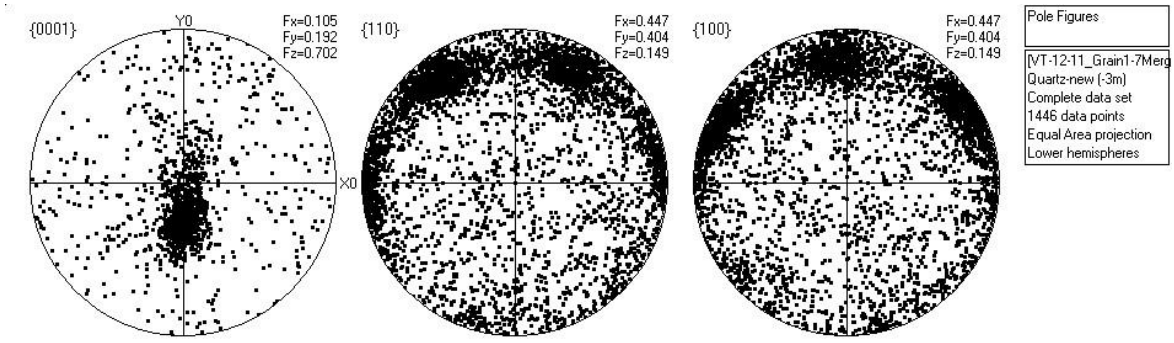
{0001}
Y0
X0
Fx=0.105
Fy=0.192
Fz=0.702
{110}
Fx=0.447
Fy=0.404
Fz=0.149
{100}
Fx=0.447
Fy=0.404
Fz=0.149
Pole Figures
[VT-12-11_Grain1-7Merg
Quartz-new (-3m)
Complete data set
1446 data points
Equal Area projection
Lower hemispheres

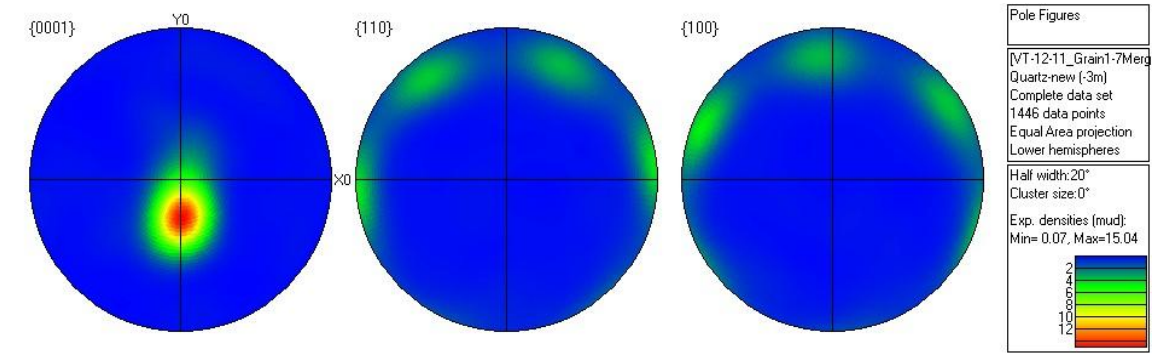
{0001}
Y0
X0
{110}
{100}
Pole Figures
[VT-12-11_Grain1-7Merg
Quartz-new (-3m)
Complete data set
1446 data points
Equal Area projection
Lower hemispheres
Half width:20°
Cluster size:0°
Exp. densities (mud):
Min= 0.07, Max=15.04
2
4
6
8
10
12

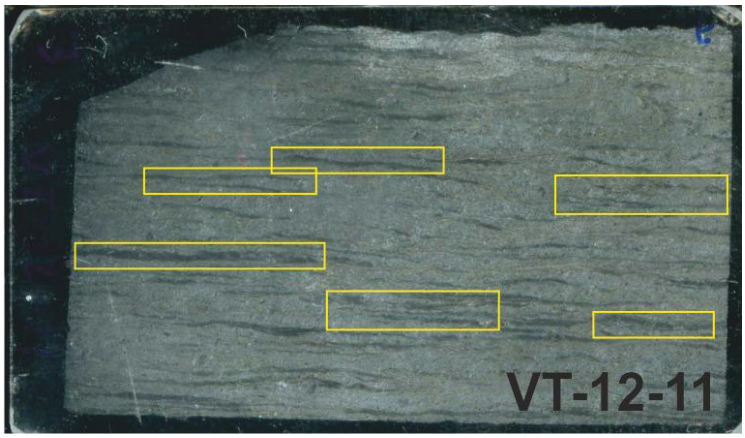
VT-12-11

VT-12-30

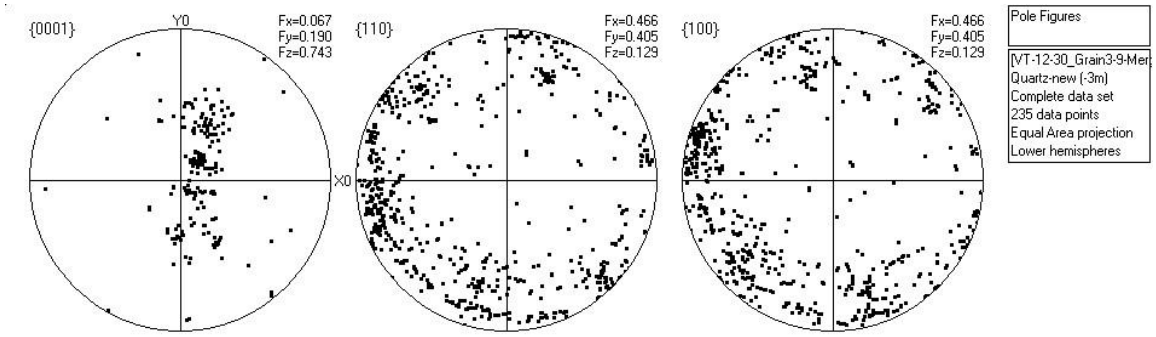
{0001}
Y0
X0
Fx=0.067
Fy=0.190
Fz=0.743
{110}
Fx=0.466
Fy=0.405
Fz=0.129
{100}
Fx=0.466
Fy=0.405
Fz=0.129
Pole Figures
[VT-12-30_Grain3-9-Mer
Quartz-new (-3m)
Complete data set
235 data points
Equal Area projection
Lower hemispheres

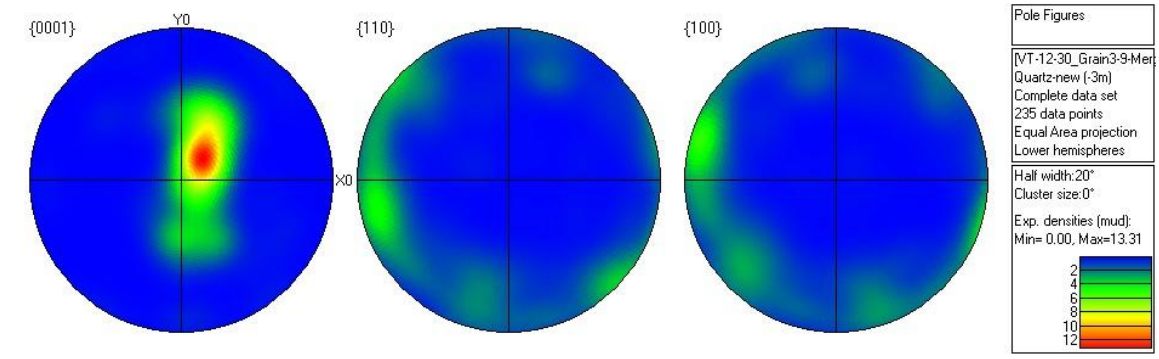
{0001}
Y0
X0
{110}
{100}
Pole Figures
[VT-12-30_Grain3-9-Mer
Quartz-new (-3m)
Complete data set
235 data points
Equal Area projection
Lower hemispheres
Half width:20°
Cluster size:0°
Exp. densities (mud):
Min= 0.00, Max=13.31
2
4
6
8
10
12

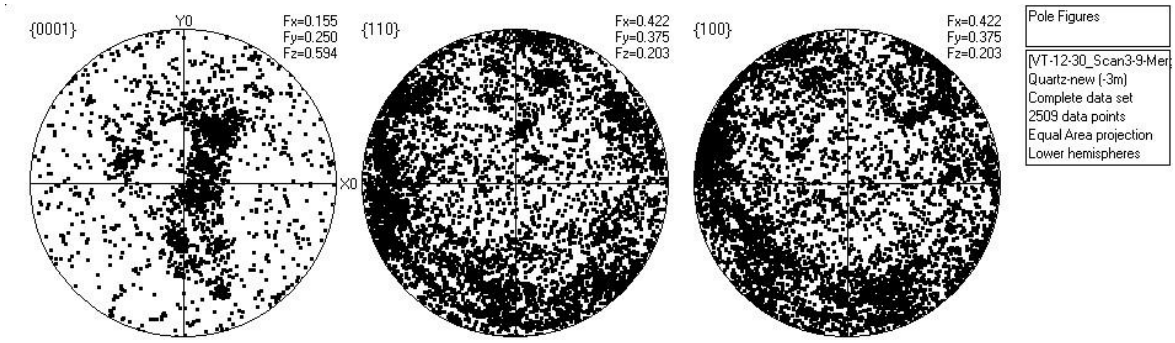
{0001}
Y0
X0
Fx=0.155
Fy=0.250
Fz=0.594
{110}
Fx=0.422
Fy=0.375
Fz=0.203
{100}
Fx=0.422
Fy=0.375
Fz=0.203
Pole Figures
[VT-12-30_Scan3-9-Mer
Quartz-new (-3m)
Complete data set
2509 data points
Equal Area projection
Lower hemispheres

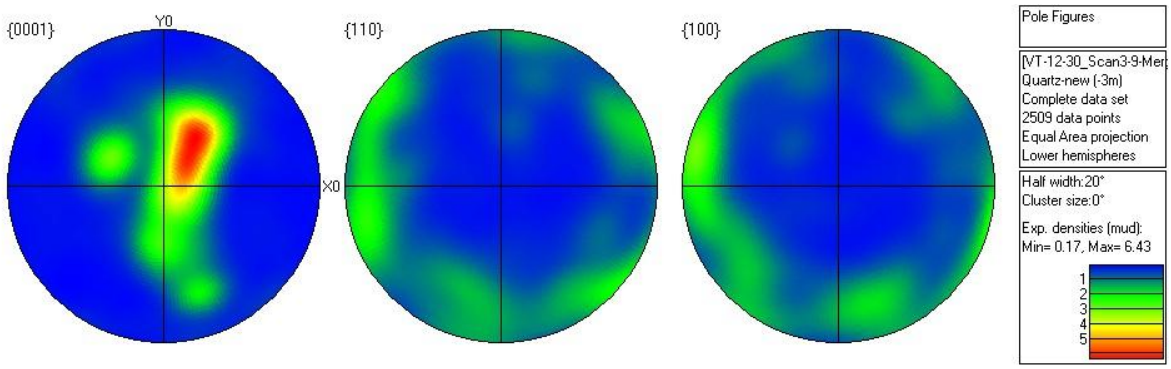
{0001}
Y0
X0
{110}
{100}
Pole Figures
[VT-12-30_Scan3-9-Mer
Quartz-new (-3m)
Complete data set
2509 data points
Equal Area projection
Lower hemispheres
Half width:20°
Cluster size:0°
Exp. densities (mud):
Min= 0.17, Max= 6.43
1
2
3
4
5

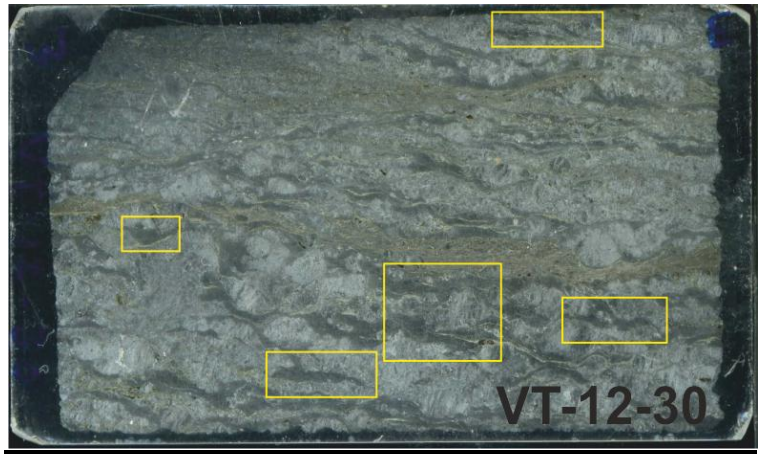
VT-12-30

VT-12-56

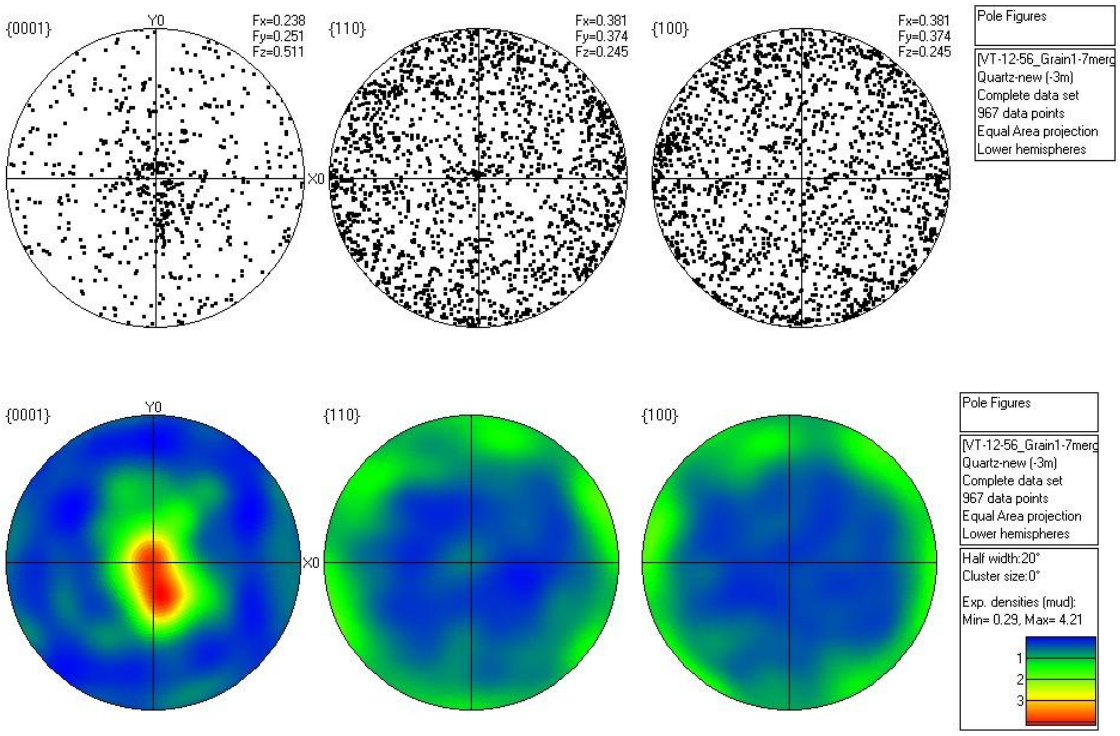
{0001}
Y0
X0
Fx=0.238
Fy=0.251
Fz=0.511
{110}
Fx=0.381
Fy=0.374
Fz=0.245
{100}
Fx=0.381
Fy=0.374
Fz=0.245
Pole Figures
[VT-12-56_Grain1-7merg
Quartz-new (-3m)
Complete data set
967 data points
Equal Area projection
Lower hemispheres
{0001}
Y0
X0
{110}
{100}
Pole Figures
[VT-12-56_Grain1-7merg
Quartz-new (-3m)
Complete data set
967 data points
Equal Area projection
Lower hemispheres
Half width:20°
Cluster size:0°
Exp. densities (mud):
Min= 0.29, Max= 4.21
1
2
3

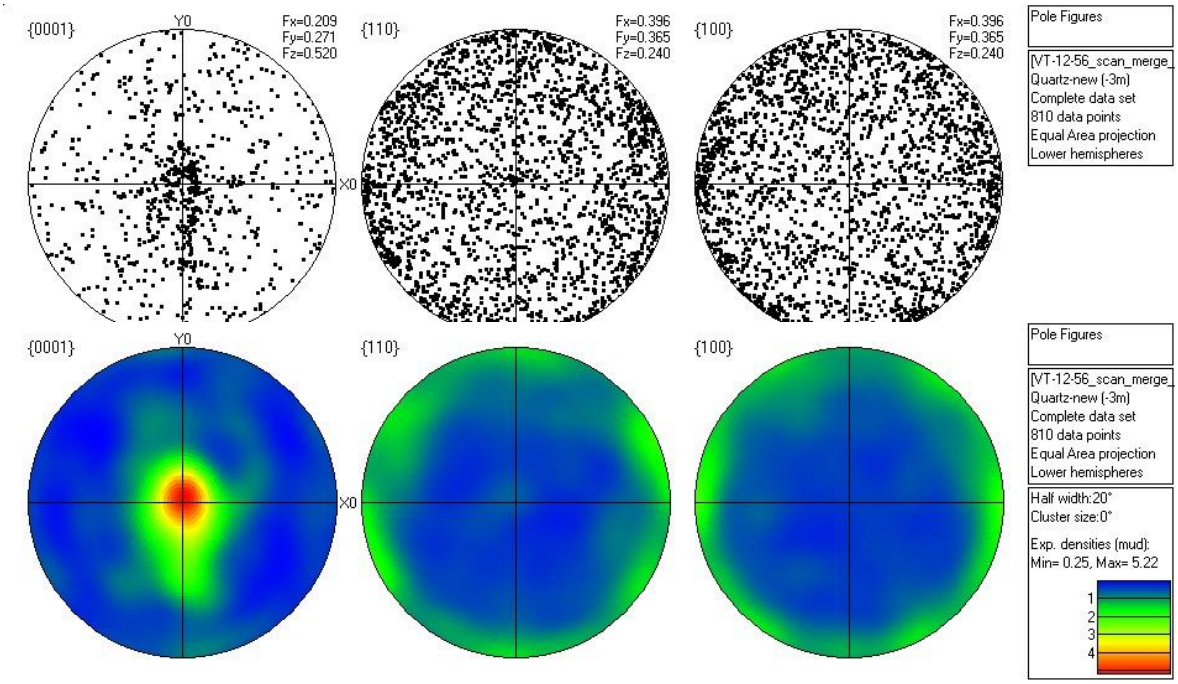
{0001}
Y0
X0
Fx=0.209
Fy=0.271
Fz=0.520
{110}
Fx=0.396
Fy=0.365
Fz=0.240
{100}
Fx=0.396
Fy=0.365
Fz=0.240
Pole Figures
[VT-12-56_scan_merge_
Quartz-new (-3m)
Complete data set
810 data points
Equal Area projection
Lower hemispheres
{0001}
Y0
X0
{110}
{100}
Pole Figures
[VT-12-56_scan_merge_
Quartz-new (-3m)
Complete data set
810 data points
Equal Area projection
Lower hemispheres
Half width:20°
Cluster size:0°
Exp. densities (mud):
Min= 0.25, Max= 5.22
1
2
3
4

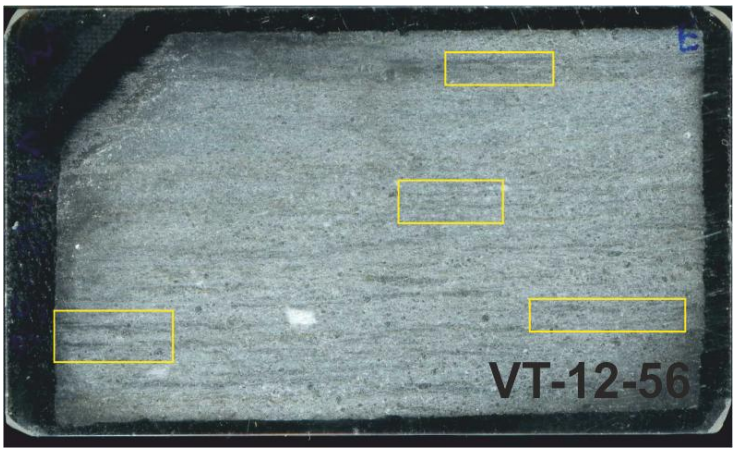
VT-12-56

VT-12-59

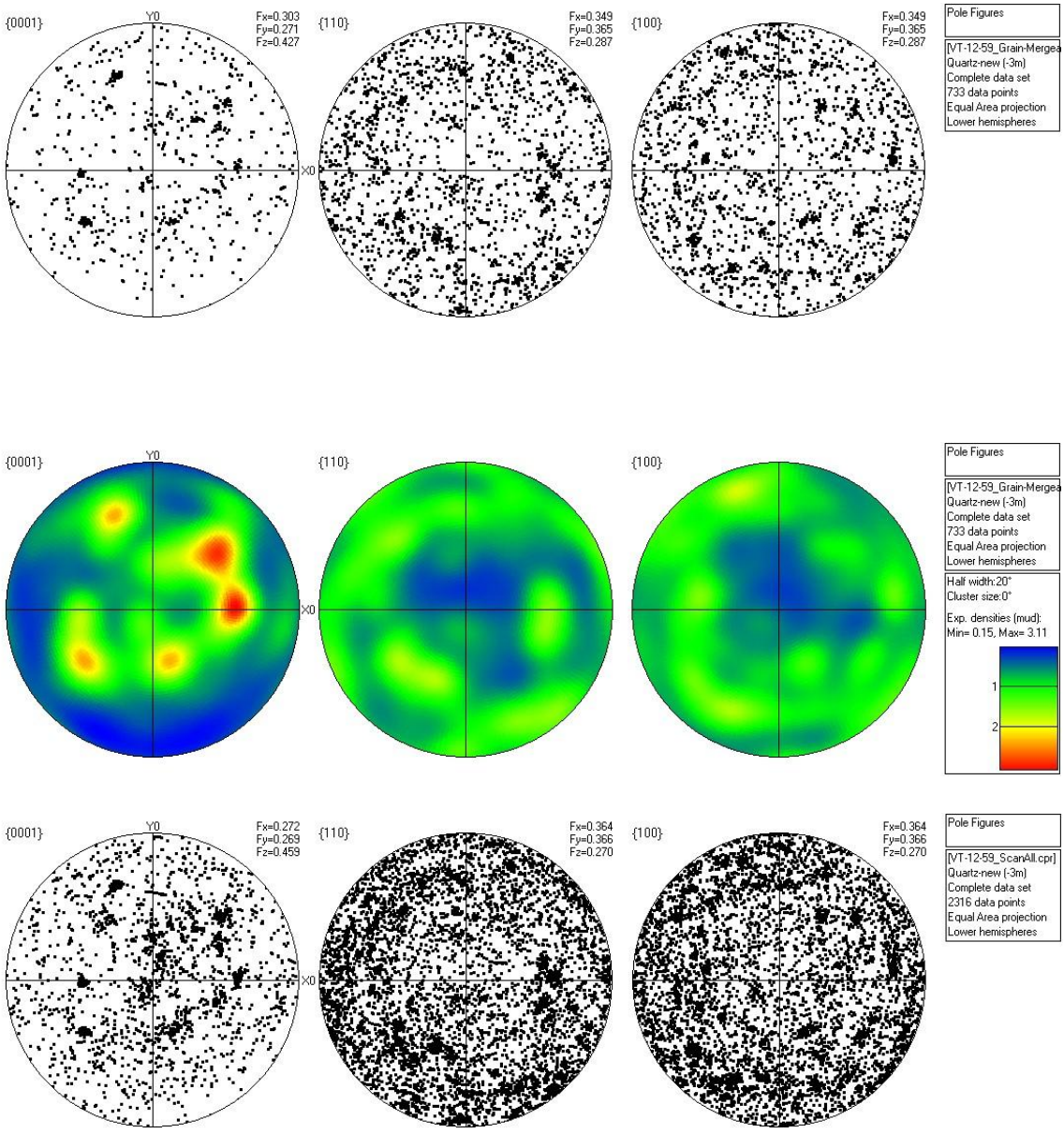
{0001}
Y0
X0
Fx=0.303
Fy=0.271
Fz=0.427
{110}
Fx=0.349
Fy=0.365
Fz=0.287
{100}
Fx=0.349
Fy=0.365
Fz=0.287
Pole Figures
[VT-12-59_Grain-Mergea
Quartz-new (-3m)
Complete data set
733 data points
Equal Area projection
Lower hemispheres
{0001}
Y0
X0
{110}
{100}
Pole Figures
[VT-12-59_Grain-Mergea
Quartz-new (-3m)
Complete data set
733 data points
Equal Area projection
Lower hemispheres
Half width:20°
Cluster size:0°
Exp. densities (mud):
Min= 0.15, Max= 3.11
1
2
{0001}
Y0
X0
Fx=0.272
Fy=0.269
Fz=0.459
{110}
Fx=0.364
Fy=0.366
Fz=0.270
{100}
Fx=0.364
Fy=0.366
Fz=0.270
Pole Figures
[VT-12-59_ScanAll.cpr]
Quartz-new (-3m)
Complete data set
2316 data points
Equal Area projection
Lower hemispheres

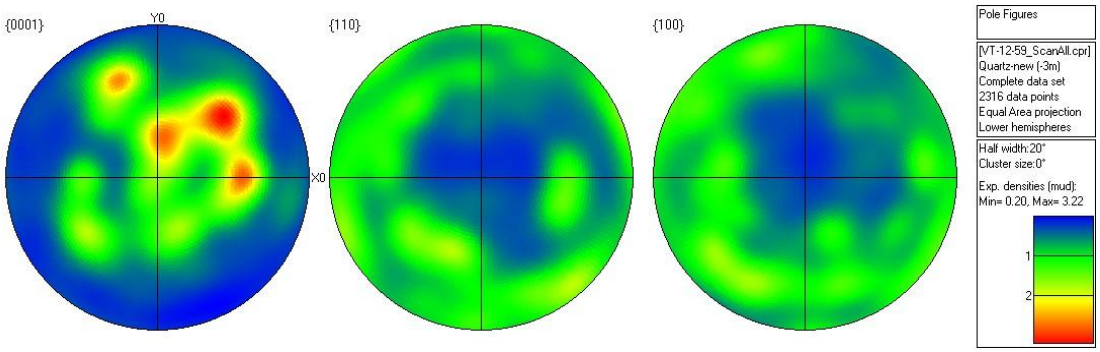
{0001}
Y0
X0
{110}
{100}
Pole Figures
[VT-12-59_ScanAll.cpr]
Quartz-new (-3m)
Complete data set
2316 data points
Equal Area projection
Lower hemispheres
Half width:20°
Cluster size:0°
Exp. densities (mud):
Min= 0.20, Max= 3.22
1
2

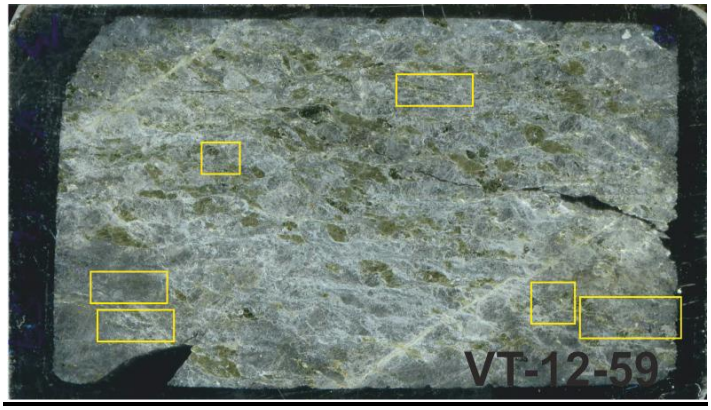
VT-12-59

VT-12-72

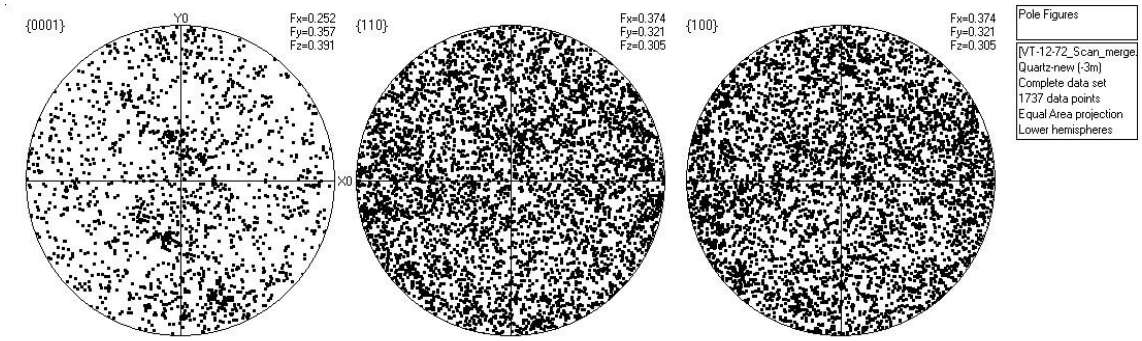
{0001}
Y0
X0
Fx=0.252
Fy=0.357
Fz=0.391
{110}
Fx=0.374
Fy=0.321
Fz=0.305
{100}
Fx=0.374
Fy=0.321
Fz=0.305
Pole Figures
[VT-12-72_Scan_merge.
Quartz-new (-3m)
Complete data set
1737 data points
Equal Area projection
Lower hemispheres

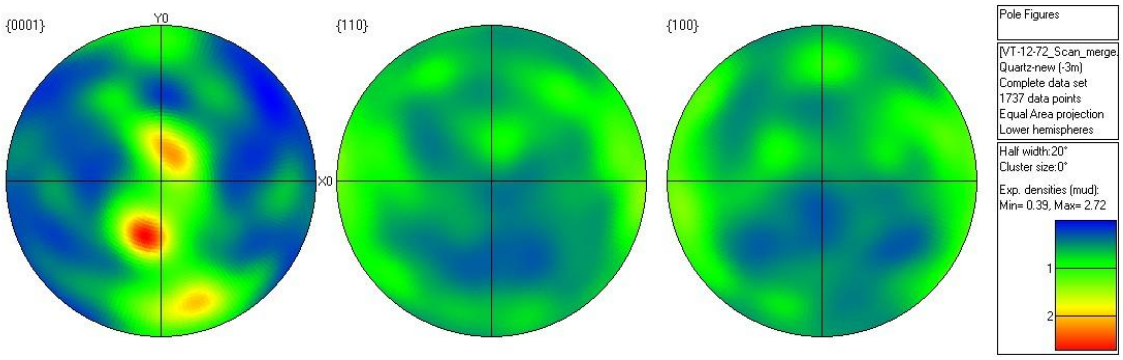
{0001}
Y0
X0
{110}
{100}
Pole Figures
[VT-12-72_Scan_merge.
Quartz-new (-3m)
Complete data set
1737 data points
Equal Area projection
Lower hemispheres
Half width:20°
Cluster size:0°
Exp. densities (mud):
Min= 0.39, Max= 2.72
1
2

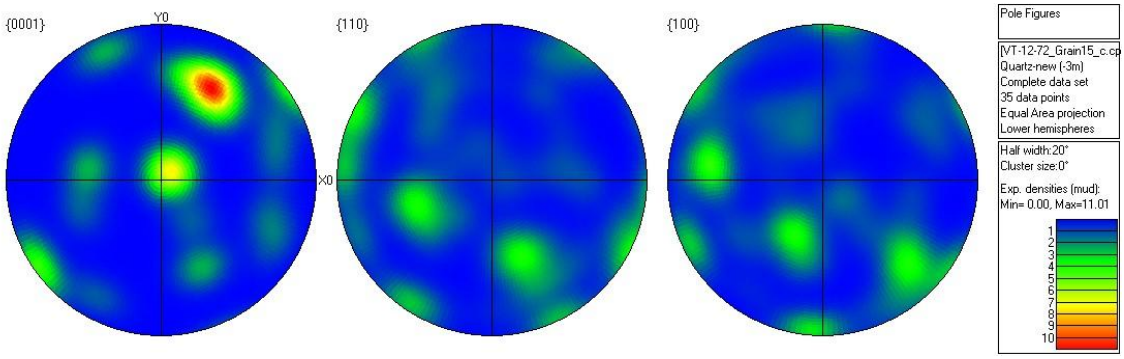
{0001}
Y0
X0
{110}
{100}
Pole Figures
[VT-12-72_Grain15_c.cp
Quartz-new (-3m)
Complete data set
35 data points
Equal Area projection
Lower hemispheres
Half width:20°
Cluster size:0°
Exp. densities (mud):
Min= 0.00, Max=11.01
1
2
3
4
5
6
7
8
9
10

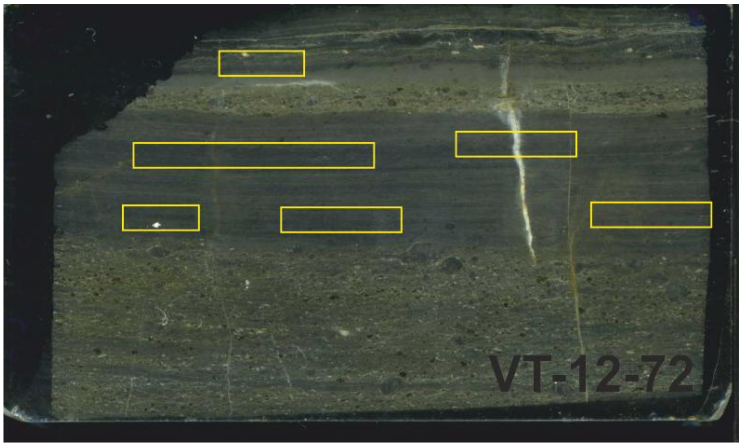
VT-12-72

VT-12-111

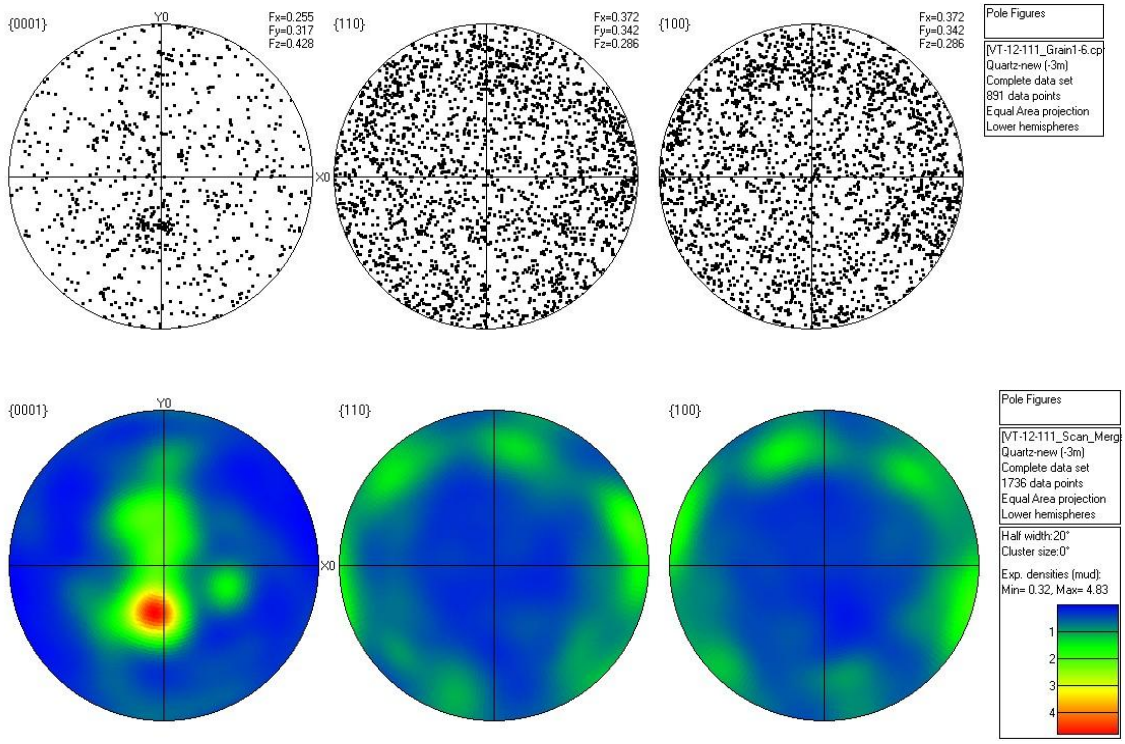
{0001}
Y0
X0
Fx=0.255
Fy=0.317
Fz=0.428
{110}
Fx=0.372
Fy=0.342
Fz=0.286
{100}
Fx=0.372
Fy=0.342
Fz=0.286
Pole Figures
[VT-12-111_Grain1-6.cp
Quartz-new (-3m)
Complete data set
891 data points
Equal Area projection
Lower hemispheres
{0001}
Y0
X0
{110}
{100}
Pole Figures
[VT-12-111_Scan_Merg
Quartz-new (-3m)
Complete data set
1736 data points
Equal Area projection
Lower hemispheres
Half width: 20°
Cluster size: 0°
Exp. densities (mud):
Min= 0.32, Max= 4.83
1
2
3
4

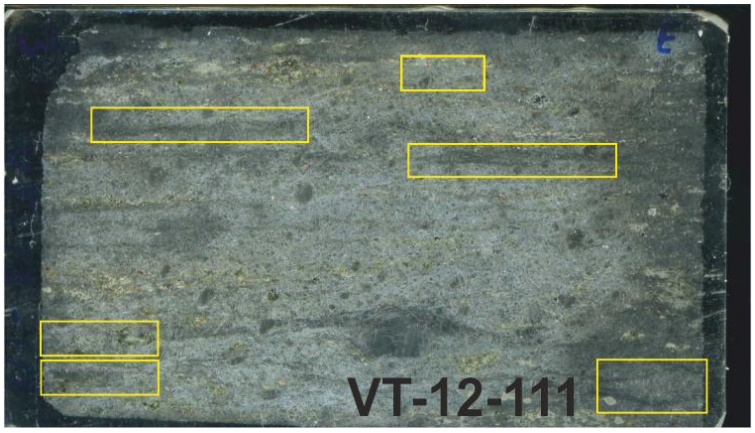
VT-12-111

VT-12-154

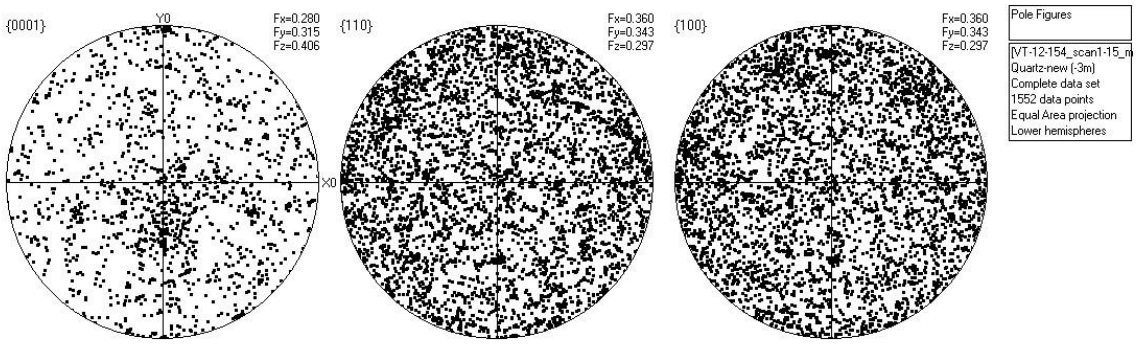
{0001}
Y0
X0
Fx=0.280
Fy=0.315
Fz=0.406
{110}
Fx=0.360
Fy=0.343
Fz=0.297
{100}
Fx=0.360
Fy=0.343
Fz=0.297
Pole Figures
[VT-12-154_scan1-15_m
Quartz-new (-3m)
Complete data set
1552 data points
Equal Area projection
Lower hemispheres

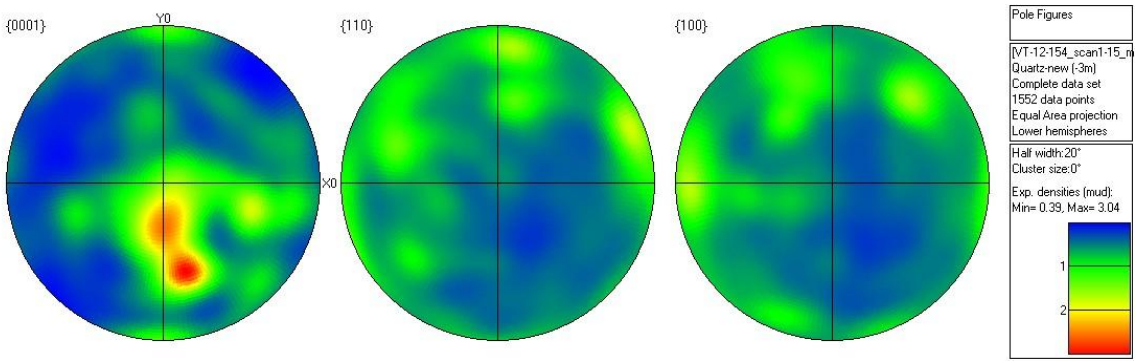
{0001}
Y0
X0
{110}
{100}
Pole Figures
[VT-12-154_scan1-15_m
Quartz-new (-3m)
Complete data set
1552 data points
Equal Area projection
Lower hemispheres
Half width:20°
Cluster size:0°
Exp. densities (mud):
Min= 0.39, Max= 3.04
1
2

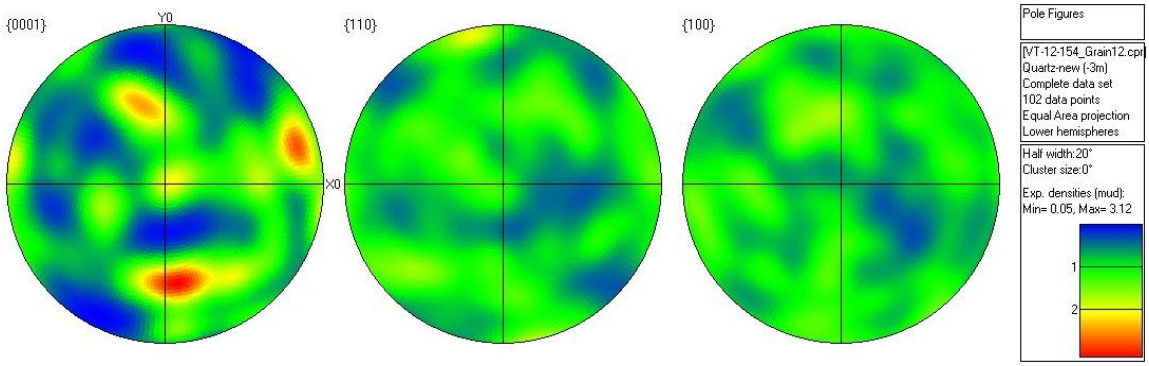
{0001}
Y0
X0
{110}
{100}
Pole Figures
[VT-12-154_Grain12.cpr
Quartz-new (-3m)
Complete data set
102 data points
Equal Area projection
Lower hemispheres
Half width:20°
Cluster size:0°
Exp. densities (mud):
Min= 0.05, Max= 3.12
1
2

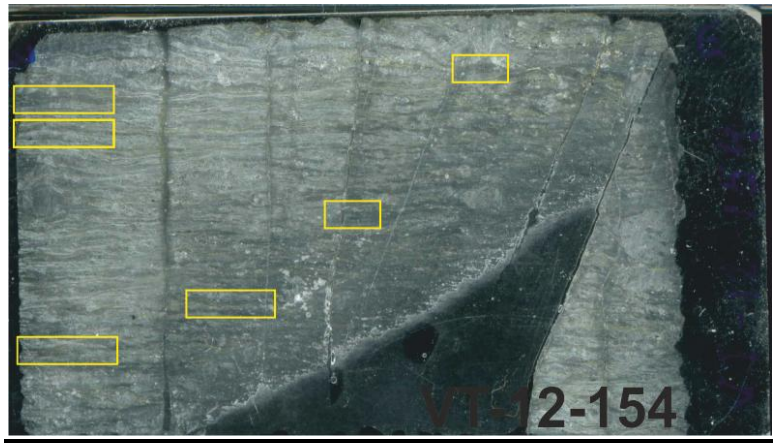
VT-12-154

VT-12-166

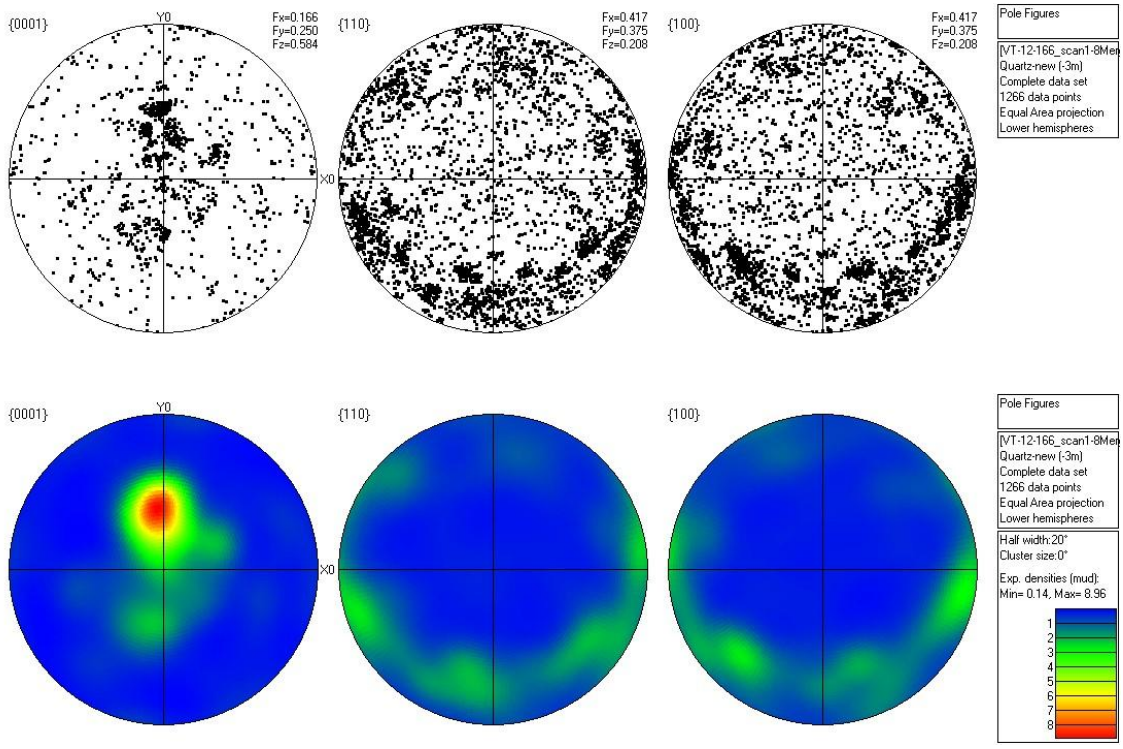
{0001}
Y0
X0
Fx=0.166
Fy=0.250
Fz=0.584
{110}
Fx=0.417
Fy=0.375
Fz=0.208
{100}
Fx=0.417
Fy=0.375
Fz=0.208
Pole Figures
[VT-12-166_scan1-8Mer
Quartz-new (-3m)
Complete data set
1266 data points
Equal Area projection
Lower hemispheres
{0001}
Y0
X0
{110}
{100}
Pole Figures
[VT-12-166_scan1-8Mer
Quartz-new (-3m)
Complete data set
1266 data points
Equal Area projection
Lower hemispheres
Half width:20°
Cluster size:0°
Exp. densities (mud):
Min= 0.14, Max= 8.96
1
2
3
4
5
6
7
8

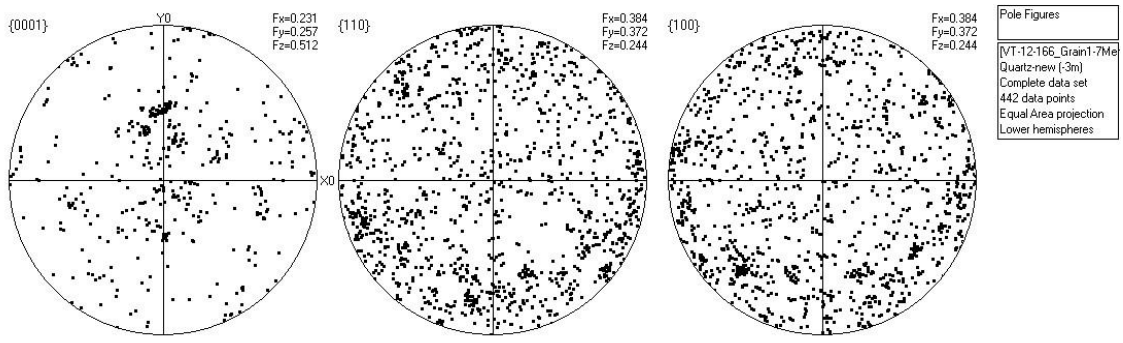
{0001}
Y0
X0
Fx=0.231
Fy=0.257
Fz=0.512
{110}
Fx=0.384
Fy=0.372
Fz=0.244
{100}
Fx=0.384
Fy=0.372
Fz=0.244
Pole Figures
[VT-12-166_Grain1-7Me
Quartz-new (-3m)
Complete data set
442 data points
Equal Area projection
Lower hemispheres

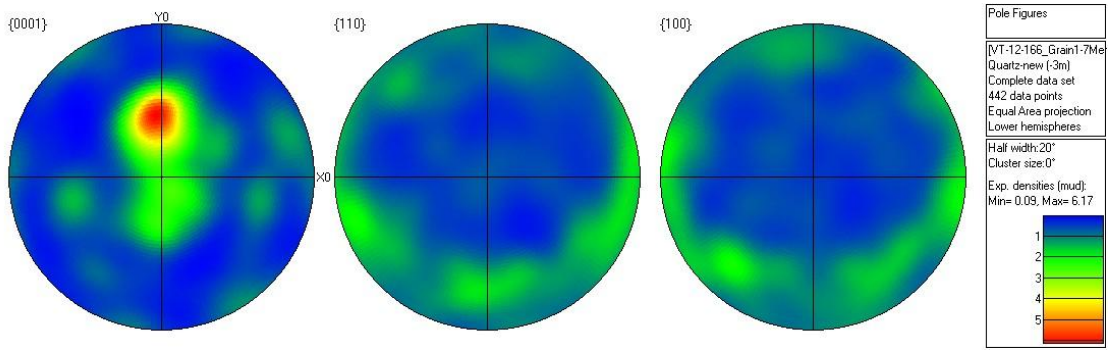
{0001}
Y0
X0
{110}
{100}
Pole Figures
[VT-12-166_Grain1-7Me
Quartz-new (-3m)
Complete data set
442 data points
Equal Area projection
Lower hemispheres
Half width:20°
Cluster size:0°
Exp. densities (mud):
Min= 0.09, Max= 6.17
1
2
3
4
5

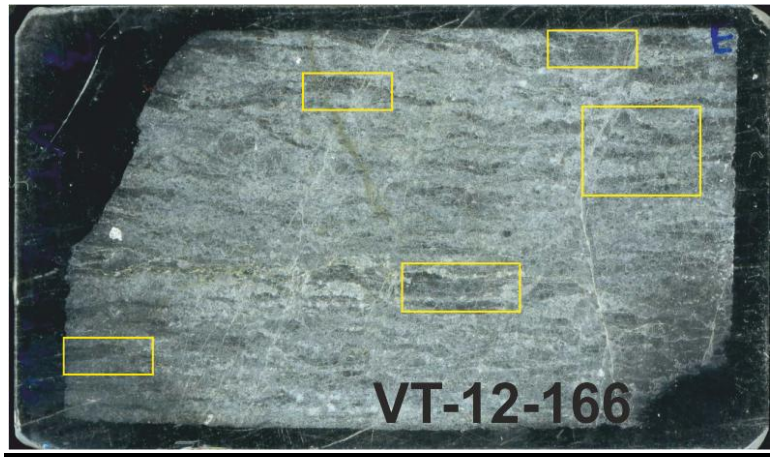
VT-12-166

VT-12-185

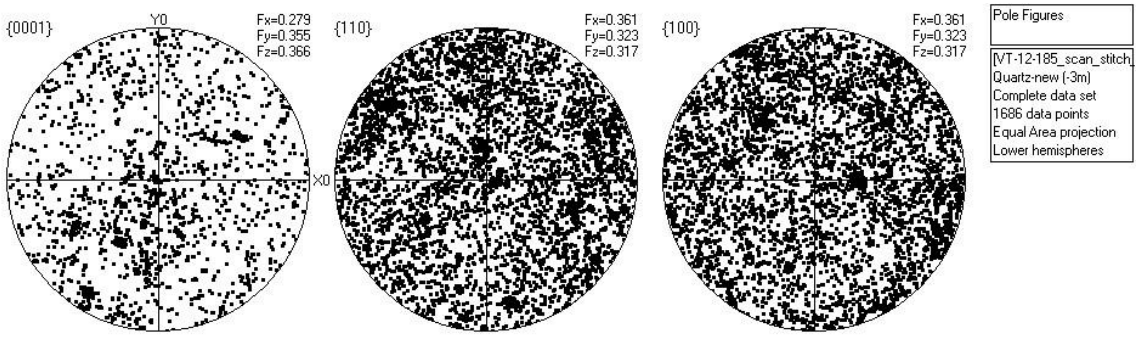
{0001}
Y0
X0
Fx=0.279
Fy=0.355
Fz=0.366
{110}
Fx=0.361
Fy=0.323
Fz=0.317
{100}
Fx=0.361
Fy=0.323
Fz=0.317
Pole Figures
[VT-12-185_scan_stitch_
Quartz-new (-3m)
Complete data set
1686 data points
Equal Area projection
Lower hemispheres

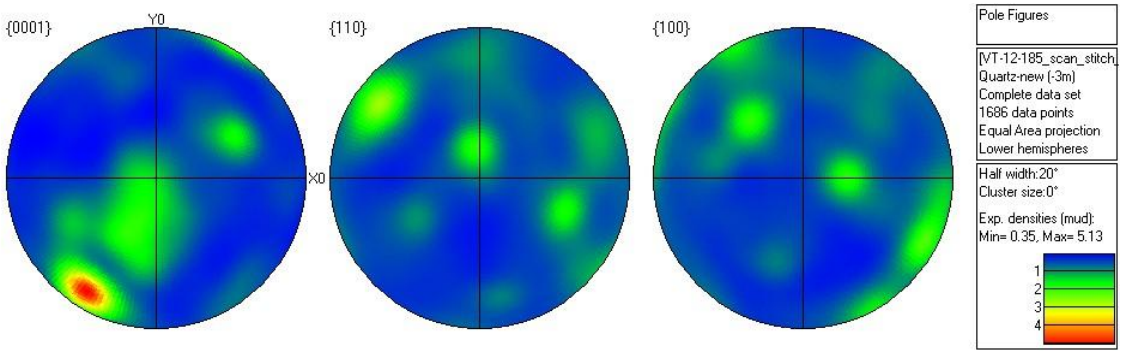
{0001}
Y0
X0
{110}
{100}
Pole Figures
[VT-12-185_scan_stitch_
Quartz-new (-3m)
Complete data set
1686 data points
Equal Area projection
Lower hemispheres
Half width:20°
Cluster size:0°
Exp. densities (mud):
Min= 0.35, Max= 5.13
1
2
3
4

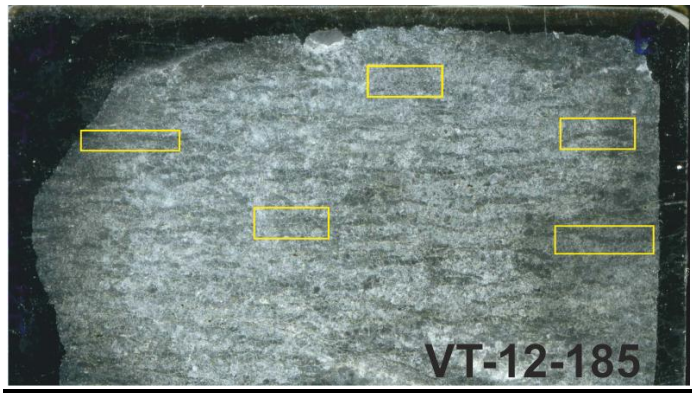
VT-12-185

Appendix C:

Fabric Analyser data

Rec_2

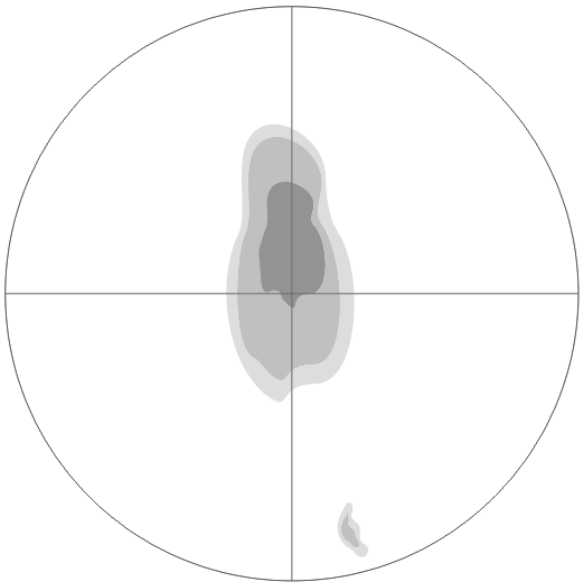

n=2027

VT-12-11

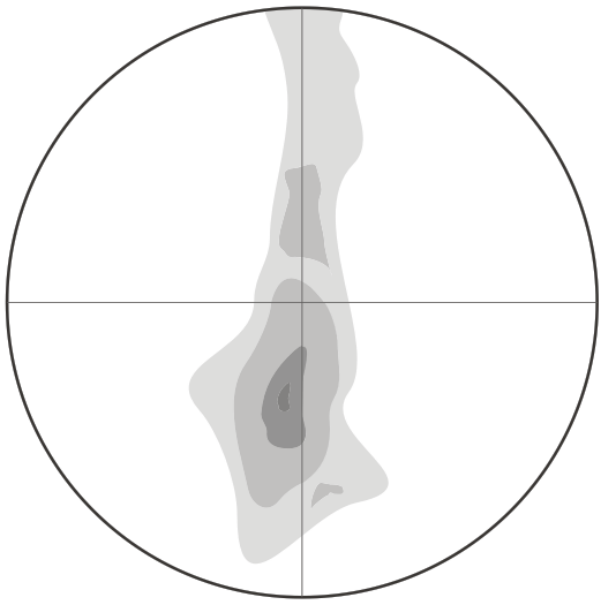

n=381

VT-12-30

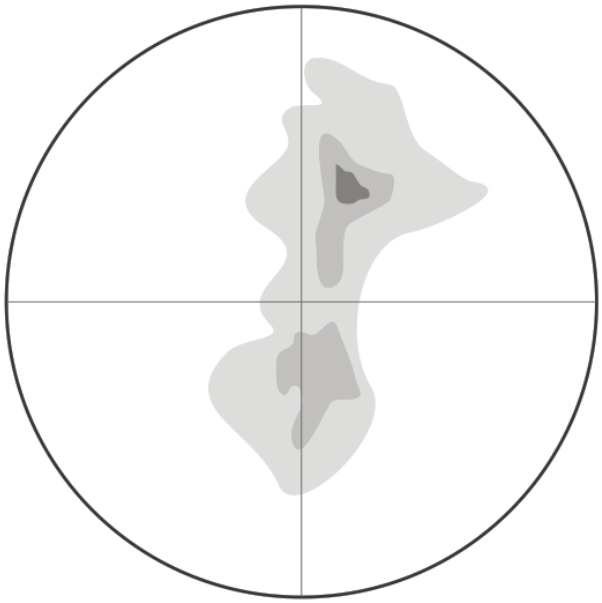

n=1132

VT-12-56

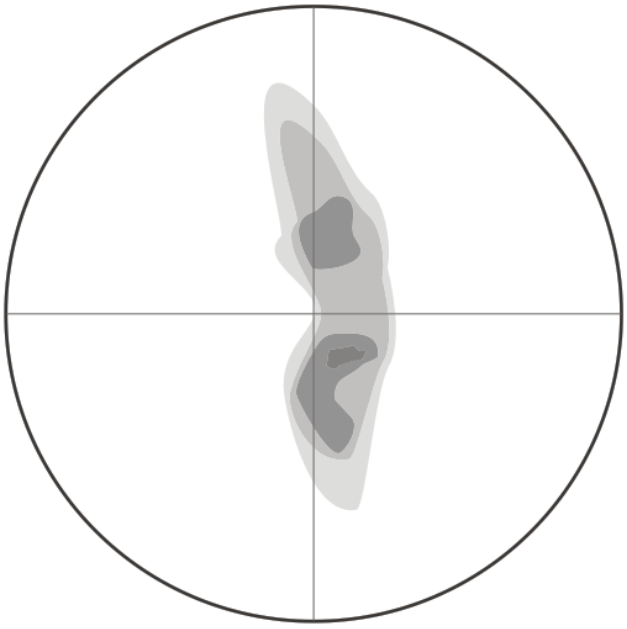

n=1348

VT-12-59

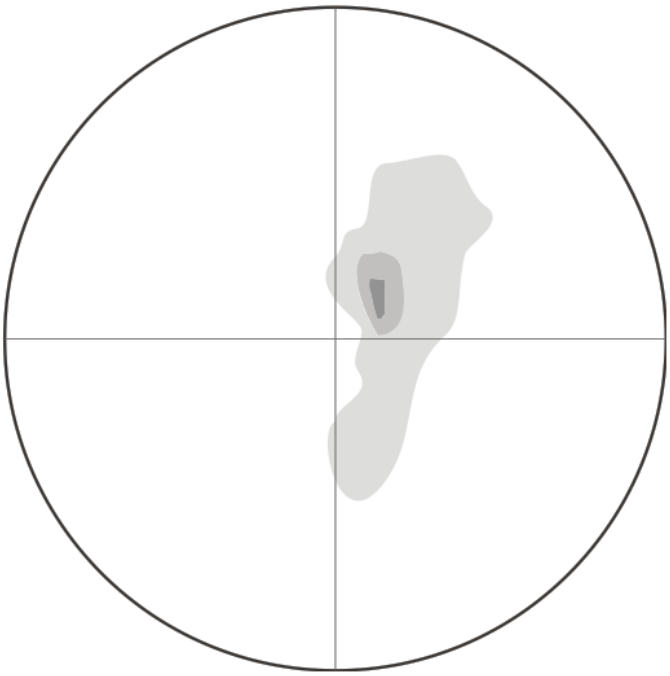

n=923

VT-12-72

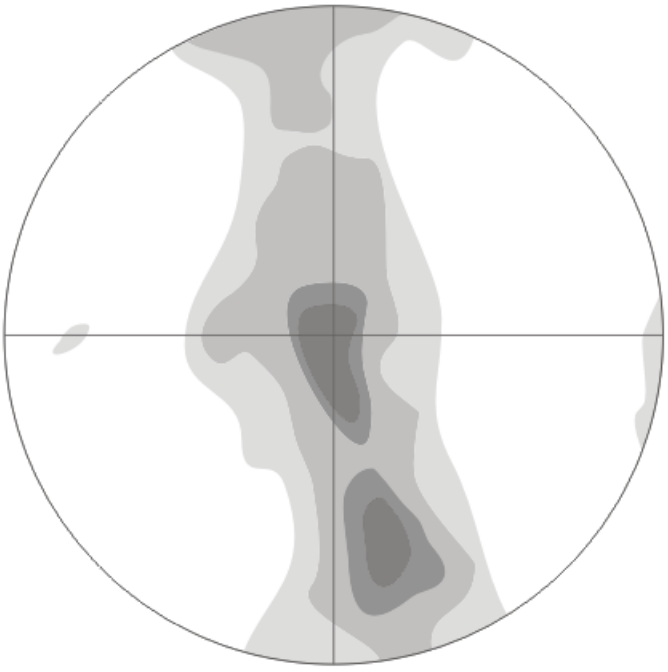

n=5278

VT-12-111

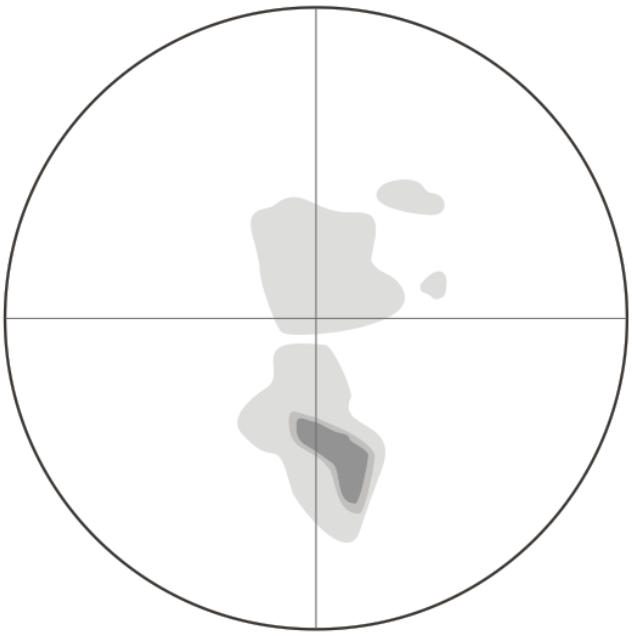

n=936

VT-12-154

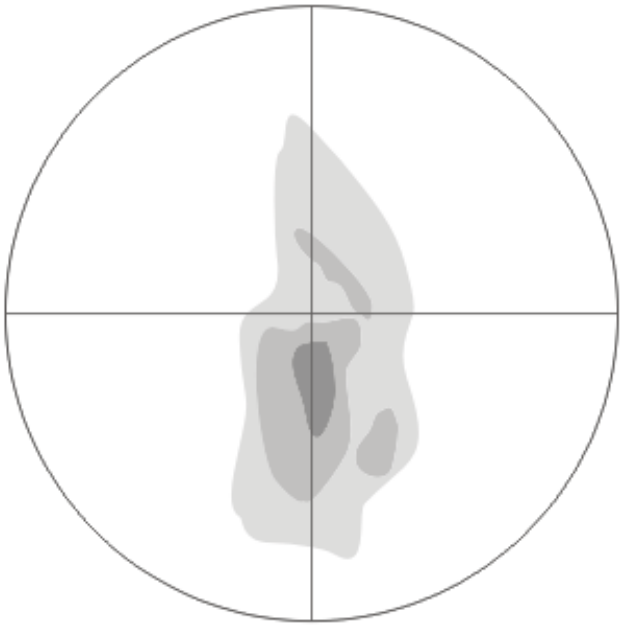

n=1165

VT-12-166

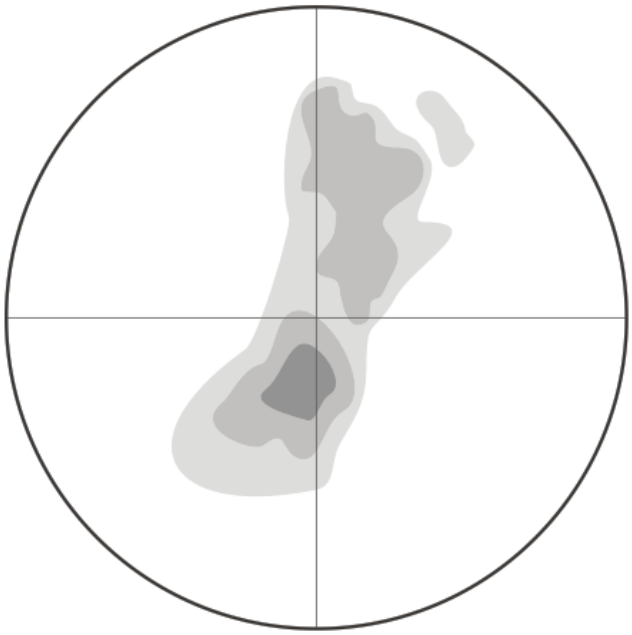

n=207

VT-12-185

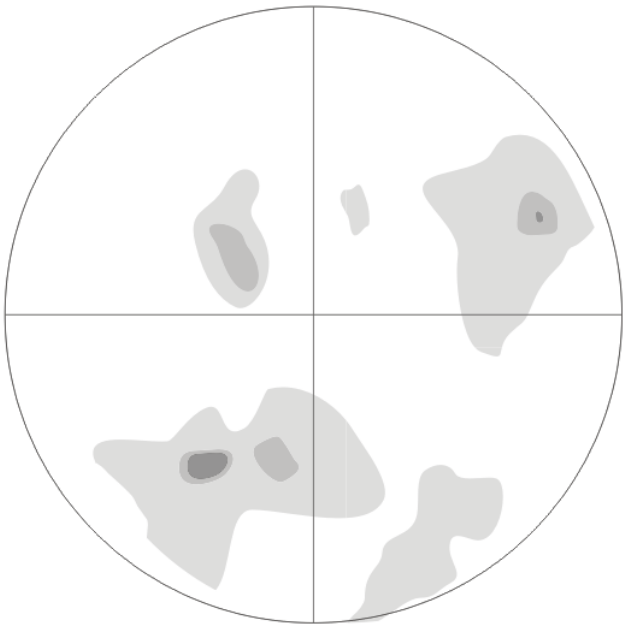

n=1068

Appendix D:

Supplementary geometric data

C.1. Initial geothermal gradient

Assuming peak metamorphism conditions of 670±50 °C and ~6.2±1.0 kbar equivalent to ~17-23 km depth based on *P-T* data of Brown et al. (2012) (Fig. C.1).

$$\frac{\mathbf{7\ km}}{17\ \mathrm{km}} = \frac{280^{\circ}\mathrm{C}}{670 \pm 50\ ^{\circ}\mathrm{C}} \qquad \frac{\mathbf{9.5\ km}}{23\ \mathrm{km}} = \frac{280^{\circ}\mathrm{C}}{670 \pm 50\ ^{\circ}\mathrm{C}}$$

Gap between 280°C and 670±50 °C; ~390 °C;

Hence initial geothermal gradient in **30-39 °C km^{-1}** range.

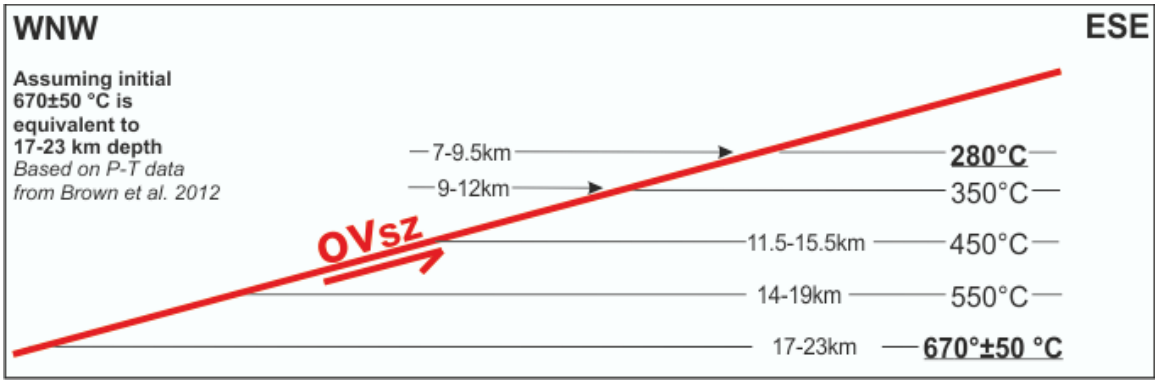

Figure C.1. Calculation of initial geothermal gradient assuming 670±50 °C equivalent to ~17-23 km depth based on *P-T* data of Brown et al. (2012).

C.2. Approximate vertical shortening

Assuming vertical section of OVsz between 1-1.5 km (Fig. C.2)

Vertical shortening based on equation: $\mathbf{e_v = \frac{l_f - l_o}{l_o}}$

e_v = vertical stretching/extension

l_f = final distance between 280-670 °C isotherms following deformation

l_o = initial distance between 280-670 °C isotherms following deformation

% shortening

$$e_v = \frac{1.5 - 10}{10} = -0.85 \quad 85\% \text{ vert. shortening}$$

$$e_v = \frac{1.0 - 10}{10} = -0.90 \quad 90\% \text{ vert shortening}$$

$$e_v = \frac{1.5 - 13}{13} = -0.884 \quad 88.4\% \text{ vert shortening}$$

$$e_v = \frac{1.0 - 13}{13} = -0.92 \quad 92\% \text{ vert shortening}$$

85-92% Vertical shortening approx.

Hence $1+e_v$ = <u>0.08-0.15</u>

1-0.85 = 0.15

1-0.9= 0.1

1-0.884=0.116

1-0.92=0.08

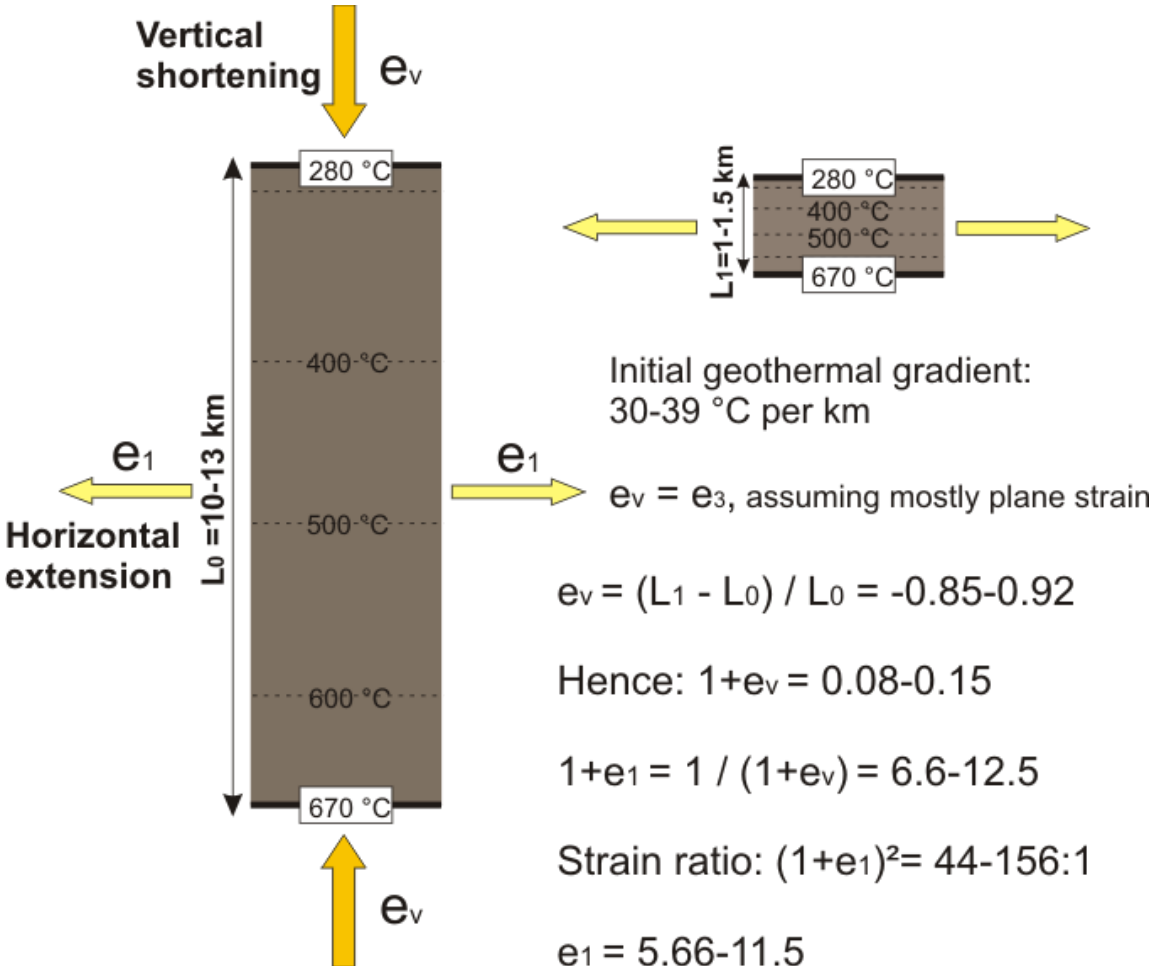

Figure C.2. Reduction of vertical spacing between 280-670 °C isotherms to ~1-1.5 km in the immediate footwall of the OVsz assuming an initial geothermal gradient ranging from 30-39 °C/km by a pure shear shortening model (e_1). Resultant stretches ($1 = e_1$) perpendicular to shortening assuming constant volume plane strain deformation. However, there was no data produced in this study that supports this particular mechanism for the telescoping of isotherms.

C.3. Quadratic elongation and approximate strain ratios based on the equation:

$$1 + e_1 = \frac{1}{1 + e_3} \quad e_v = e_3 \text{ assuming mostly plane strain (Fig. C. 2)}$$

$$1 + e_1 = \frac{1}{0.15} = 6.66$$

$$1 + e_1 = \frac{1}{0.1} = 10$$

$$1 + e_1 = \frac{1}{0.116} = 8.8$$

$$1 + e_1 = \frac{1}{0.08} = 12.5$$

Hence, strain ratios based on the equation $(1+e_1)^2$ are as follows:

6.66^2=44; 10^2= 100; 8.8^2=77.44; 12.5^2=156

Therefore strain ratio(R_s); <u>44-156:1</u>

C.4. Horizontal stretching (e_1)

<u>$1+e_1$ Therefore;</u>

	<u>% Horizontal extension</u>
e_1 = 5.66	**566%**
e_1 = 7.80	**780%**
e_1 = 9.00	**900%**
e_1 = 11.5	**1150%**

References:

Brown, S. R., Gibson, H. D., Andrews, G.D.M., Thorkelson, D.J., Marshall, D.D., Vervoort, J.D., Rayner N., 2012. New constraints on Eocene extension within the Canadian Cordillera and identification of Phanerozoic protoliths for footwall gneisses of the Okanagan Valley shear zone. Lithosphere 4, 354-377.

Appendix E:

Late to Post-kinematic volcanism within the Okanagan Mountain Provincial Park

Two post-kinematic dacitic outliers are mapped in northern limb of the pericline that defines the OVsz within the Okanagan Mountain Provincial Park (Fig. D.1) Dikes that feed into the outliers cut through the mylonitic gneiss. Euhedral to subhedral K-feldspar, hornblende, biotite phenocrysts are common in the felsic lavas which also contain minor subhedral, partly resorbed quartz xenocrysts in a vitrophyric groundmass. The outliers lack any of penetrative shear zone fabric suggesting they post-date the main phase of Eocene deformation. The outliers appear to be deposited within a paleotopographic low created by a small graben down-dropped along late, north-northeast trending high-angle faults that parallel the boundaries of the outliers. The long-axes of feldspar and hornblende phenocrysts within the lavas also parallel the boundaries (Fig. D.1). Despite being well within the ductily deformed structural section of the shear zone (~300-400m structural depth), the contacts of the mylonitic gneiss beneath theses outliers are cataclasized, brecciated and chloritized (Fig. D.1), indicating the felsic lavas were emplaced following the majority of exhumation facilitated by the OVsz.

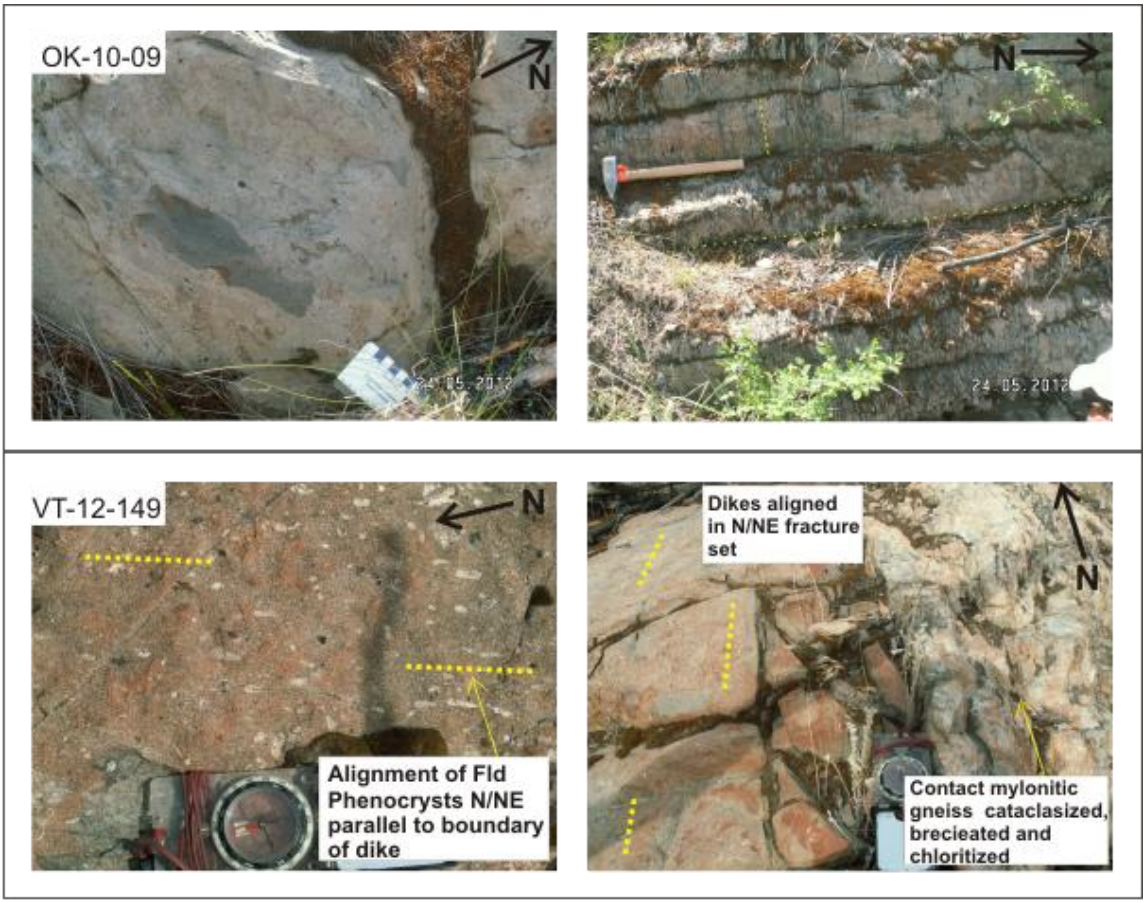

Figure D.1. Outcrop appearance of the two dacitic outliers both approximately 300-400m down the vertical structural section of the OVsz. Note the alignment of the long axes of the orthoclase and hornblende phenocrysts in a NNE direction parallel to the strike of the high angle brittle fracture set in which the outliers are aligned. The contact with mylonitic gneiss is highly fractured, brecciated and chloritized.

These outliers are tentatively correlated with the Marama Formation based on previous mapping of similar felsic lava flows within and east of the OVsz (Church 1973, 1985; Bardoux, 1993). Cooling ages for volcanic rocks of these formations range from 48.4 Ma (whole rock) to 53.1 Ma (K/Ar-biotite) (Church 1973, 1985) suggesting the mid-lower section of the OVsz (i.e ~300-400m estimated structural depth) on which the lavas were extruded was exhumed to the surface by this time. The cooling ages of these regional volcanic outliers are coeval with the ages of leucosome, dikes and plutons interpreted to have been generated at mid-crustal depths (Bardoux, 1993). This suggests that ductile deformation lower in the structural succession may have been still ongoing while the mid-lower section of the OVsz was already at the surface.

References:

Bardoux, M. 1993. The Okanagan Valley normal fault from Penticton to Enderby—Southcentral British Columbia. Ph.D. Dissertation, Carleton University, Ottawa, Ontario, 292 p.

Church, B.N. 1973. Geology of the White Lake Basin, British Columbia. Department of Mines and Petroleum Resources, Bulletin 61, 3-141.

Church, B.N. 1985. Volcanology and structure of Tertiary outliers in south-central BritishColumbia. Field Trip Guidebook, B.C. Ministry of Energy. Mines, and Petroleum Resources, 46p.